IOWA STATE UNIVERSITY
Digital Repository

Retrospective Theses and Dissertations

Iowa State University Capstones, Theses and Dissertations

1987

An experimental and theoretical study of a hydronic radiant ceiling panel heating system

Zhuanglin Zhang
Iowa State University

Follow this and additional works at: https://lib.dr.iastate.edu/rtd

 Part of the Mechanical Engineering Commons

Recommended Citation
Zhang, Zhuanglin, "An experimental and theoretical study of a hydronic radiant ceiling panel heating system " (1987). *Retrospective Theses and Dissertations*. 9320.
https://lib.dr.iastate.edu/rtd/9320

This Dissertation is brought to you for free and open access by the Iowa State University Capstones, Theses and Dissertations at Iowa State University Digital Repository. It has been accepted for inclusion in Retrospective Theses and Dissertations by an authorized administrator of Iowa State University Digital Repository. For more information, please contact digirep@iastate.edu.

www.manaraa.com

INFORMATION TO USERS

The most advanced technology has been used to photograph and reproduce this manuscript from the microfilm master. UMI films the original text directly from the copy submitted. Thus, some dissertation copies are in typewriter face, while others may be from a computer printer.

In the unlikely event that the author did not send UMI a complete manuscript and there are missing pages, these will be noted. Also, if unauthorized copyrighted material had to be removed, a note will indicate the deletion.

Oversize materials (e.g., maps, drawings, charts) are reproduced by sectioning the original, beginning at the upper left-hand corner and continuing from left to right in equal sections with small overlaps. Each oversize page is available as one exposure on a standard 35 mm slide or as a 17″ × 23″ black and white photographic print for an additional charge.

Photographs included in the original manuscript have been reproduced xerographically in this copy. 35 mm slides or 6″ × 9″ black and white photographic prints are available for any photographs or illustrations appearing in this copy for an additional charge. Contact UMI directly to order.

UMI

Accessing the World's Information since 1938

300 North Zeeb Road, Ann Arbor, MI 48106-1346 USA

Order Number 8805155

An experimental and theoretical study of a hydronic radiant ceiling panel heating system

Zhang, Zhuanglin, Ph.D.

Iowa State University, 1987

U·M·I
300 N. Zeeb Rd.
Ann Arbor, MI 48106

PLEASE NOTE:

In all cases this material has been filmed in the best possible way from the available copy. Problems encountered with this document have been identified here with a check mark __✓__.

1. Glossy photographs or pages _____
2. Colored illustrations, paper or print _____
3. Photographs with dark background _____
4. Illustrations are poor copy __✓__
5. Pages with black marks, not original copy __✓__
6. Print shows through as there is text on both sides of page _____
7. Indistinct, broken or small print on several pages __✓__
8. Print exceeds margin requirements _____
9. Tightly bound copy with print lost in spine _____
10. Computer printout pages with indistinct print _____
11. Page(s) _____ lacking when material received, and not available from school or author.
12. Page(s) _____ seem to be missing in numbering only as text follows.
13. Two pages numbered _____. Text follows.
14. Curling and wrinkled pages _____
15. Dissertation contains pages with print at a slant, filmed as received _____
16. Other _____

_____

_____

U·M·I

An experimental and theoretical study of a hydronic radiant ceiling panel heating system

by

Zhuanglin Zhang

A Dissertation Submitted to the
Graduate Faculty in Partial Fulfillment of the
Requirements for the Degree of
DOCTOR OF PHILOSOPHY

Major: Mechanical Engineering

Approved:

Signature was redacted for privacy.

In Charge of Major Work

Signature was redacted for privacy.

For the Major Department

Signature was redacted for privacy.

For the Graduate College

Iowa State University
Ames, Iowa

1987

TABLE OF CONTENTS

LIST OF TABLES

LIST OF FIGURES

ABSTRACT

The objective of this study is to improve the design of hydronic radiant panel systems through the understanding of the thermal performance of panel systems. The scope of this study includes performing experiments using testing facilities and the radiant panel ceiling in the Energy Research House, and developing a theoretical model that can predict heat transfer from a radiant ceiling panel.

In the experimental part of this study, a solar-radiant heating system was field tested to examine the feasibility of using a radiant system coupled to a solar heating system to provide space heating. Through experimental testing a system energy flow chart was made which showed how solar energy is utilized by the system through its various components. It was also found that room temperatures could be maintained at comfort levels using hot water from a solar storage tank at only about 32°C. This verified the concept that a radiant panel ceiling, due to its extended heat transfer surface, can effectively utilize low temperature heat sources such as solar energy. By operating the solar collector at a low temperature, the collector efficiency was also improved; an average efficiency of 40% was maintained in the test. A monthly averaged analysis showed that about 50% of the heating load was met by solar energy when using these combined systems in March, 1985.

A study on the transient thermal response of the radiant ceiling and room enclosure was also performed. This study provided a data pool

for checking the theoretical model to be developed in the later part of this study.

Another experimental study performed at the Energy Research House was a comparison of radiant heating and forced-air heating. Its major objective was to determine if radiant heating saves energy compared to forced-air heating. The experiment was carried out by alternatively operating the two systems and recording all relevant data during a ten-week testing period. It was concluded that the radiant heating was 15 to 20% more energy efficient than forced-air heating in normal winter conditions.

Theoretical modeling of the radiant panel heating system was performed in three steps. First, a panel unit was isolated from whole panel in order to to set up a domain. Numerical methods were used to solve heat transfer in this domain. Then a semi-analytical correlation was developed. Finally, a complete model was built by integrating heat output per panel unit along the entire tubeline, thus establishing an interrelationship between various system parameters. The model predicted the thermal behavior of the radiant panel to a reasonable accuracy.

ACKNOWLEDGEMENTS

I wish to express my gratitude to my Major Professor, Dr. Michael B. Pate, for his exceptional guidance and enthusiastic support throughout this study, without which this work has not been possible. I also wish to thank Professors Arthor E. Bergles, Ron M. Nelson, Theodore Okiishi, Paul W. Peterson, and Howard E. Shapiro, who served in my advisory committee, for their constant encouragement and valuable opinions.

Further thanks are due to the members of the Building Energy Utilization Laboratory. It has been a very pleasant experience for me to work with them. Very special appreciations are due to Mr. Richard P. Rusk and Mr. Ti Liu who were a tremendous help to me at the earlier stages of this work.

I also wish to express my deep appreciation to the Iowa State University Graduate College and the Mechanical Engineering Department whose financial support made this study possible.

Finally, I wish to thank my wife Ning Tang with whom I shared many joys and frustrations of working toward the completion of this study. I am also deeply indebted to my dearest daughter, Panpan, who has paid a dear price of not being able to stay with her parents during these years.

NOMENCLATURE

A	surface area (Chapter 2)
A	constant coefficient of $\theta_{i,j}$ (Chapter 5)
A'	constant coefficient of $\theta_{i,j}$ in Eq. (5.27)
A_C	collector effective area (Chapter 2)
B	constant coefficient of $\theta_{i,j-1}$ (Chapter 5)
Bi	Biot number, convection parameter, defined in Eq. (5.16) and Eq. (6.8)
C	constant coefficient of $\theta_{i,j+1}$ (Chapter 5)
C	grid size increment factor, Eq. (5.4)
C_p	specific heat of plaster (Chapter 5)
CT	correction term, Eq. (6.48)
d	tube diameter
D	constant coefficient of $\theta_{i-1,j}$ (Chapter 5)
DA	X length of curvilinear portion of the ceiling unit (Chapter 5)
E	constant coefficient of $\theta_{i+1,j}$ (Chapter 5)
F	constant coefficient of $\theta_{i,j}^{n+1}$ in Eq. (5.27)
F_R	collector heat removal factor (Chapter 2)
F	view (shape) factor
Fo	Fourier number (Chapter 3)
Fo	constant defined by Eq. (5.20)
G_T	total radiation incident on A_C (Chapter 2)
h	convective heat transfer coefficient

h	tank height (Chapter 2)
$\bar{h}$	equivalent heat transfer coefficient (Chapter 6)
Hi	nondimensional heat transfer coefficient defined in Eq. (6.11)
$\dot{I}$	enthalpy of water (Chapter 7)
k	thermal conductivity of plaster
l	tube separation distance or tube spacing
L	nondimensional tube spacing defined in Eq. (6.15)
Δl	distance between nodes at ith row and (i+1)th row (Chapter 5)
ΔL	Δl in nondimensional form (Chapter 5)
m	number of nodes at each row (Chapter 5)
m	panel section thickness including tube diameter or tube cover thickness (Chapter 6)
M	nondimensional tube cover thickness defined in Eq. (6.16)
Δm	grid length along side (Chapter 5)
ΔM	Δm in nondimensional form (Chapter 5)
MC	storage heat capacity (Chapter 2)
$(\dot{m}c)_c$	collector loop capacitance rate (Chapter 2)
$(\dot{m}c)_r$	radiant loop capacitance rate (Chapter 2)
$(\dot{m}c)_t$	tank loop capacitance rate (Chapter 2)
n	number of nodes at each column (Chapter 5)
N	number of the vertical temperature measurements of the

	storage tank (Chapter 2)
Δn	grid length along side (Chapter 5)
ΔN	Δn in nondimensional form (Chapter 5)
P	constant in Eqs. (5.22) and (5.27)
Pi	radiation parameter, defined in Eq. (5.15) and Eq. (6.7)
q	heat flux or heat output from ceiling unit
Q	q in nondimensional form (Chapter 5)
Q	energy consumption for the Research House (Chapter 4)
Q	constant defined in Eq. (5.25)
q_r	heat flux due to radiation (Chapter 5)
Q_e	heating energy extracted from the tank (Chapter 2)
Q_h	heating energy delivered to radiant system (Chapter 2)
Q_l	heat losses (Chapter 2)
Q_T	total incident solar energy (Chapter 2)
Q_u	useful energy collected by the collector (Chapter 2)
Qi	nondimensional heat output from panel section defined in Eq. (6.20)
r	correlation coefficient (Chapter 4)
R	copper tube radius (Chapter 5)
R	thermal resistance (Chapter 6)
Ri	nondimensional thermal resistance defined in Eq. (6.18)
S	total stretched length of tubes embedded in the panel (Chapter 7)
t	time

T ceiling surface temperature

$\bar{T}$ scaled radiant panel temperature (Chapter 3)

t_1, t_2 initial and final operating time, respectively (Chapter 2)

T_0 initial enclosure temperature (Chapter 3)

T_0 tube (isothermal boundary) temperature (Chapter 5 and 6)

T_a outdoor temperature (Chapter 2)

T_a average room temperature (Chapter 5)

T_n tank temperature at each level with equal spacing (Chapter 2)

T_s steady-state ceiling temperature (Chapter 3)

T_o, T_i collector outlet and inlet temperatures, respectively (Chapter 2)

T_s, T_r panel surface and room air temperatures, respectively (Chapter 2)

T_{t2},T_{t1} mean final and initial temperatures of the tank during the period t_1 to t_2 (Chapter 2)

T_∞ ambient temperature (Chapter 6)

Ti sink-source temperature ratio defined in Eq. (6.9)

Ti_a averaged nondimensional temperature defined in Eq. (6.14)

U_L overall heat transfer coefficient of the collector (Chapter 2)

UA overall heat transfer coefficient for the Research House

Ui nondimensional thermal transmittance defined in

Eq. (6.28)

x ceiling unit horizontal coordinate (Chapter 5)

X x in nondimensional form (Chapter 5)

y ceiling unit vertical coordinate (Chapter 5)

Y y in nondimensional form (Chapter 5)

Greek Symbols

α thermal diffusivity of plaster

ϵ ceiling surface emissivity

ϵ convergence parameter (Chapter 5)

θ nondimensional temperature defined in Eq. (6.34)

θ T in nondimensional form (Chapter 5)

θ_a T_a in nondimensional form (Chapter 5)

ρ density of plaster

σ Stefan-Boltzman's constant

$\tau\alpha$ product of collector absorptivity and transmissivity (Chapter 2)

ϕ nondimensional temperature defined by Eq. (6.34)

CHAPTER 1 INTRODUCTION

The use of hydronic radiant panel systems in both residential and industrial space heating dates back to the 1940s. Although the decades that followed did not witness widespread applications of such systems, panel heating persists and pertinent research continues because of interest in building energy conservation.

The most systematic research in this field was organized and conducted in the 1950s by ASHRAE, then known as ASHVE (American Society of Heating and Ventilating Engineers), at its research laboratory located in Cleveland, Ohio. The results of this work was reported in ASHVE Transactions. Based partly on this research, a chapter on Panel Heating and Cooling Systems was later written into the ASHRAE Handbook (1987). This document serves as a valuable guide for the design of panel systems.

The major advantage of panel heating systems is that they conserve energy while improving thermal comfort. This advantage has stimulated extensive research on the physiological effects of panel systems and on heat transfer characteristics in panels, both theoretical and experimental. Recently, Howell (1986) conducted a literature survey on all aspects of designing radiant heating and cooling systems. The past work consists mainly of three parts: improved thermal comfort, cost effectiveness, and heat transfer characteristics of radiant systems. Although radiant cooling has drawn some attention from researchers, most past studies deal with heating systems.

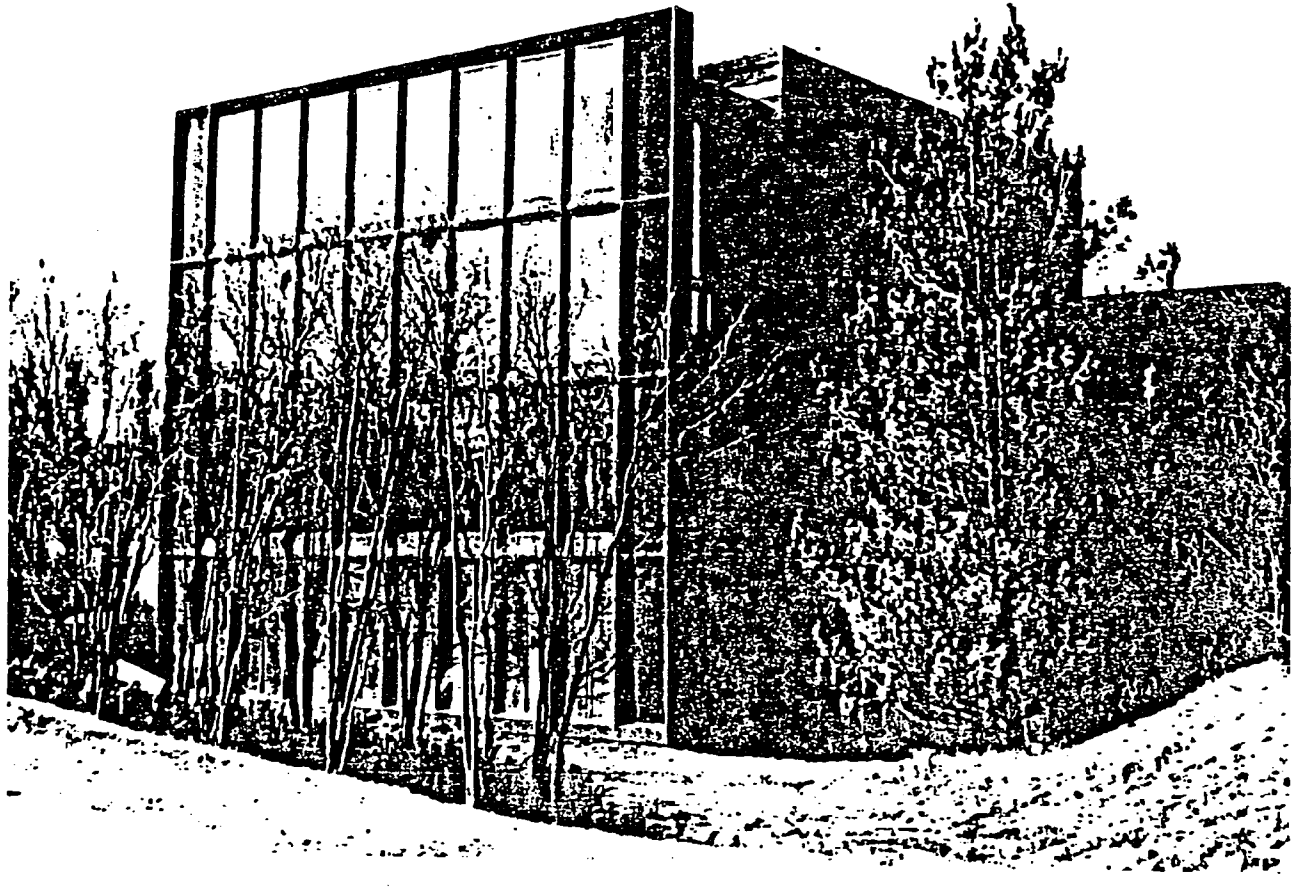

FIGURE 1.1. The ISU Energy Research House

system in order to gain a better understanding of its transient thermal behavior. Specifically, Chapter 2 focuses on the temperature response of the radiant system under different operating conditions. Particular attention is placed on obtaining a qualitative understanding of the thermal behavior of the panel and room enclosure in order to form a basis for the numerical studies and computer simulations reported in the theoretical part of this study.

The energy efficiency of the panel heating system is compared with that of a forced-air heating system in Chapter 4. Both systems are installed in the Energy Research House. This comparison between the energy consumptions for the radiant system and the forced-air system quantifies the cost-effectiveness of the hydronic panel heating installation.

The studies described above are experimentally oriented and based on extensive testing performed at the ERH during the 1984/1985 and 1985/1986 heating seasons. These experimental studies, particularly the transient study reported in Chapter 3, validate many assumptions that are used in the theoretical models and provide useful data with which model predictions can be compared. These theoretical models are described below and presented in Chapters 5 through 7.

A numerical study of heat transfer in the ceiling panel is reported in Chapter 5. This study focuses on a two-dimensional panel unit and employs the finite-difference method to solve the heat output from the panel unit. Effects of the convective heat transfer

coefficient, the tube spacing, and the tube cover thickness on the heat output are also examined theoretically.

A different approach to the above problem is presented in Chapter 6. Instead of using a numerical method, a semi-analytical correlation between the heat output from the radiant panel unit and various affecting parameters is established. The correlation for the heat output is expressed in terms of nondimensional parameters.

Based on this correlation, a new method was developed in Chapter 7 for performing a hydronic radiant panel calculations and design. This new method integrates the heat output from the two-dimensional unit over the entire tube length in a panel, thus providing a useful relation between heat output from the whole panel and other system parameters. This method can also be extended to other types of heating panels.

CHAPTER 2 AN INVESTIGATION OF A RESIDENTIAL SOLAR SYSTEM COUPLED TO A RADIANT PANEL CEILING

Introduction

A heating system consisting of a water-ethylene glycol solar collector system supplying energy to a hydronic radiant ceiling has potential for residential applications. This potential is based on the fact that solar collectors are more efficient at lower fluid and plate temperatures, while radiant heating systems can be operated at fluid temperatures well below those required by typical water-to-air coils used in forced-air systems. As a consequence, using the combination of solar and radiant heating systems, a greater fraction of solar energy can be utilized for residential heating.

Although successful utilization of a solar-radiant heating system was reported as early as 1957, few buildings or residences constructed since then have incorporated this type of heating system. One explanation for this lack of use is that a complete evaluation of the thermal performance of such a system has not been reported. This lack of knowledge coupled with higher construction cost does not encourage widespread use of solar-radiant heating systems. In addition, past radiant heating studies have implied that the use of solar heating may not be feasible. For example, widely accepted HVAC design literature (ASHRAE 1987) suggests a 55 to 60°C surface temperature for a radiant ceiling of moderate height (i.e., 2.5 to 3 m). This, in turn, would

require 65°C or higher water temperatures supplied from a solar collector or storage tank. For a standard flat-plate collector, this high temperature results in a low collector efficiency (Duffie and Beckman 1980).

It is possible, however, to operate a radiant system with a low panel temperature, as this study shows. This low temperature operation not only improves the solar collector efficiency but also minimizes heat losses throughout the rest of the system. The important questions that arise are how the heating system performs at low temperatures (i.e., slightly above room temperature) and whether this performance is adequate to heat a residence.

This Chapter presents the results of an experimental analysis of a solar-radiant heating system installed at Iowa State University (ISU) Energy Research House (ERH). The heating system tested consists of 24 solar collectors, a 4540-liter storage tank, a solar-to-radiant heat exchanger, and a hydronic radiant ceiling. The complete system was well instrumented with thermocouples and flow-meters. The experimental data emphasize the dynamic thermal behavior of each component in the solar-radiant system. Special attention has been placed on analyzing data for two 24-hour periods: a clear-sky day and the third of three consecutive cloudy days. These two periods represent two extreme operating conditions for the heating system. A thermal performance evaluation based on the data collected over a much longer period of time is also included. This evaluation covers each component including

the flat-plate collector, the water storage tank, the solar-to-radiant heat exchanger, and, finally, the room enclosure that contains the radiant ceiling. An overall performance evaluation of the complete system using the results of each component is also presented. Although the experiments did not include the most severe winter months (January and February), this study provides insight into the operation and potential usefulness of a solar-radiant heating system.

Experimental Facilities

The ERH is the primary facility for residential energy research at Iowa State University. The 300 m^2, three bedroom, single-family residence located near the ISU campus in Ames, Iowa, consists of three floors of living space with a greenhouse on the south side. The design of the house incorporates several energy-efficient elements and an active solar system to reduce external energy consumption. Among specialized systems included in the ERH that are pertinent to this study are an array of 24 flat-plate collectors vertically mounted on the south wall (40 m^2 total area), a storage tank, heat exchangers, and a hydronic radiant heating system installed in the ceiling. A schematic of these systems is shown in Figure 2.1.

The liquid (45% water, 55% ethylene glycol) solar collectors are Lennox LSC 18-1 type flat-plate collectors. Each collector has four major components:

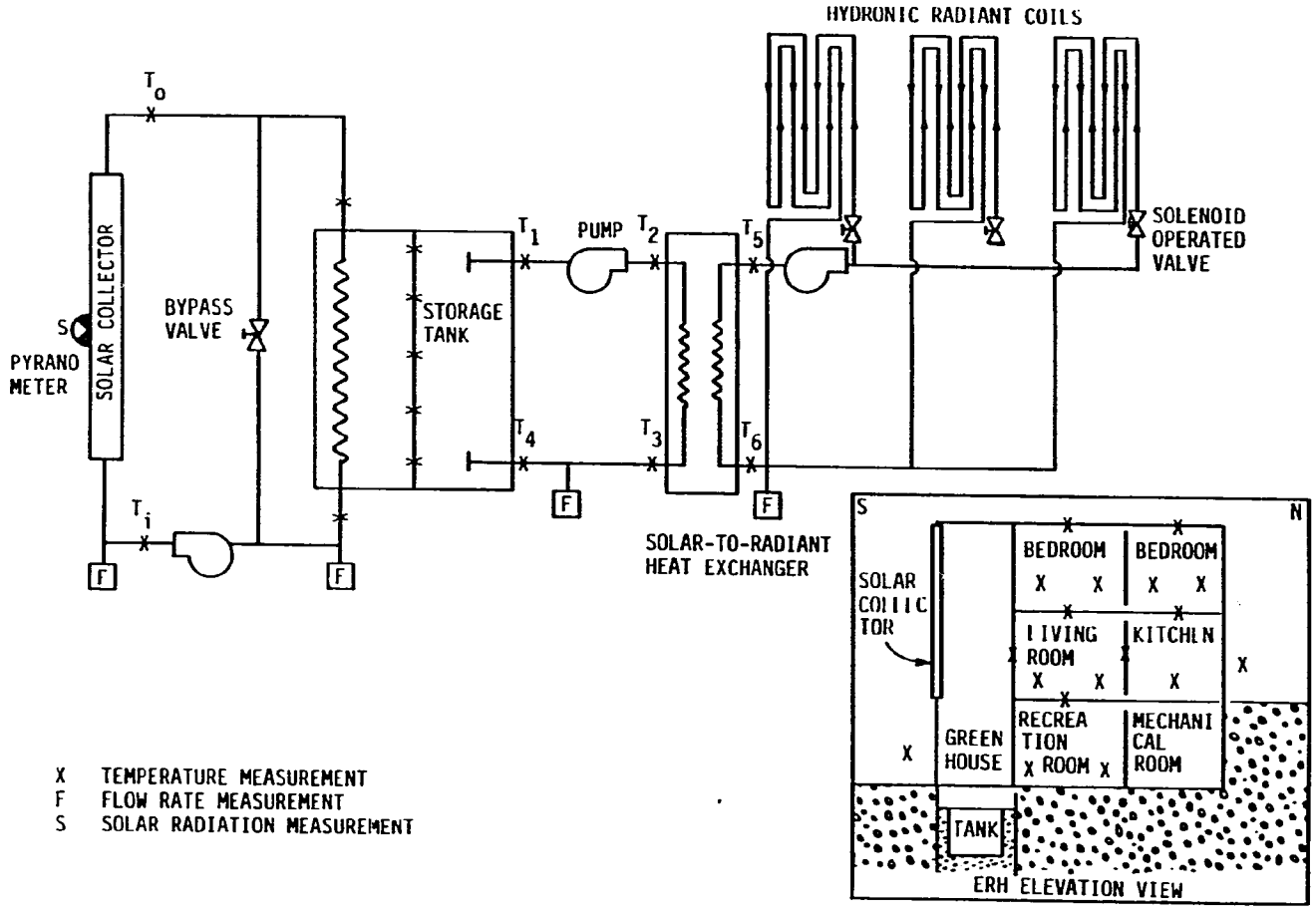

FIGURE 2.1. A schematic of the solar-radiant heating system

- covers — two 3.2-mm, low-iron, transparent glass sheets, surface-etched to reduce reflections
- absorber plate — parallel copper tubes bonded to a steel plate electroplated with black chrome on bright nickel
- insulation — a semi-rigid fiberglass board without facing, 8.9 cm beneath the absorber plate and 2.5 cm around the sides of the collector enclosure
- frame — extruded aluminum, anodized for protection against corrosion, having weep holes for ventilation and moisture removal.

Figure 2.2 shows a schematic diagram of the collector.

The hot-water storage system includes a 4540-liter concrete storage tank and a copper, spiral-finned-tube heat exchanger connected to the solar collectors. The hot water for the load is extracted directly from the tank. This arrangement eliminates the temperature drop in a heat exchanger installed on the radiant side of the tank, but it has the disadvantage of reducing thermal stratification whenever the storage tank is used to supply heating loads. The storage tank, as shown in Figure 2.3, is insulated with 15.2 cm of styrofoam on the sides and bottom. In addition, the tank cover is insulated with 30.5 cm of polyurethane. The tank is below grade inside a greenhouse that is located between the collector wall and the residential part of the house.

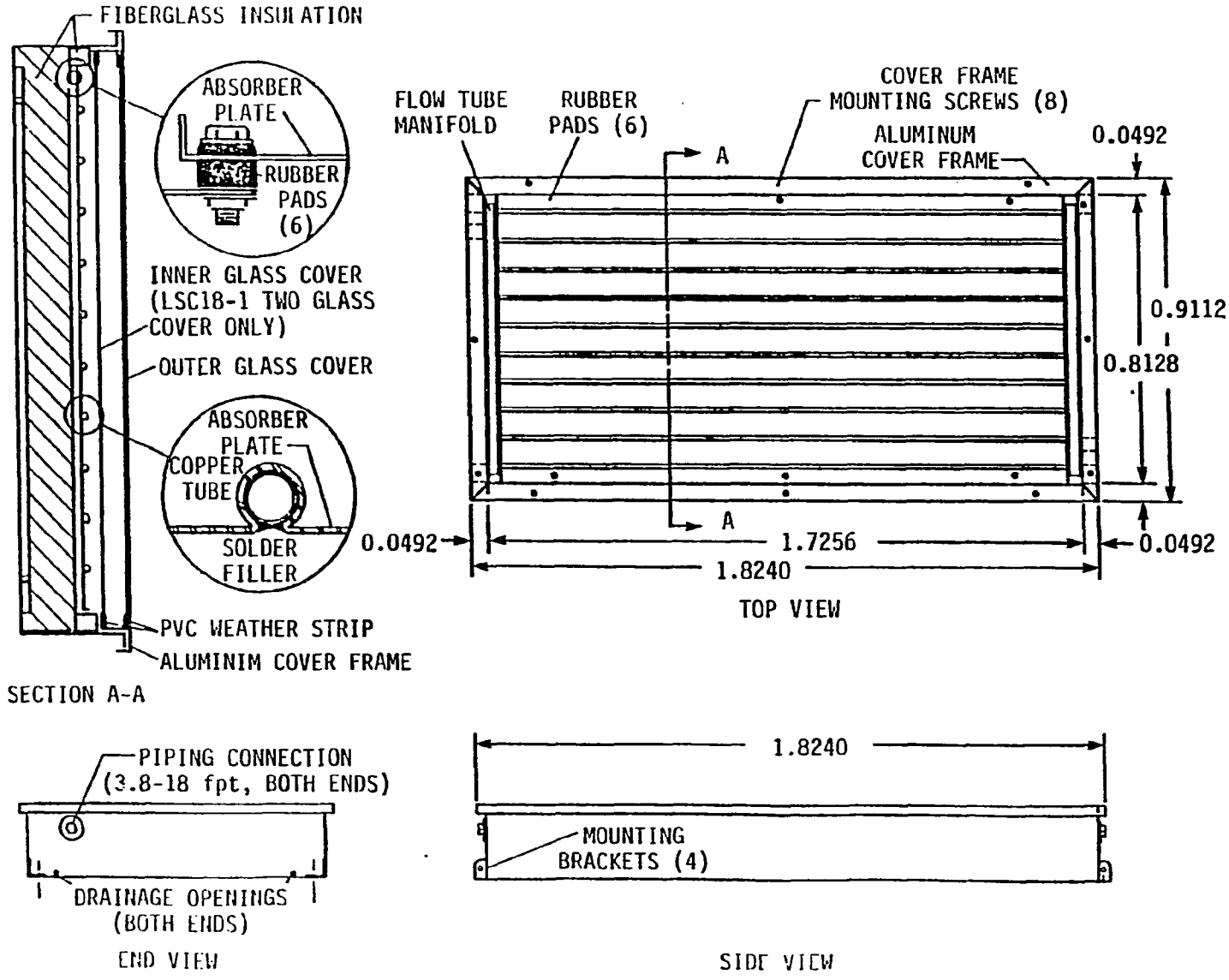

FIGURE 2.2. Schematic diagram of the collector (dimension in meters)

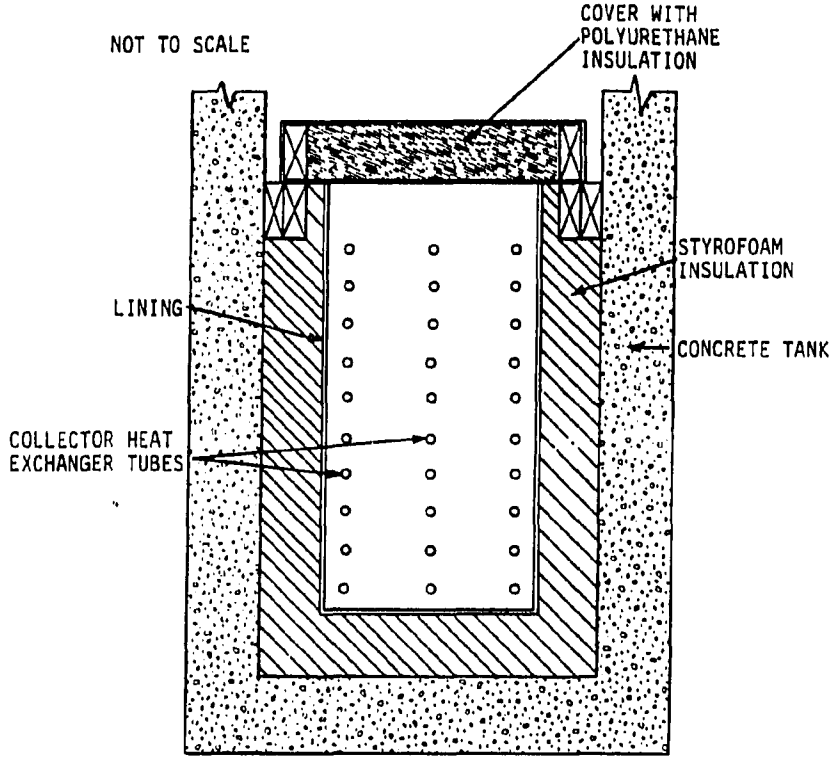

FIGURE 2.3. Cross-sectional view of the storage tank

The radiant heating system consists of a closed-loop water system, which gains heat from the storage tank through a solar-to-radiant heat exchanger as shown in Figure 2.1. The heat exchanger is needed to isolate the hydrostatic pressure of the three-story radiant system from the storage tank. Heat can also be supplied to the radiant system by a heat pump or by electric resistance heaters, but they were not used in the present study. The house heating load is divided into separate zones, each having a motorized, on-off valve for room temperature

control. Under fully loaded conditions (i.e., all valves are open), the radiant system has a total mass flow rate of 27.5 kg/min. The radiant panel ceiling consists of 10-mm-I.D. copper tubes embedded in a 2.54-cm layer of plaster that has an approximate surface emissivity of 0.9. The tube pattern for each room consists of a single supply and return line, arranged so that the tubes are adjacent and parallel to each other as shown in Figure 2.1. The tubes are separated by a distance of 15.2 cm. This arrangement helps achieve a high degree of temperature uniformity which will be discussed in Chapter 3.

Instrumentation and System Control

Temperatures were measured at 15 locations including the heat exchangers, pipes, solar collectors, outside air, greenhouse, and storage tank (as shown in Figure 2.1). Thermal stratification in the storage tank was measured by five thermocouples placed in a vertical array with the top thermocouple 38.1 cm below the water level and each successive thermocouple 50.8 cm deeper. An average temperature for the radiant ceiling in each room was measured by connecting five thermocouples in parallel. Room air temperatures were measured using radiation-shielded thermocouples. The outdoor air temperature was estimated using an average of temperature measurements taken near the north and south sides of the house; the north side was shaded while the south side was exposed to the sun.

A differential temperature controllor was installed to monitor the collector plate temperature and the storage tank temperature and to turn on the collector pump if the plate temperature exceeded the tank temperature by a set amount. The operation of the radiant heating system was controlled by thermostats installed in each zone. If the room temperature dropped below the 21°C set-point temperature, then a motorized valve opened, and hot water was supplied to the pipes embedded in the plaster ceiling.

The temperatures were measured using copper-constantan thermocouples connected to a Fluke 2240B datalogger through isothermal block connectors. The datalogger provided reference junction compensation that improved the accuracy of temperature measurements. The measurement uncertainty was approximately ±0.2°C. The flow rate measurements were made using strain-gage type flow-meters with an uncertainty of ±0.2 l/min. The instantaneous total solar radiation was taken by an Eppley precision pyranometer mounted on the center of the collector assembly. The flow-meters and the pyranometer were also read by the Fluke 2240B. Experimental data were taken at 20-minute intervals.

Solar Collector

Figure 2.4 shows the solar radiation incident on the vertical south-facing collector wall for typical clear-sky days and typical overcast days. The clear-day radiation peaked at 725 W/m^2, while the

radiation on a typical overcast day never exceeded 66 W/m^2, an order of magnitude lower.

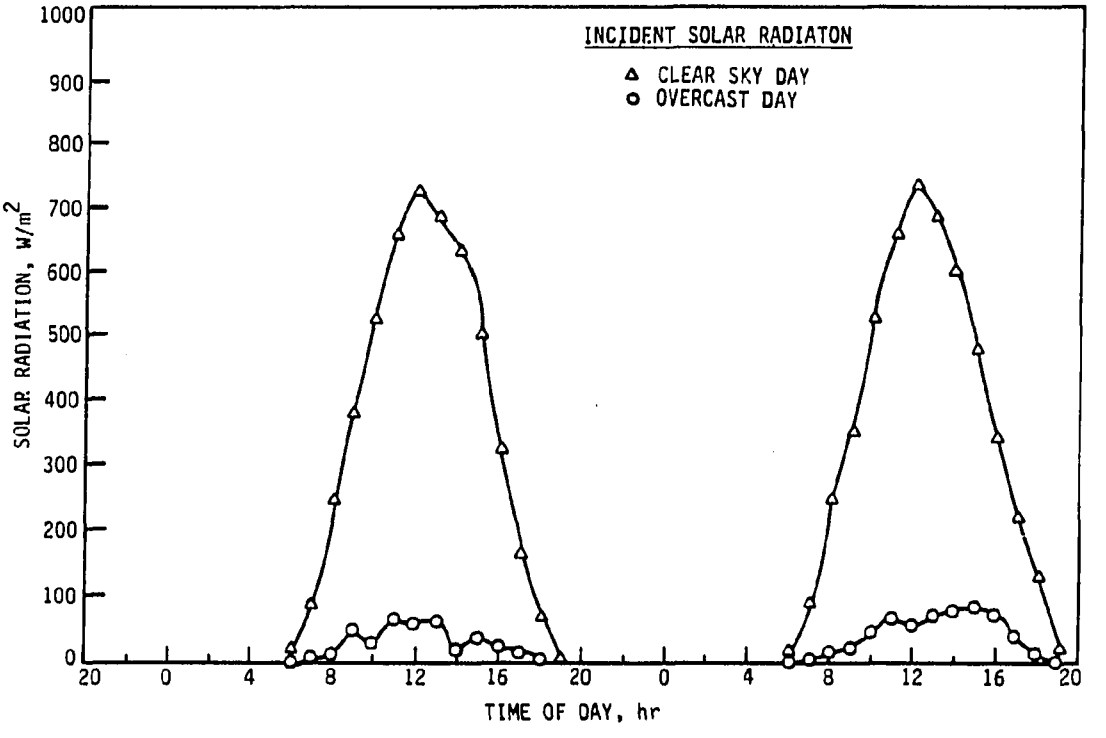

FIGURE 2.4. Incident solar radiation for the two test days

The collector efficiency was calculated from experimental data on a daily basis as follows:

$$\eta = \frac{Q_u}{Q_T} \tag{2.1}$$

where the useful energy from the collector was calculated from collector inlet and outlet temperature measurements

$$Q_u = \int_{t_1}^{t_2} (\dot{m}c)_c (T_o - T_i) dt \qquad (2.2)$$

and the total incident radiation was calculated by integrating Figure 2.4

$$Q_T = A_c \int_{t_1}^{t_2} G_T dt \qquad (2.3)$$

The collector efficiency was evaluated for two different sets of conditions:

1. Charging mode only, on a typical clear-sky day (i.e., no energy extraction from tank) — flow rate V = 35 l/min; average outdoor temperature T_a = 5.1°C; Q_T = 663.2 MJ/day; Q_u = 283.4 MJ/day; η = 42.7%
2. Fully operational (i.e., simultaneously adding energy to tank and supplying energy to radiant system) — flow rate V = 51 l/min; average outdoor temperature T_a = 11.6°C; Q_T = 557.6 MJ/day; Q_u = 238.1 MJ/day; η = 41.2%

The efficiency changed only slightly from the first test to the second test, even though the outdoor temperature was considerably higher on the latter. This change was modest because the second test was performed when energy was being extracted from the storage tank. Energy extraction had the effect of reducing thermal stratification in the tank by causing disturbances when water was pumped directly from

the tank to the solar-to-radiant heat exchanger and then discharged back to the tank. The net result was that the collector inlet temperature increased by approximately the same amount as the outdoor temperature, while G_T changed only slightly; thus the collector efficiency remained unchanged. This is in agreement with solar collector theory which shows that the decrease in collector efficiency is directly proportional to the difference between the collector inlet temperature and the outdoor temperature (i.e., collector ambient temperature) as follows (Duffie and Beckman 1980):

$$\eta = F_R(\tau a) - F_R U_L(T_i - T_a)/G_T \qquad (2.4)$$

The above variations in collector efficiency are small and of the same order of magnitude as the experimental uncertainty. An analysis of these data and additional experiments suggested that under normal conditions (outdoor temperature above -5°C, wind speed under 10 km/hr), the daily collector efficiency is approximately 40%, and 2.5×10^5 kJ of solar energy can be charged into the storage tank on a clear-sky day in March. Using a clearness index of 52% given in Cinquemani et al. (1978), a total of 40×10^5 kJ of solar energy could be collected during the month of March. Therefore, the monthly averaged daily useful solar energy is about 1.35×10^5 kJ/day.

It is worthy of note that the measured collector efficiency is fairly close (within 5%) to the manufacturer's performance curve (Lennox 1979). The incident solar radiation, however, is less by about 25% than the value predicted by theory using the solar data given in (Cinquemani et al. 1978).

Storage Tank

The storage tank is an important component of the solar-radiant system. It must be well insulated to minimize heat loss. For example, the storage tank investigated in this study was insulated with 15.2 cm of styrofoam on the bottom and sides and 30.5 cm of polyurethane on the tank cover, as shown in Figure 2.3.

Figure 2.5 compares the thermal behavior of the storage tank with the overall heating system and enclosure during a 24-hour period on a clear-sky day. Specifically, the outdoor air, room air, storage tank, and collector-outlet temperatures have been plotted. The room air temperature is the average air temperature in the living room, which is located in the center of the house as shown in Figure 2.1. The temperature of the storage tank is from the middle thermocouple in the tank. The vertical array of five thermocouples in the storage tank verified that the tank was well mixed (i.e., not stratified) when the pump was supplying hot water to the solar-to-radiant heat exchanger.

Figure 2.6 shows the same plot for a 24-hour period of overcast conditions. The collector outlet temperature is not shown on the overcast plot or after daylight hours on the clear-day plot, since the collector was not providing useful energy at these times. The outdoor temperatures were about the same for both the clear-sky day and the overcast day, as can be seen in Figures 2.5 and 2.6. The obvious difference between the two plots is that the temperature of the storage tank decreased significantly after several cloudy days. On the clear-

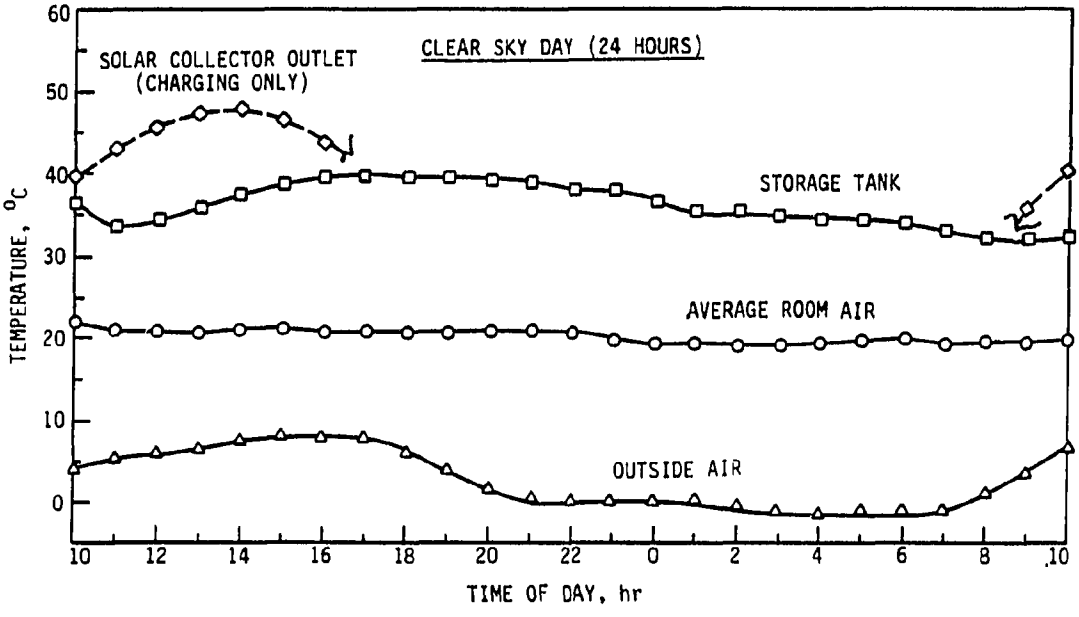

FIGURE 2.5. System temperature fluctuations on a clear-sky day

sky day, the storage tank was about 15°C warmer than the room temperature, while on overcast days the difference decreased to about 3°C. In addition, Figure 2.5 shows the storage tank charging when the collector outlet temperature is greater than the storage tank temperature. The discharging of the storage tank can also be observed during those periods when the collectors are not providing useful energy.

The heat loss from the storage tank was estimated as the first step in evaluating the thermal performance of the tank. Determining

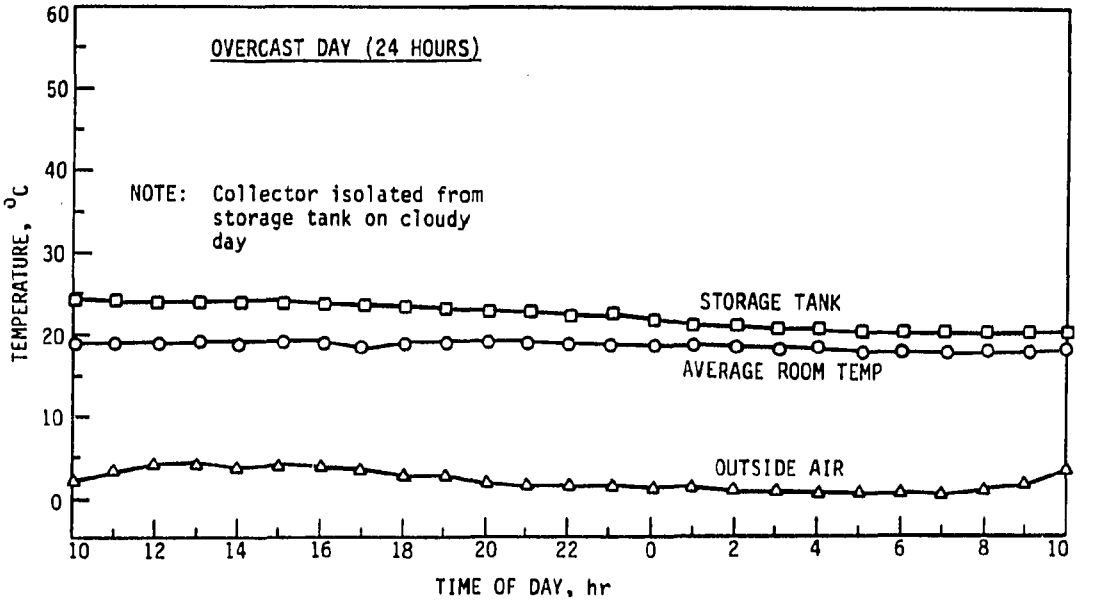

FIGURE 2.6. System temperature fluctuations on a cloudy day

this heat loss required measuring the mean tank temperature. When the radiant system was operational, temperatures were observed to be uniform throughout the tank because of disturbances caused by pumping water to and from the tank. In contrast, when the tank was in a solar charging mode only, considerable thermal stratification in the range of 20°C was observed, as shown in Figure 2.7. Additional data showed that water temperatures on the same horizontal level were fairly uniform, differing by less than 2°C. This one-dimensional behavior was observed even though the storage tank has three dimensions (i.e., 1.6 m X 1.5 m

X 2.4 m) that are of the same order of magnitude. The mean storage tank temperature during stratification was thus calculated as follows:

$$T_t = \frac{1}{h}\int_0^h T(y)\,dy \cong \frac{1}{N}\sum_{n=1}^{N} T_n \qquad (2.5)$$

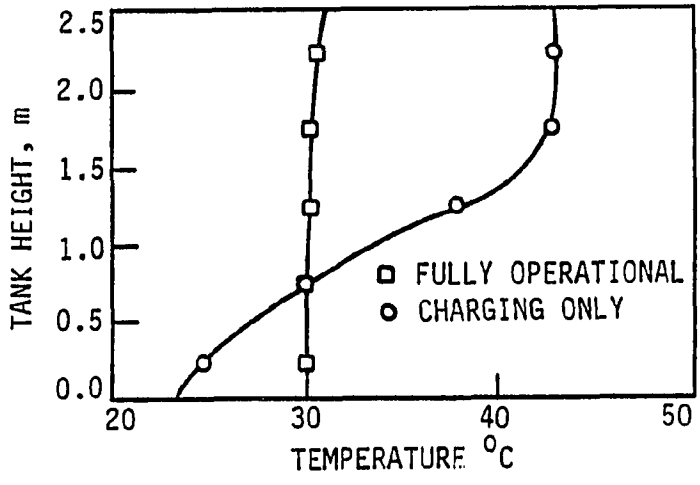

FIGURE 2.7. Thermal stratification in the storage tank

The following equation along with experimental data was used to estimate the tank heat loss over a time period t_1 to t_2:

$$Q_l = MC(T_{t1} - T_{t2}) + Q_u - Q_e \qquad (2.6)$$

The energy extracted from the tank, Q_e, was calculated as follows:

$$Q_e = \int_{t_1}^{t_2} (\dot{m}c)_t (T_1 - T_4)dt \qquad (2.7)$$

where T_1 and T_4 are the supply and return temperatures of the line connecting the storage tank to the solar-to-radiant heat exchanger (see Figure 2.1). A heat loss from the tank of 1.8×10^3 kJ/hr was measured for the following operating conditions:

- fully operational, stratification negligible
- outdoor temperature, -5 to 5°C
- tank mean temperature, 27.5°C
- room temperature, 20°C.

These operating conditions are representative of those conditions that were used in evaluating the collector efficiency. The daily heat loss for the storage tank is estimated at 0.43×10^5 kJ/day.

A wide range of experiments using Eq. (2.6) indicated that the heat loss from the tank, Q_1, depended on four factors: room temperature, tank mean temperature, degree of tank stratification, and outdoor temperature. Of these four, the tank mean temperature was observed to be the dominant factor affecting the tank loss. For example, for an increase in tank mean temperature from 27.5 to 40°C, the tank heat loss rate increased from 1.8×10^3 to 3.8×10^3 kJ/hr, resulting in a 24-hour loss as high as 0.9×10^5 kJ. Therefore, almost two-thirds of the average daily solar gain would be lost if the storage tank temperature had to be maintained at this high level. In contrast, the outdoor temperature is the least important of the above factors because there is no direct thermal contact between the tank and the outside air.

It is well known that stratification improves the performance of solar systems. Not only does it increase the collector efficiency by reducing the collector inlet temperature, but it also minimizes the tank loss by lowering the temperature at the bottom of the tank. Unfortunately, no perceivable stratification was observed in the tank when the radiant system was operating, as previously discussed. Therefore, high temperature operations are impractical for this system.

Solar-To-Radiant Heat Exchanger

The radiant flow loop receives energy from the storage tank via a shell and tube type heat exchanger as shown in Figure 2.1. Except for small amounts of energy lost from piping systems, the energy received by the radiant flow loop serves to warm the occupied spaces.

Figure 2.8 shows water temperatures entering and leaving the storage tank and the solar-to-radiant heat exchanger during a clear-sky day. Charging of the storage tank during daylight hours can be observed along with discharging at night. The heat lost from the supply and return pipes connecting the storage tank to the heat exchanger is not shown, but it can be significant since the heat exchanger is located in the mechanical room, which is some distance from the storage tank location. Even so, this heat loss is useful energy gain to the heated spaces. The total net heat removed from the storage tank is bounded by the storage tank inlet (T_4) and outlet (T_1) temperature curves in Figure 2.8.

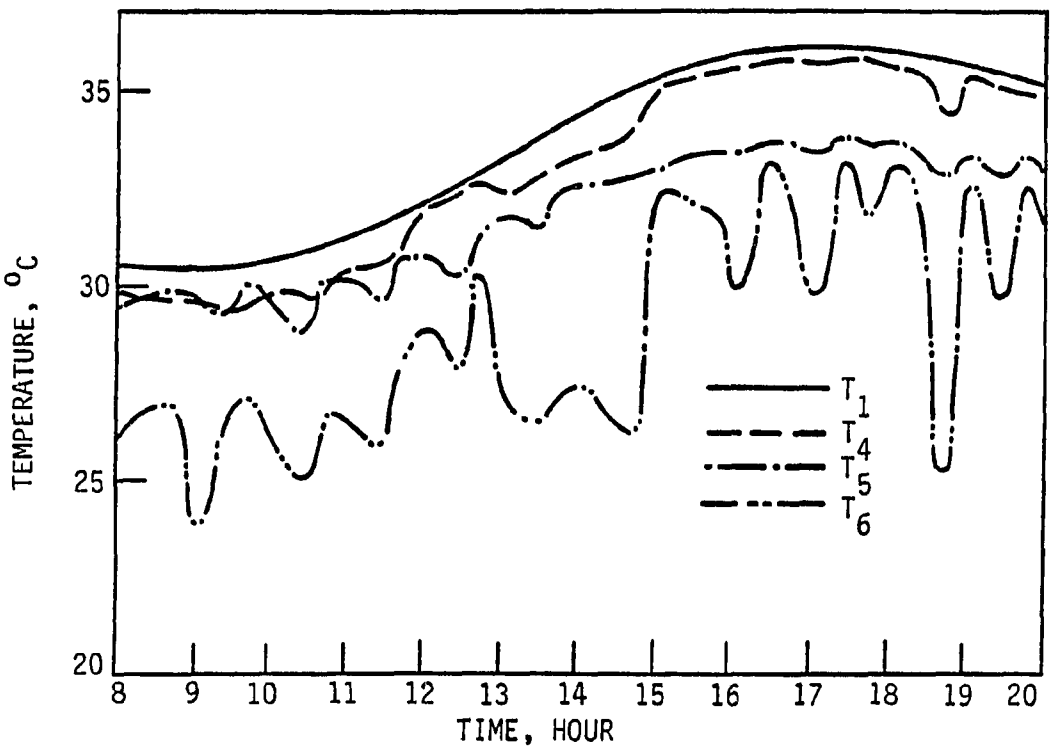

FIGURE 2.8. Solar-to-radiant temperature fluctuations on a clear-sky day

The temperature fluctuations on both sides of the heat exchanger are caused by the controls on the radiant heating system. When no heat is required (i.e., all motorized valves are shut), the circulating pump for the radiant ceiling is off. With this pump turned off, the water from the storage tank loses very little energy as it passes through the solar-radiant heat exchanger. At these times, the outlet temperature

is approximately equal to the inlet temperature. In contrast, when the pump is on, energy is extracted from the storage tank loop, as shown by the sharp drop in the temperature of the water leaving the heat exchanger and reentering the storage tank. The well-mixed storage tank shows no fluctuations but rather a steady increase in temperature as energy is added to the tank from the solar collectors. The temperature of the water leaving the heat exchanger on the radiant side is only meaningful when the pump is on, but in general this temperature increases as the storage tank temperature increases.

Figure 2.9 shows the storage tank and heat exchanger temperatures during the overcast day. The temperatures are much closer to room temperature than during the clear-sky day, since the storage tank has been discharged considerably during the third consecutive cloudy day. A steady decline is seen in all temperatures, and there appears to be no fluctuations from the control system, because the radiant system is operating continuously at maximum capacity. In fact, the temperature of the room air is decreasing slightly (see Figure 2.6), suggesting that the storage tank charge is not high enough to make up for all of the heat losses from the envelope.

The energy transferred to the radiant ceiling from the heat exchanger can be calculated as:

$$Q_h = \int_{t_1}^{t_2} (\dot{m}c)_r (T_6 - T_5) dt \qquad (2.8)$$

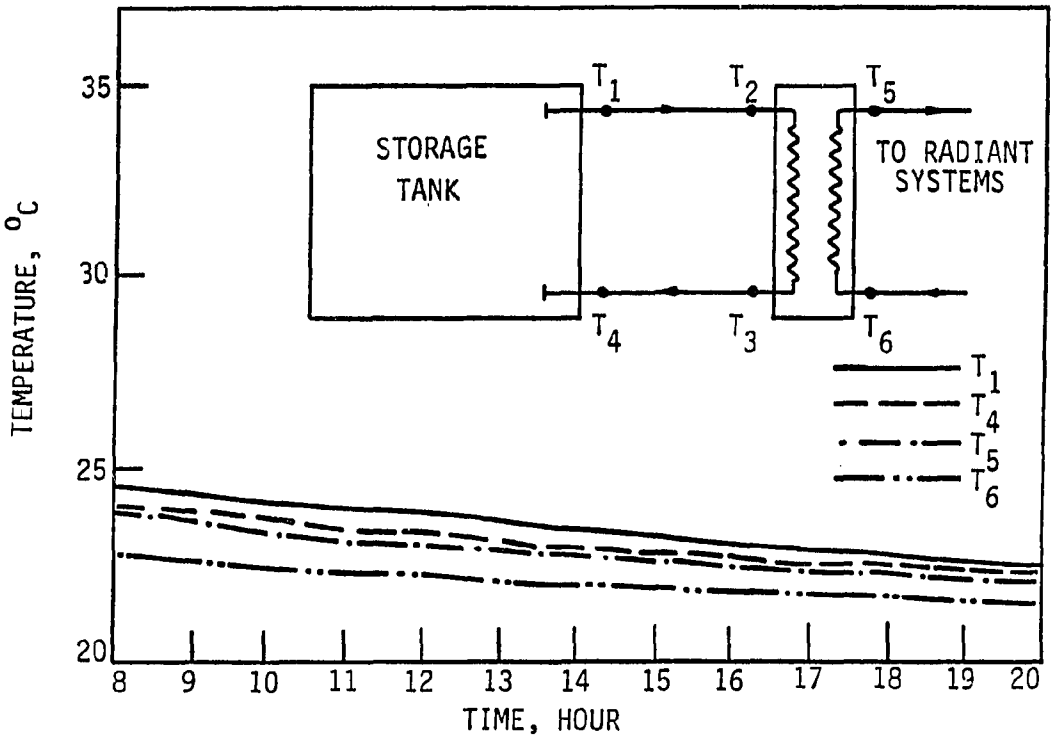

FIGURE 2.9. Solar-to-radiant temperature fluctuations on a cloudy day

where T_5 and T_6 are shown in Figures 2.8 and 2.9. This energy was calculated to be 1.43 X 10^5 kJ/day for the cloudy day. The total energy supplied to the solar-to-radiant heat exchanger from the storage tank (i.e., Q_e) for the cloudy day was calculated to be 1.7 X 10^5 kJ/day using Eq. (2.7). Since the pump work is negligible, the solar-to-radiant heat exchanger, including the pipeline, is seen to operate at an efficiency of 84%. In other words, of 100 kJ energy extracted

from the storage tank, 84 kJ was utilized by the radiant system for heating, and the rest was lost from the pipeline and heat exchanger shell. However, even this heat loss contributed to heating the residence since the piping and heat exchangers are located inside the residence. Additional experiments also resulted in an approximate efficiency of 85% for the heat exchanger and piping.

In contrast to the cloudy day, the efficiency of the heat exchanger was more difficult to evaluate on clear-sky days because of its much more dynamic behavior (as seen in Figure 2.8). Nevertheless, the efficiency of the solar-to-radiant heat exchanger was observed to remain relatively constant at approximately 85% for water temperatures less than 35°C. Based on this estimate, the monthly average energy finally supplied to the radiant system is around 0.78×10^5 kJ/day when an appropriate cloud cover factor for this location is taken into consideration.

Radiant Ceiling and Enclosure

Radiant ceiling and room air temperatures were measured throughout the house. These temperatures provided an indication of the dynamic behavior of the radiant heating system and envelope as they interact with the solar system. The living room, located on the middle level adjacent to the greenhouse, was selected as an appropriate space for a detailed analysis of the dynamic behavior of an enclosure.

Two sets of outdoor conditions were used to study the radiant ceiling and enclosure response. These conditions are the same as those used in earlier sections of this Chapter, namely, a clear-sky day and an overcast day. As previously noted, the overcast day is the third consecutive cloudy day, which resulted in a significant lowering of storage-tank temperatures.

Figures 2.10 and 2.11 show the temperature response for the living room during the clear-sky day and the overcast day, respectively. Because the temperature of the storage tank has been lowered by the third consecutive overcast day, the room air temperature in Figure 2.11 shows a slight but continuous decrease. This decrease indicates that the storage system cannot provide adequate heat to the radiant system. However, the air temperature only decreased 1.5°C in 24 hours, thus remaining within the comfort range. In contrast, the room air temperature for the clear sky day in Figure 2.10 shows that the solar collector and storage tank system are capable of supplying adequate energy to the radiant heating system. The 2°C swing in room air temperature is within the normal operating range of a typical residential system. Interestingly, the period of the temperature swing is much larger than in a typical forced-air system and, in fact, follows solar irradiation.

The temperature difference between the ceiling and wall, as shown in Figures 2.10 and 2.11, is a rough indicator of the heat transfer from the heating system. The overcast day with its steadily decreasing

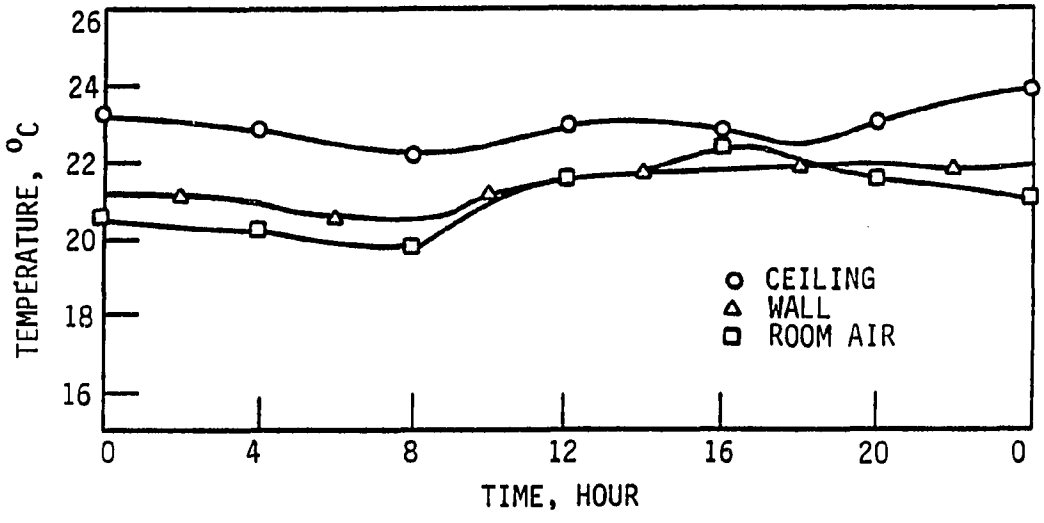

FIGURE 2.10. Living room temperature responses during a clear-sky day

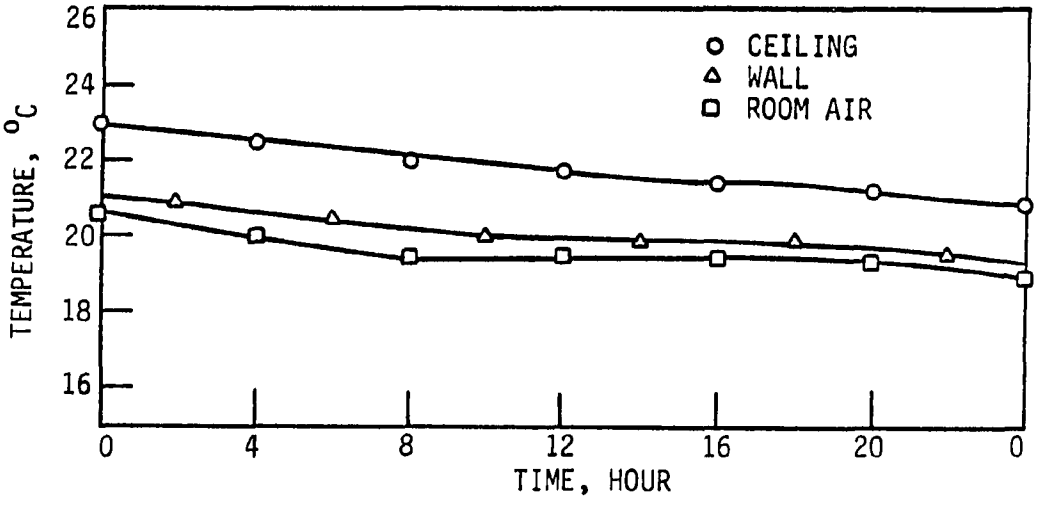

FIGURE 2.11. Living room temperature responses during a cloudy day

storage tank temperature shows that heat transfer to the room is approximately constant over the 24-hour period. This behavior is consistent with the fact that solar irradiation has little effect on envelope heat losses during an overcast period. In contrast, the clear-sky day case in Figure 2.10 shows considerable variation in heat transfer from the ceiling over the 24-hour period. This dynamic behavior is due to the control system used to supply hot water to the tubes in the ceiling, as well as to changes in the storage tank temperature caused by charging during the day and discharging at night. Another important factor, though, is that envelope heat losses decrease considerably during daylight hours. Uncontrollable heat additions also occur from the adjacent greenhouse (see Figure 2.1) and from natural convection from the lower levels of the house through the open stairwell. The nighttime behavior of the living room shows that periods of maximum heat transfer from the ceiling and maximum envelope losses coincide.

Additional insight into the dynamic behavior of the radiant ceiling and enclosure can be gained by comparing the wall and room air temperatures. Since the wall temperature is generally greater than the room air temperature, the room air is thus heated by the radiant ceiling via radiation to the wall. An exception, though, occurs during a short period in the afternoon on a typical sunny day as shown in Figure 2.10. At this time the room air temperature exceeds the wall temperature, either because of solar heating of the envelope or convection flow changes in the space or adjacent spaces.

A thermal performance evaluation of the radiant ceiling and enclosure must take into account the fact that the mechanism for transferring heat from the radiant flow loop to the air is a combination of radiation heat transfer between a highly emissive ceiling and other surfaces in the enclosure (floor and walls) and convective heat transfer between all surfaces and the air.

The radiant energy transferred from the ceiling to the enclosure can be approximated by a simple radiation heat transfer model (Holman 1981):

$$Q = \frac{\sigma(T_1^4 - T_2^4)}{\frac{1-\epsilon_1}{A_1\epsilon_1} + \left\{A_1F_{12} + \left(\frac{1}{A_1F_{13}} + \frac{1}{A_2F_{23}}\right)^{-1}\right\}^{-1} + \frac{1-\epsilon_2}{A_2\epsilon_2}} \qquad (2.9)$$

where the subscript 1 denotes the ceiling, 2 the internal surface of the wall, and 3 the floor. This model treats the carpet-covered floor as an adiabatic surface and the other surfaces as isothermal. Because the walls in the living room are not homogeneous, this model is considered an approximation only. The energy transferred to all spaces in the house was estimated as 0.95×10^5 kJ/day.

The energy transferred directly to the air from the ceiling by convection can be approximated using an equation given in Jennings (1978) as follows:

$$q = 0.3328(T_s - T_r)^{1.25} \qquad (2.10)$$

where q is in W/m^2 and T in °C. It should be noted that Eq. (2.10) could possibly overestimate the convection heat transfer, as equations in other references (ASHRAE 1987) result in considerably lower heat transfer coefficients for heated ceilings. Applying Eq. (2.10) directly, the convective heat transfer for all of the ceilings in the house is about 0.46×10^5 kJ/day. Comparing this value to the total energy supplied by the solar-to-radiant heat exchanger (i.e., 1.43×10^5 kJ/day), the convection was approximately 33% of the total energy transferred and the radiation about 66%.

The fact that the energy balance on the radiant system agrees as well as it does (i.e., 66% for radiation, 33% for convection, only 1% unaccounted) must be considered coincidental, because these calculations contain inaccuracies due to experimental uncertainties, and Eqs. (2.9) and (2.10) are only rough approximations of the phenomena in this study. In addition, heat losses to the outside through the ceiling were not considered. Although the roof of the house is well insulated with an experimentally determined U value of 0.16 $W/(m^2°C)$, which is a very low value, the conduction loss is still likely to be much greater than 1%.

Overall System Performance

The component studies can be combined into a performance evaluation for the complete solar-radiant heating system. Figure 2.12 is an energy flow chart for the overall solar-radiant heating system.

Using 100% to represent the daily solar energy incident on the collector, approximately 60% of this energy is lost to the atmosphere from the collector and connecting pipes. The remaining 40% is transferred to the storage tank as useful energy, Q_u. Part of the useful energy is lost to the surrounding earth by heat conduction through the walls of the tank, while part is transferred through the tank cover to the greenhouse area. The overall storage tank loss is 14%, and the energy extracted from the storage tank, Q_e, is thus 26%. Approximately 3% is lost from the heat exchanger jacket and connecting pipes. Although this piping loss and the loss through the tank cover eventually contribute to heating the residence, they are classified as uncontrollable heating energy because they cannot be distributed in a controlled manner throughout the occupied spaces.

The energy received by the radiant loop from the heat exchanger, Q_h, is thus 23% of the solar insolation. This represents the net energy usable by the hydronic radiant heating system. Of this energy, a very small percentage is lost through the roof to the atmosphere, while another small amount is lost from the insulated pipeline that connects the heat exchanger to the radiant coil. Of the energy transferred from the ceiling to the enclosure, 15.5% is by radiation heat transfer and 7.5% is by convection heat transfer. The difference between the house heating load and the energy supplied by the solar-radiant heating system can be met by auxiliary energy, Q_a. It is important to note that the percentages shown in Figure 2.12 are only approximations due to reasons discussed previously.

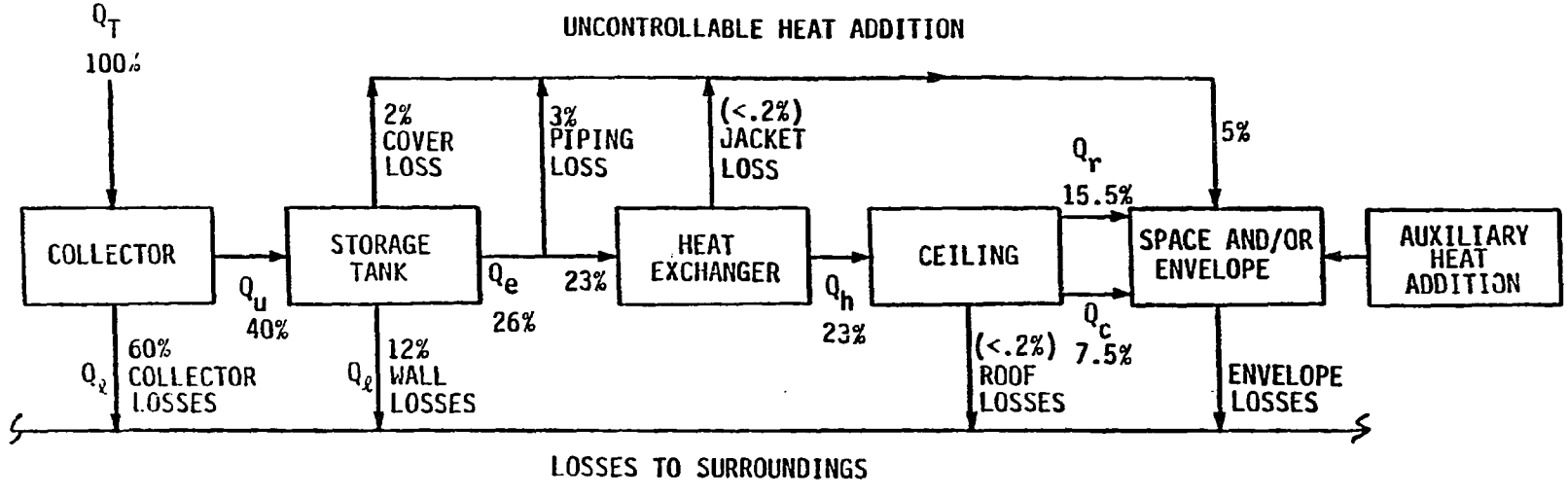

FIGURE 2.12. Energy flow chart of solar-radiant heating system

Figure 2.13 is a bar chart that provides a quantitative view of the complete system. The values are for monthly averaged daily quantities. As noted from the last section, during a typical March day when the average outdoor temperature was 2.1°C, about 1.70 X 10^5 kJ/day energy was extracted from the storage tank and approximately 1.43 X 10^5 kJ/day was supplied to the radiant system to maintain the house at a comfortable 19.6°C. Assuming the average outdoor temperature for March as 0°C, the energy requirement for this house is approximately 1.5 X 10^5 kJ/day. Since the average solar energy supplied by the system is approximately 0.77 X 10^5 kJ/day, the solar-radiant system can provide approximately 50% of the heating energy requirement.

An interesting observation from this experiment is that the house was maintained in the comfort zone using water at a temperature only slightly above the room air. Specifically, the temperatures of the hot water running through the radiant coils ranged from 24°C to 30°C, while the room air temperatures were in the 20 to 21°C range. Thus, low-temperature radiant heating is feasible for a well-insulated house and mild winter seasons.

Although these experiments did not cover the entire winter season, the preceding system analysis can be used to predict the performance of the system for additional winter months.

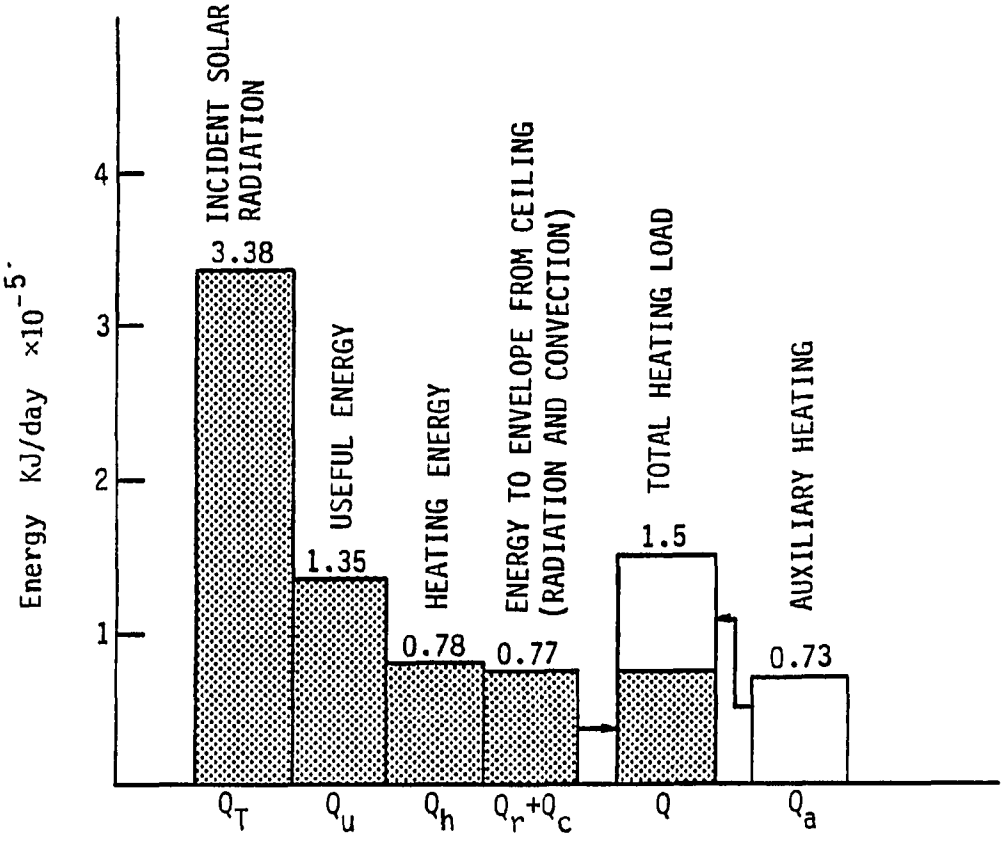

FIGURE 2.13. Energy bar chart of solar-radiant heating system

Conclusion

The dynamic behavior and the thermal performance of a solar collector-radiant heating system installed at the ISU Energy Research House was analyzed for both a clear-sky day and an overcast day. Significant insight into the operation and performance of this system

was obtained by observing transient temperatures throughout the system. Of special importance is the fact that the house was heated from the solar storage tank, even though the storage tank temperatures were only slightly higher than the room temperatures. On the clear-sky day the storage tank temperature was generally about 15°C warmer than the room temperature, and the system operated satisfactorily using only periodic operation of the radiant heating system. In contrast, the temperature difference decreased to 3°C after three consecutive cloudy days, and continuous operation of the radiant heating system was required to maintain the room temperature in the comfort zone.

The dynamic interaction between the radiant ceiling and room was also different for the overcast day and the clear-sky day. The temperature at the radiant ceiling remained a constant 2°C different from the room air temperature over the 24-hour period during the overcast day. In contrast, the temperature differences for the clear-sky day varied from a minimum of 0°C to a maximum of 3°C over a 24-hour period.

An evaluation of the thermal performance of each component showed that the flat-plate collector had an efficiency of 40% in a mild winter month and that the storage tank heat loss is significant when the tank mean temperature reaches 35°C and above. A performance evaluation of the solar-to-radiant heat exchanger showed that about 85% of useful solar energy can be provided for radiant heat via a solar-to-radiant heat exchanger. It was estimated that radiation constitutes about two-

thirds and convection about one-third of the energy transferred to the enclosure from the ceiling panel. t was also estimated that 50% of the house heating load can be supplied by solar energy using a radiant heating system during mild winter months (assuming 0°C outdoor temperature). The final conclusion is that despite the low temperature of the energy source, the combined systems worked well in providing space heating.

CHAPTER 3 AN EXPERIMENTAL STUDY OF THE TRANSIENT RESPONSE OF A RADIANT PANEL CEILING AND ENCLOSURE

Introduction

Although many studies in radiant heating field have been done in the past 40 years, few papers have studied the transient thermal response of a combined enclosure and radiant-panel heating system. A study of this type is important for designing energy-efficient radiant heating systems and for implementing computer-aided control systems.

This Chapter reports the results of transient experiments performed on a radiant heating system and enclosure. These experiments consisted of supplying water at different temperatures and flow rates to the radiant ceiling and then monitoring the thermal response of the ceiling and enclosure for a period of several hours. An analysis of the results provided insight into the transient behavior of a radiant ceiling and enclosure.

Experimental Facilities

Enclosure and radiant-panel ceiling

The experiments in this study were performed at the Energy Research House from November 1984 to February 1985. The master bedroom, located on the top floor in the northwest corner, was isolated and used as a testing enclosure. The enclosure consists of a radiant

ceiling, a carpet-covered floor, and four walls. The four walls, originally designed for envelope testing purposes, have different compositions and, thus, different thermal resistances. The west wall, with an average thermal resistance of 3.5 $m^2°C/W$ (20 $h·ft^2·F/Btu$), is the only wall that is adjacent to the outside. The north wall is separated from the outside by a closet area and window. The south wall is adjacent to one of the other bedrooms. The east wall parallels the hallway. All of the rooms in the house, except the master bedroom, were maintained at a temperature of approximately 15.5°C (60F) by using a forced-air system and an electrical furnace.

The radiant panel essentially consists of a standard plaster ceiling in which copper tubes have been embedded as shown in Figure 3.1. The 0.95 cm (3/8-in.) copper tubes are arranged at 15.2 cm (6-in.) intervals, and the supply-return lines run parallel and counterflow to each other as shown in Figure 3.2. This particular pattern was used to achieve a high ceiling temperature uniformity.

Radiant heating mechanical systems

The Research House has several options for heating the water supply for the radiant system. These options include solar collectors with energy storage in a water storage tank, a heat pump, an in-line electrical heater, and a standard domestic hot-water heater that can be directly mounted in the radiant flow loop. The last option was used in this study because the hot-water heater provided the best method of

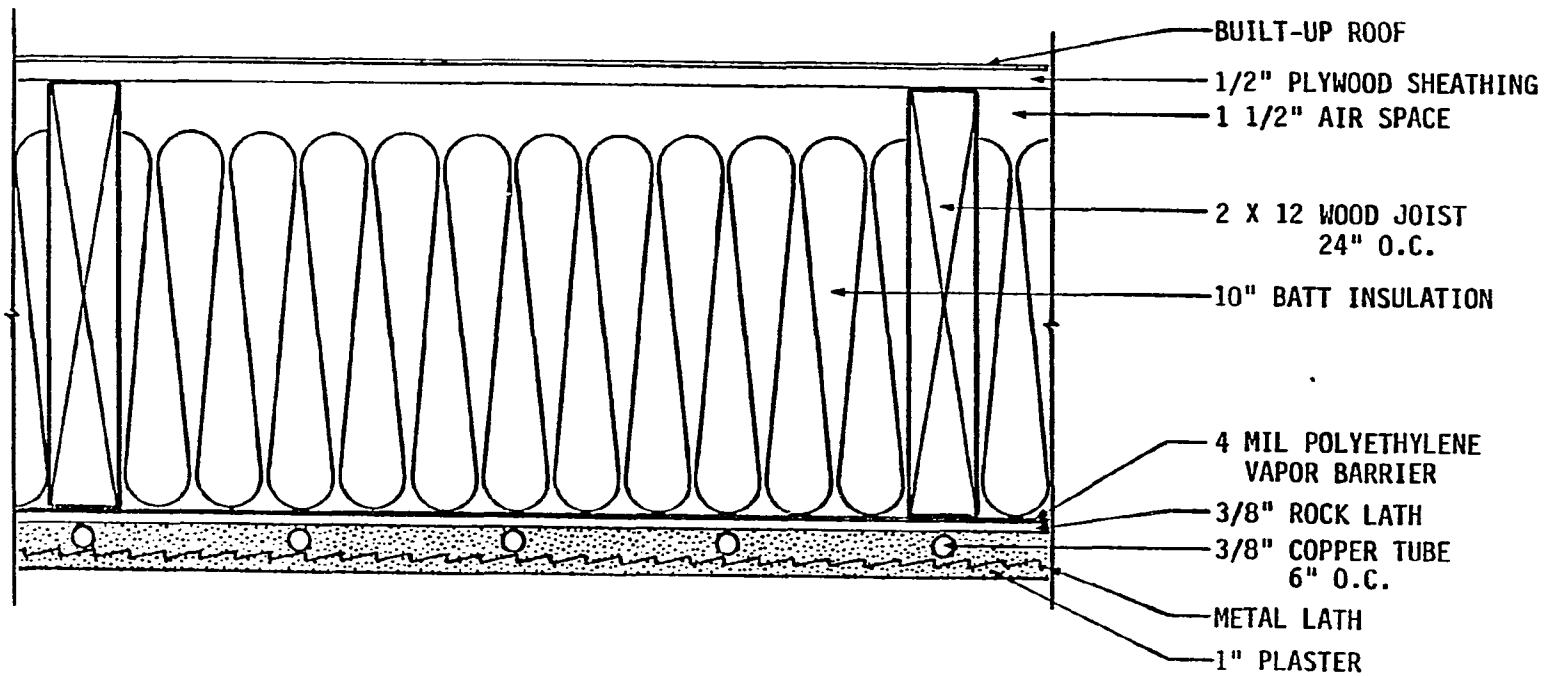

FIGURE 3.1. Cross-sectional view of radiant panel ceiling

controlling supply temperatures during transient testing. Figure 3.3 is a schematic of the radiant heating mechanical system as installed in the test house.

Instrumentation

Temperatures in the enclosure, such as the ceiling surface, wall surface, and room air, were measured by using copper-constantan thermocouples. Thermocouples were attached to the surfaces by running the leads along the surface for approximately 10.2 cm (4 in.) in order to minimize thermocouple errors associated with lead losses. The radiant ceiling temperature was measured in detail by installing a thermocouple every 7.6 cm (3 in.) across the middle of the ceiling. Thermocouples were attached to the surface of the ceiling plaster directly underneath each embedded tube path. Tubes buried in the plaster were located by using an infrared camera. The room air temperature distribution was measured by using thermocouples installed approximately 61 cm (2 ft) from each wall at a distance of 46 cm (1.5 ft) and 152 cm (5.0 ft) from the ceiling. These measurements were used to observe vertical temperature stratifications. Wall surface temperatures were measured at points directly adjacent to thermocouples mounted in the air. The temperatures of the supply and return water were measured by attaching thermocouples to the exposed copper tube surface and then covering the tube with a layer of insulation. Two outdoor temperatures were recorded: one on the flat roof and the other on the north window.

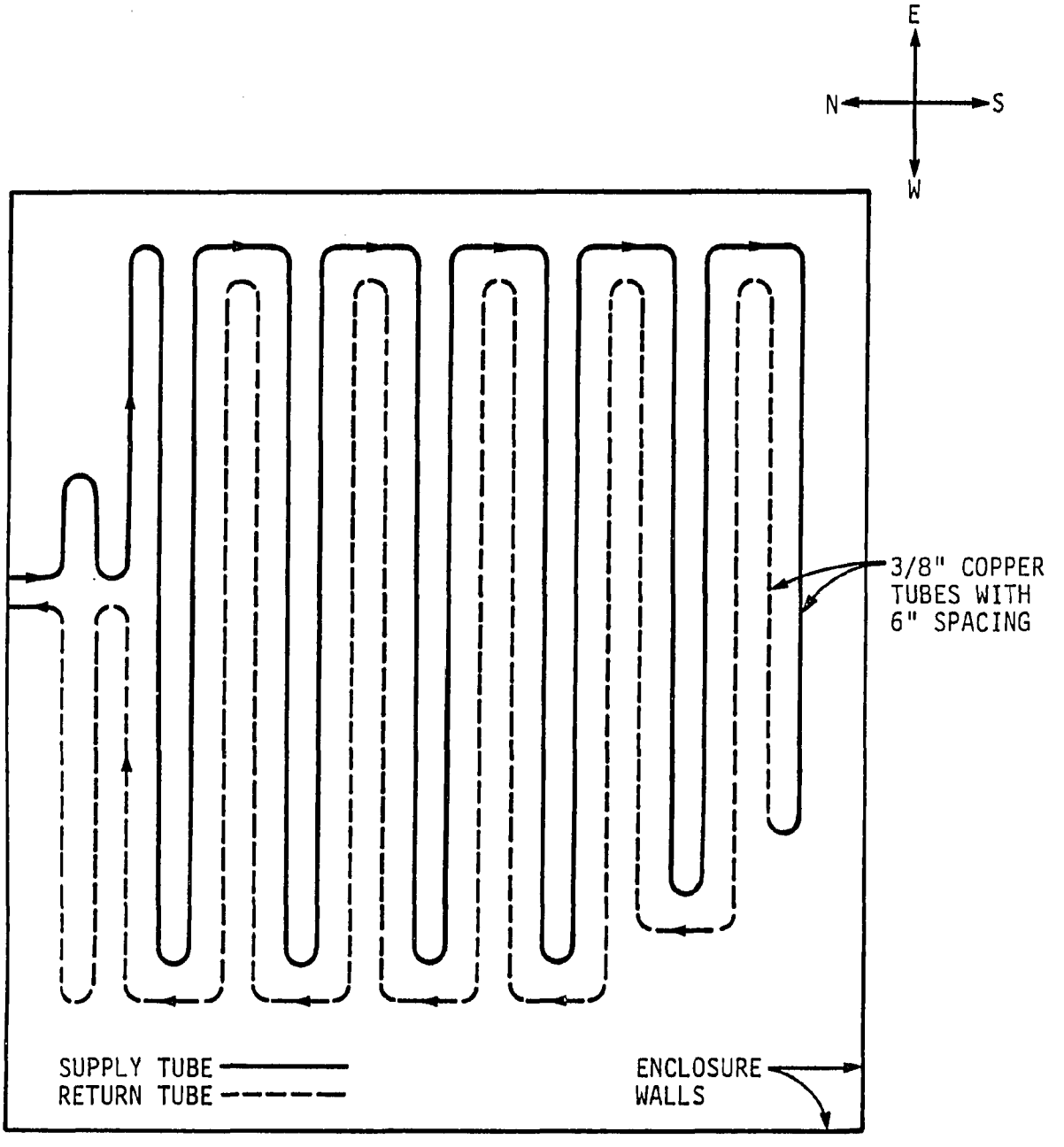

FIGURE 3.2. Copper tube pattern in radiant ceiling, a plane view

Water flow rate was measured by a strain-gage type flow-meter with a gage bridge adapter. The same data logger as in the previous study was used to record temperatures and mass flow rates. Each thermocouple was connected to an isothermal reference junction provided by the data logger. In addition, thermocouples were taken from the same wire roll from which samples were periodically checked for accuracy. Experimental uncertainties for temperature measurements were estimated to be ±0.2°C (0.4F). Experimental uncertainties for mass flow rates were ±0.2 l/m (0.05 gpm).

Experimental Test Description

The thermal responses of the ceiling, the walls, and the room air were observed by recording thermocouple readings at an intervals of 15 minutes. The major independent variables during any given test were (1) temperature of the supply water, (2) water mass flow rate, (3) outdoor temperature and other weather conditions, and (4) initial room and wall temperatures. Of these four variables, only the outdoor temperature could not be controlled. The temperature of the supply water was set by adjusting the thermostat in the water heater while the flow rate was set by controlling a throttle valve. The initial temperatures of the enclosure were eliminated as independent variables by referencing temperature transients to the initial temperature so as to form a scaled radiant-panel temperature as follows:

$$\bar{T} = T - T_0 \tag{3.1}$$

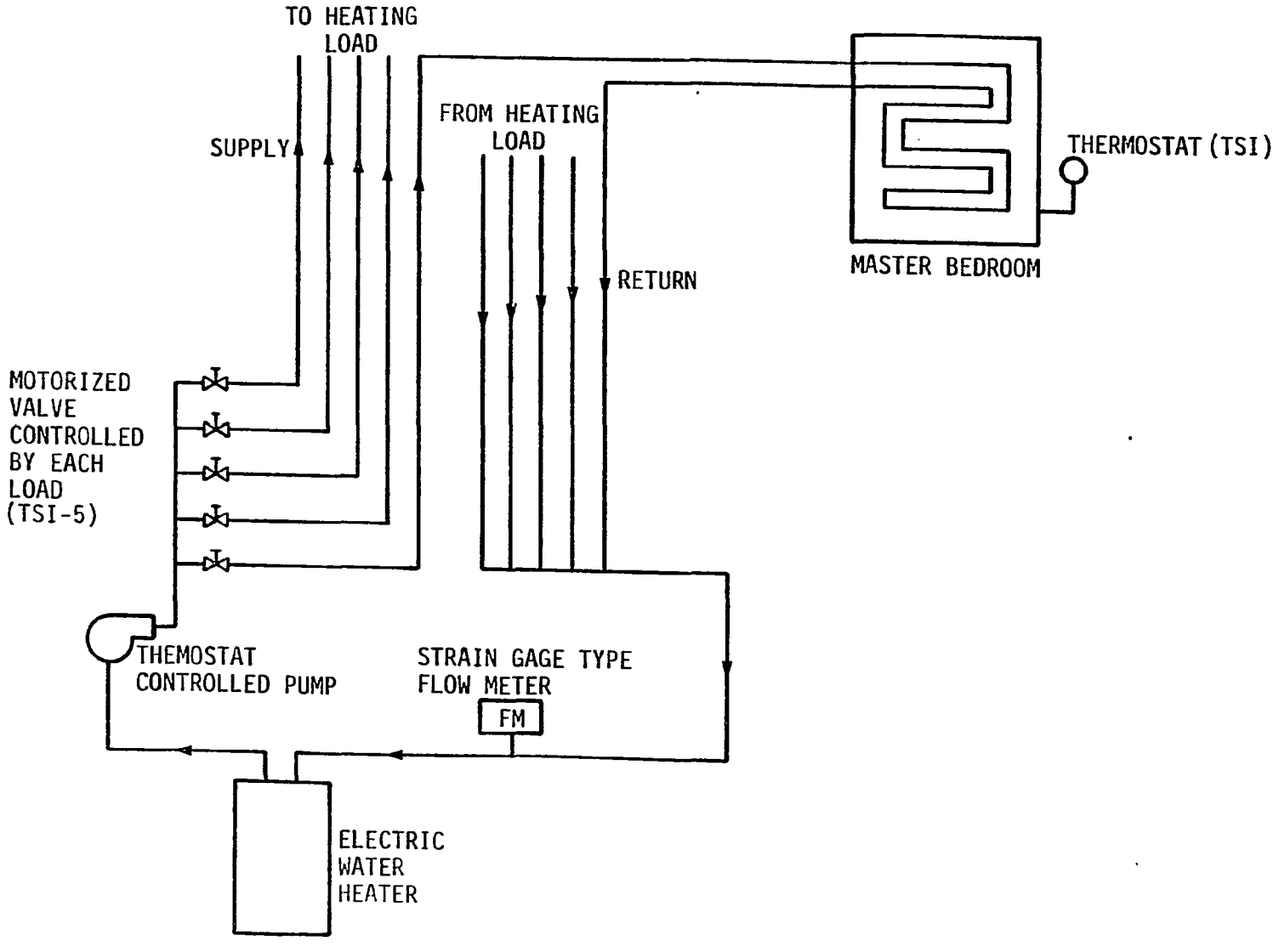

FIGURE 3.3. Schematic of radiant heating mechanical system

For a given temperature and mass flow rate, each test lasted approximately seven to nine hours. The thermal response pattern manifested itself only after this time duration. During experiments performed at higher temperatures and higher flow rates, the supply temperature was sometimes unstable because of the limited capacity of the heater. Even so, the heat capacity of the plaster ceiling tended to buffer these fluctuations.

Results and Discussion

Ceiling temperature distribution

Figure 3.4 is a plot of ceiling temperatures measured every 7.6 cm (3 in.) across the center of the room and perpendicular to the tubing path. The data scatter in Figure 3.4 is a combinations of measurement uncertainty and, to greater extent, actual temperature variations in the ceiling. These variations are mainly caused by the variations of the plaster cover thickness and the distribution of the metal lath inside the ceiling panel.

Figure 3.4 shows that the surface of the ceiling directly below the tubes is consistently warmer than the surface between the tubes. This temperature difference varies with time and, to a lesser extent, with location for those reasons discussed in the previous paragraph. The variation of ceiling temperatures with location can be represented by a parameter S, which is the area enveloped by the two imaginary

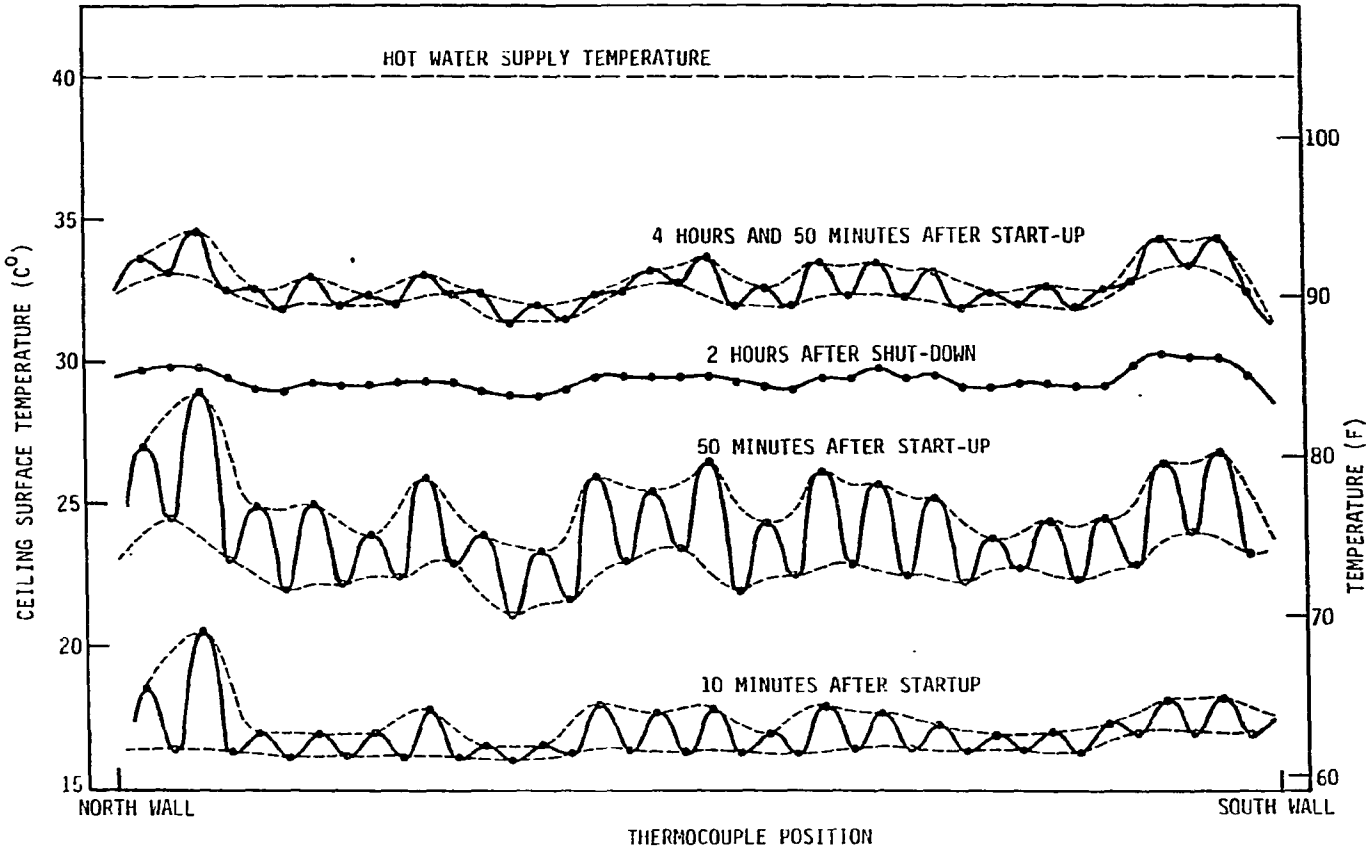

FIGURE 3.4. Surface temperatures across middle of ceiling, perpendicular to tubing path

temperature curves shown in Figure 3.4. Parameter S increases as the ceiling and room warm up and then decreases as steady state is approached. The reason for this behavior may be that during heat-up it takes time for heat to diffuse to the space between the tubes and during steady state, when the tube region is no longer being heated, the temperature of the center region finally catches up. Figure 3.4 also shows parameter S going to zero two hours after the radiant system is shut off. This results in a more uniform ceiling temperature.

In terms of average temperature differences between the peaks (i.e., tube regions) and valleys (i.e., regions between tubes) shown in Figure 3.4, the temperature differences vary from a maximum of approximately 2.5°C (4.5F) after one hour of operation to a minimum of zero after shut-off. The steady-state temperature difference is probably less than the 1°C (1.8F) shown for the four-hour, 50-minute heating period.

Figure 3.4 shows the overall change in ceiling temperature after the radiant heating system is started. It appears to take about one hour to heat the ceiling the first 8°C (14F) and then another four hours to heat the ceiling another 8°C (14F). The net result is that it takes about five hours to heat the ceiling 16°C (29F). This was accomplished with a hot-water supply temperature of 40°C (104F). The temperature difference between the hot-water supply and the 33°C (91F) ceiling is about 7°C (13F).

Transient response of ceiling panel

An investigation of the transient ceiling temperature for a variety of conditions provides additional insight into the thermal response of the ceiling. A scaled radiant-panel temperature defined by Eq. (3.1) was used to eliminate initial temperature as an independent variable. Figure 3.5 compares transient response curves for three different water supply temperatures at a constant flow rate. In contrast, Figure 3.6 compares transient response curves for two different water flow rates at a constant supply temperature.

Figure 3.5 shows that the ceiling can be heated faster by using a higher water temperature in the radiant system. For example, the ceiling temperature can be increased by 18°C (32F) in 1.5 hours by using 55°C (131F) water, but it takes at least twice that long to heat the ceiling to the same temperature using 42°C (108F) water. This observation suggests that varying the supply water temperature may be an appropriate method of controlling room air temperature in a radiant heating system that has considerable thermal mass storage. This approach would be especially appropriate when night set-back is used and rapid heating of the room is required just prior to occupancy.

While the thermal response appears to be dependent on water supply temperature, it shows little dependence on the water flow rate. In fact, the differences shown in Figure 3.6 are probably caused by variations in outdoor temperature, since the lower flow rate raises the ceiling temperature even faster than the higher flow rate, which has a

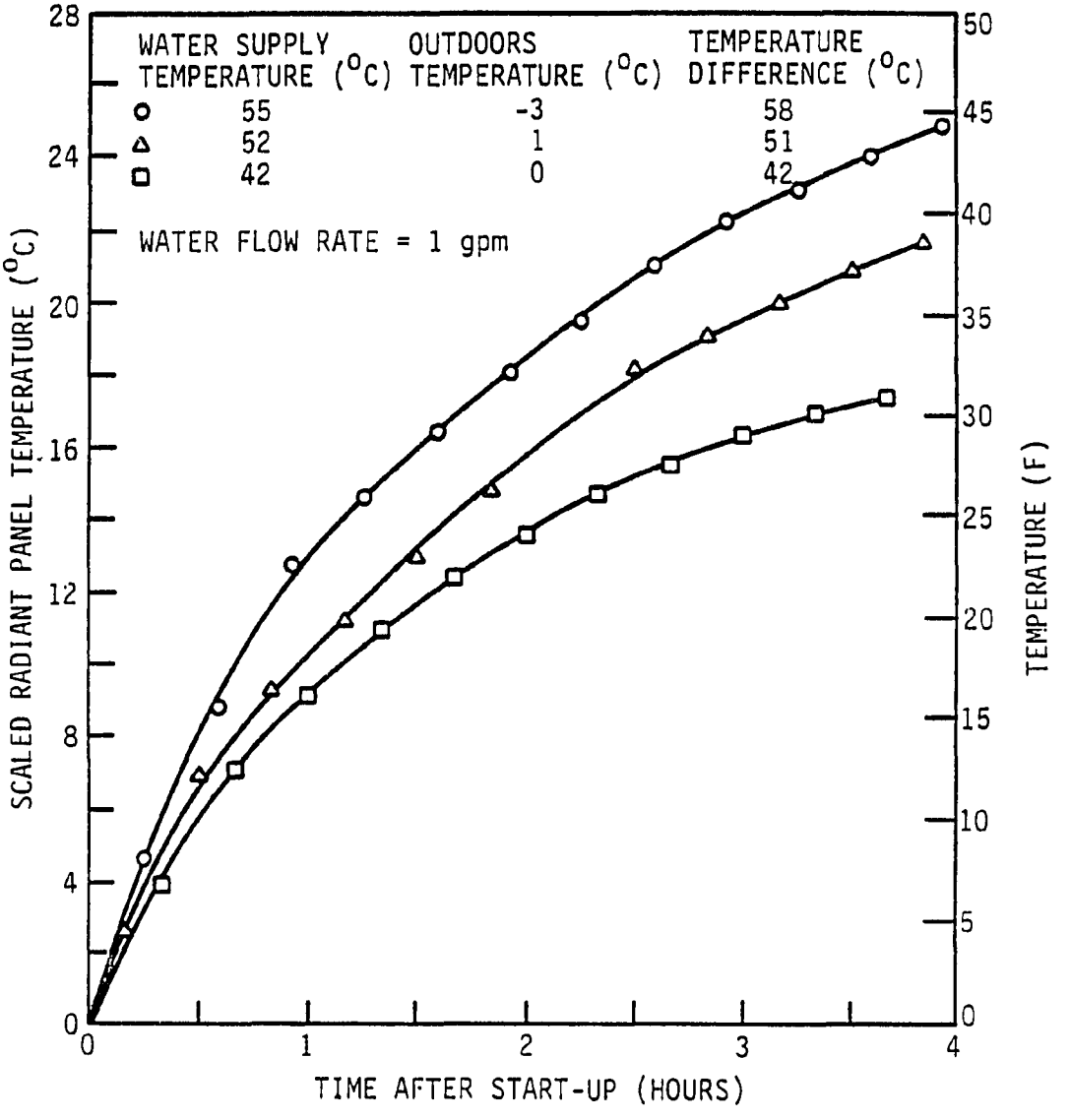

FIGURE 3.5. Thermal response of radiant ceiling for different water supply temperatures

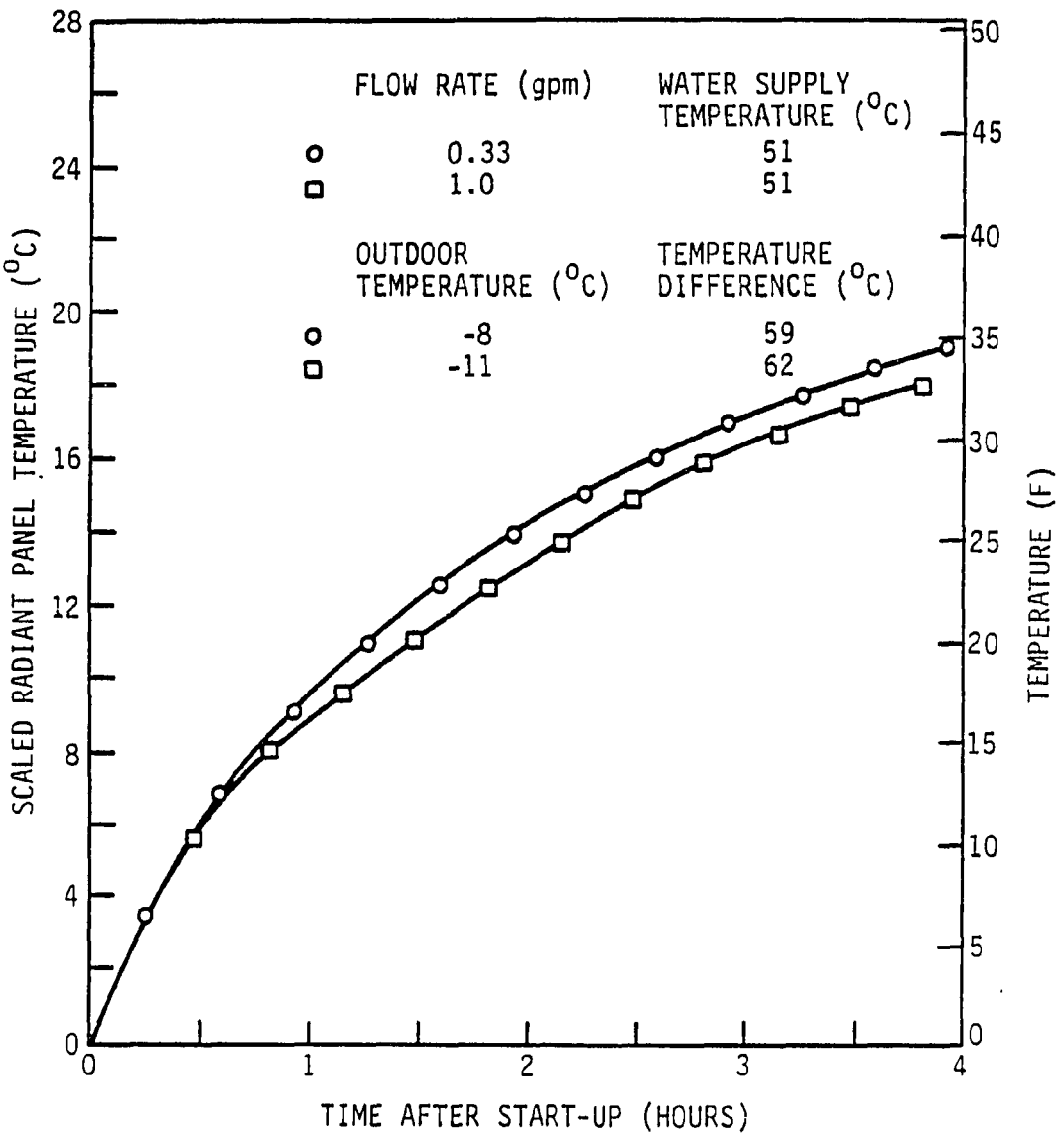

FIGURE 3.6. Thermal response of radiant ceiling for different water flow rates

3°C (5.4F) lower outdoor temperature. Even though the flow rate has very little effect on the local ceiling temperature rise, especially in the region where the tube enters the room as seen in Figure 3.6, it does affect the overall average ceiling temperature since the fluid in the tube that leaves the room is at a lower temperature. Therefore, the thermal response of the ceiling as a whole is indirectly affected.

The characteristic response curves shown in Figures 3.5 and 3.6 are basically exponential since the heat transfer mode from the hot tube to the ceiling surface is transient conduction. However, unlike many unsteady conduction problems having solvable simplified forms, this thermal response problem is complicated for a number of reasons. First, the dominant heat transfer mode between the ceiling and the floor, walls, door, and window is radiation. Radiation heat transfer gets more complicated when shape factors and emissivities are taken into account. Second, the complex ceiling structure and the relatively large ratio of unheated area to heated area in the ceiling panel makes a one-dimensional model less applicable and the two-dimensional model too involved. The unpredictable variation in the ceiling plaster thickness worsens this situation. Third, the presence of free-convection as a secondary heat transfer mechanism cannot be neglected. These reasons inhibit any attempt at an analytical solution for predicting the thermal response of the ceiling panel.

A comparison of time response characteristics for several residential heating sources by McNall (1975) has shown that radiant

ceilings may be the most difficult systems to approximate as a first-order system because of their low temperature. Even so, a rough estimate of the ceiling temperature can be obtained by approximating it as a first-order system (Chapman 1984):

$$\frac{T_s - T}{T_s - T_0} \propto \exp\left(-\frac{at}{L^2}\right) \propto \exp(-Fo) \tag{3.2}$$

where T_S is steady-state ceiling temperature, Fo is the Fourier number, and L is characteristic length.

Even though Figures 3.5 and 3.6 have not reached steady state, the steady state temperature appears to be linearly dependent on supply water temperature, T_{sw}, as follows,

$$T_s = C_2 \cdot T_{sw} \tag{3.3}$$

Therefore, at any instant, i.e., for any given Fo, the temperature difference ratio is constant,

$$C_1 = \frac{T_s - T}{T_s - T_0} \tag{3.4}$$

and the ceiling temperature, T, can be expressed as

$$T = C_2(1 - C_1) \cdot T_{sw} - C_1 T_0 \tag{3.5}$$

Constants C_1 and C_2 are less than unity so that the linearity $C_2(1 - C_1)$ is positive. Eq. (3.5) thus shows that the ceiling temperature is approximately linearly proportional to temperature of the supply water. This analysis is valid only for a constant outdoor condition. The outdoor condition has an effect on the temperature rise pattern, which can be deduced from Figure 3.6.

Transient response of room air and walls

Figure 3.7 shows room air temperatures measured 61 cm (2 ft) from the wall at two different heights: 46 cm (1.5 ft) and 152 cm (5.0 ft). These wall and air temperature curves are representative of the other walls with the exception that stratification is generally less than that shown in Figure 3.7 (i.e., the air temperature curve at 46 cm is generally much lower). The slow response of a radiant heating system with high thermal mass storage is obvious. To heat the room to a comfortable 20°C (68F) from an initial 12°C (54F) requires more than 2.5 hours. Figure 3.7 also shows that the air-temperature transient and the wall-temperature transients are similar. This similarity is understandable since the air is being heated primarily by natural convection from the enclosure, especially the floor, and the air has a low thermal mass storage.

One of the interesting observations from Figure 3.7 is that the air temperatures are higher than the wall temperatures. This indicates that heat transfer is from the air to the wall and that air movement is downward in the wall region. The conclusion to be drawn from Figure 3.7 is that the air is probably heated by the floor (the temperature of the carpet covered floor was not measured) through natural convection. Additional heating of the air may occur by convection from the ceiling since the overall flow pattern for the enclosure is probably air rising in the center region of the room, moving outward, and then moving downward along the walls. Thus the walls appear to be heated by

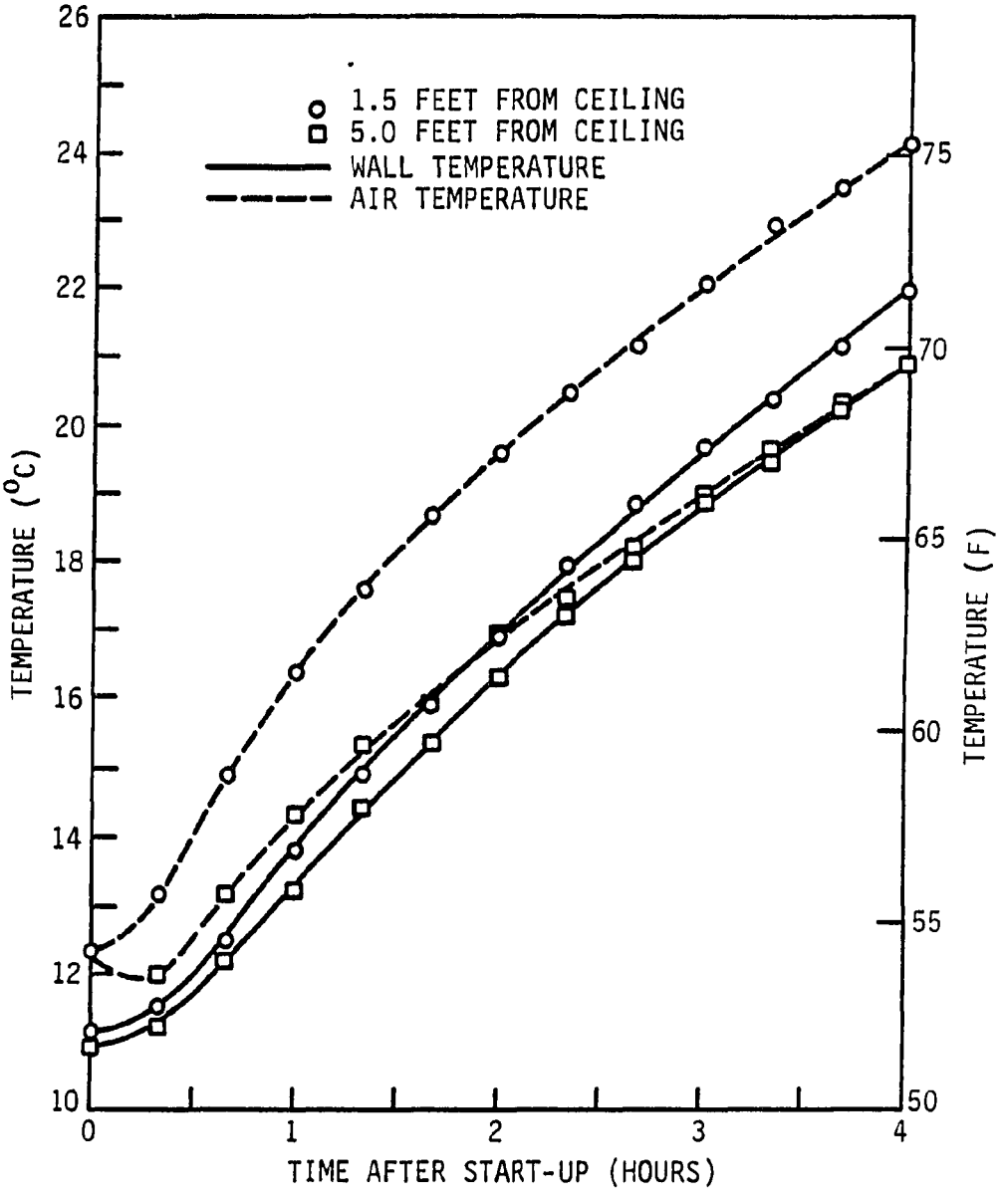

FIGURE 3.7. Comparison of wall and air temperature transients at two different distances from ceiling

radiation from the ceiling and natural convection from the air. Some of the above observations may not be applicable to typical residences since adjacent rooms in the test house were maintained at an atypical 15.5°C (60F). In addition, further studies and measurements are required before the stratification, the airflow pattern, and the actual mechanism for heating the room are fully understood and verified.

Profiles of air stratification after the radiant system has been in operation are shown in Figure 3.8. As noted previously, the air in the room is probably heated by convection from the floor and ceiling. This free convection occurs simultaneously with radiation heat transfer between the ceiling and the enclosure surfaces and with no obvious thermal lag. The warmer air near the floor rises because of its lower density while the cooler air moves in from other parts of the room to fill the vacancy. For comfort and energy conservation, stratification should be minimized; the stratification observed in these tests was less than that found in conventional forced-air heating systems (McQuiston and Parker 1982) As noted previously, these stratification tests are not considered conclusive, and additional tests must be performed before the air movement in the room is fully understood.

As was seen in Figure 3.7, the thermal response of the wall and air is very slow when heated by a hot-water radiant system. This is a problem that needs to be addressed when implementing hot-water (low-temperature) radiant panels as compared to implementing electric or infrared (high-temperature) radiant panels such as spot radiant and

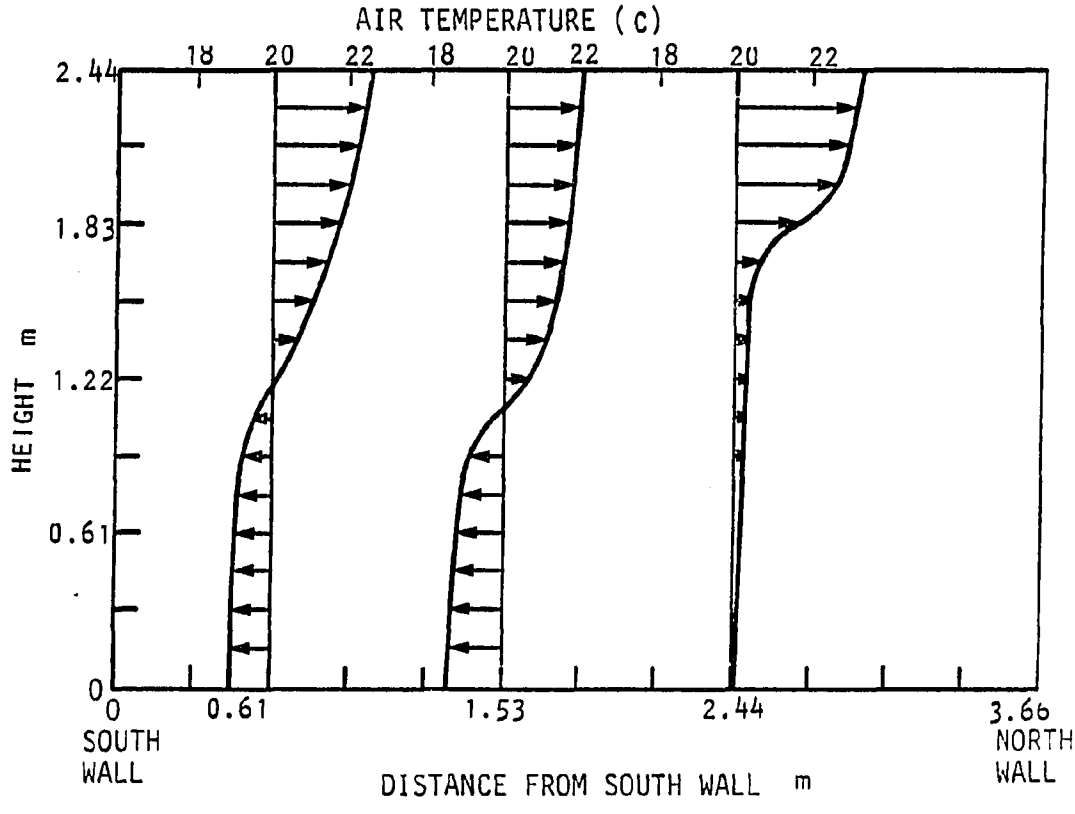

FIGURE 3.8. Stratification of air at three different locations in room

fast-acting ceilings. The main cause of this sluggish response is the fact that the ceiling panel itself takes a considerable time to approach its operative temperature after the step input of hot water temperature.

Transient response of overall enclosure

Figure 3.9 shows the thermal responses of the enclosure as a whole (i.e., ceiling temperatures, wall temperatures, and supply and return water temperatures) during a heat-up transient. The supply water temperature was maintained in the 42-48°C (108-118F) range, which is much lower than the suggested value of 55°C (131F) for a ceiling of moderate height (ASHRAE 1987). The outdoor average temperature at night (first six hours) was -8°C (18F), while the outdoor average temperature for the remaining period was approximately 6°C (43F). The room temperature increased steadily during the 24-hour testing period. Air and wall temperatures followed a similar trend. In addition, steady-state conditions were approached but not reached.

Figure 3.9 shows that the ceiling temperature is generally about 8°C (14F) higher than the wall temperature. The ceiling temperature is also shown to be uniform since the surface temperatures in the vicinity of the supply and return lines differ by less than 2°C (3.6F) during most of the testing period. The difference in temperature between the fluid in the tubes and the ceiling surface is also shown.

The temperature decrease of the fluid as it flows through the radiant system provides an indication of how much heat is supplied to the ceiling. This heat is used to compensate heat losses from the enclosure, or it is stored in the structure, in the ceiling, walls, and floor. Evidence of both phenomena can be observed in Figure 3.9. During the first part of the test when the maximum heat addition

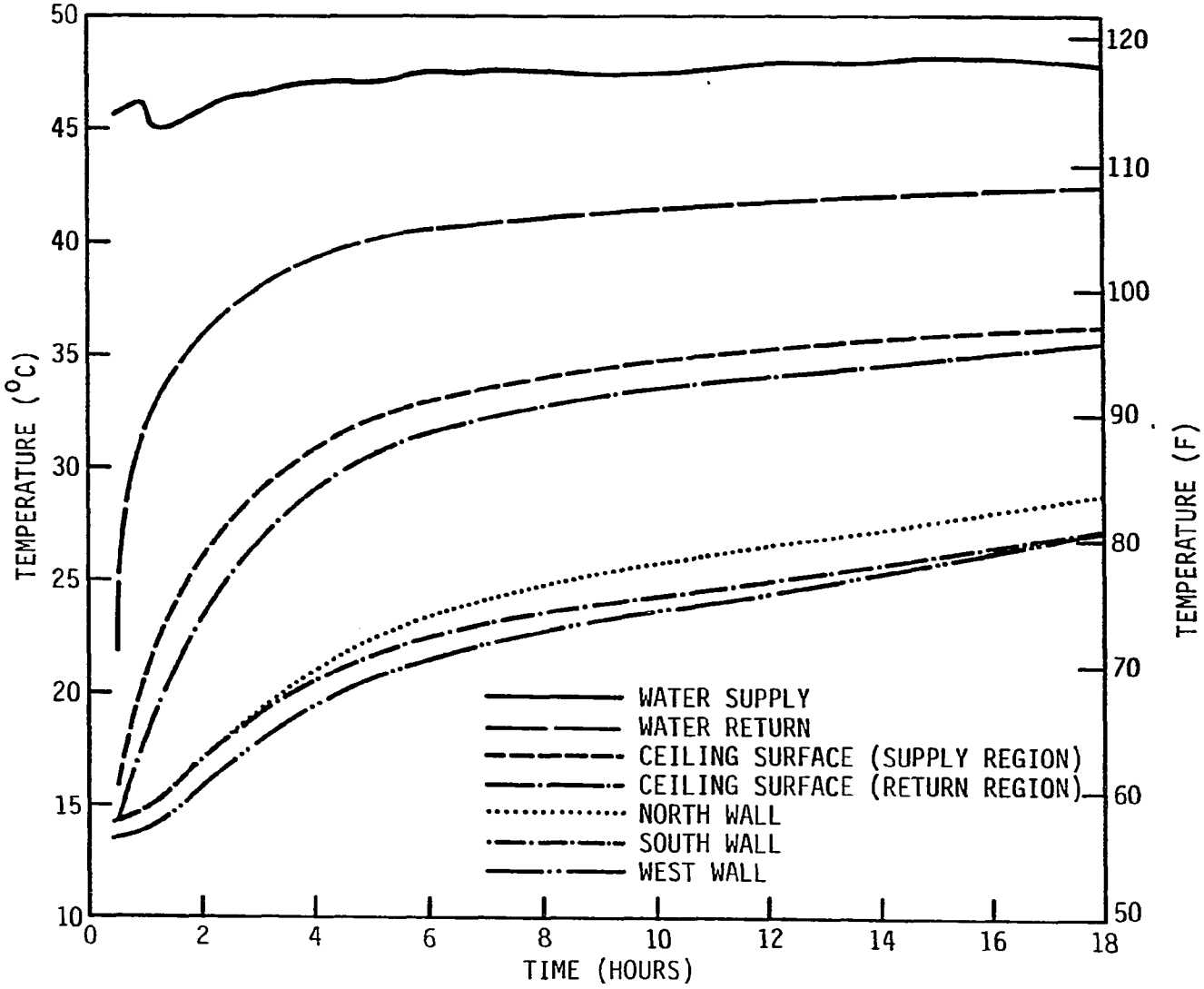

FIGURE 3.9. Thermal response of enclosure and radiant heating system during heat-up

occurs, the heat is primarily stored. In the latter stages of the transient, when the temperatures of the structure have leveled off somewhat, most of the heat addition is probably used to replace heat losses through the walls and ceiling.

Figure 3.10 shows the response of the ceiling and wall temperatures after the water supply to the radiant system was shut off. This reduced the heat addition to zero. The water temperatures are not shown since the flow rate is zero and the measured temperatures are not representative of the water temperature in the ceiling. During this test, the change in thermal storage replaces heat losses through the envelope. The ceiling surface has the highest rate of temperature decay because heat is transferred not only to the walls and floor but also through the roof. Figure 3.10 shows that all temperatures in the enclosure approach each other. After 15 hours, the maximum temperature difference between the ceiling and walls has dropped from 9°C (16F) to 1.5°C (2.7F).

Conclusion

This study has contributed to the understanding of the transient behavior of radiant heating panels and enclosures exposed to this type of heating system. The following conclusions were drawn from this study.

1. The pattern of tubes as installed in the ceiling provided a high degree of temperature uniformity. No evidence of

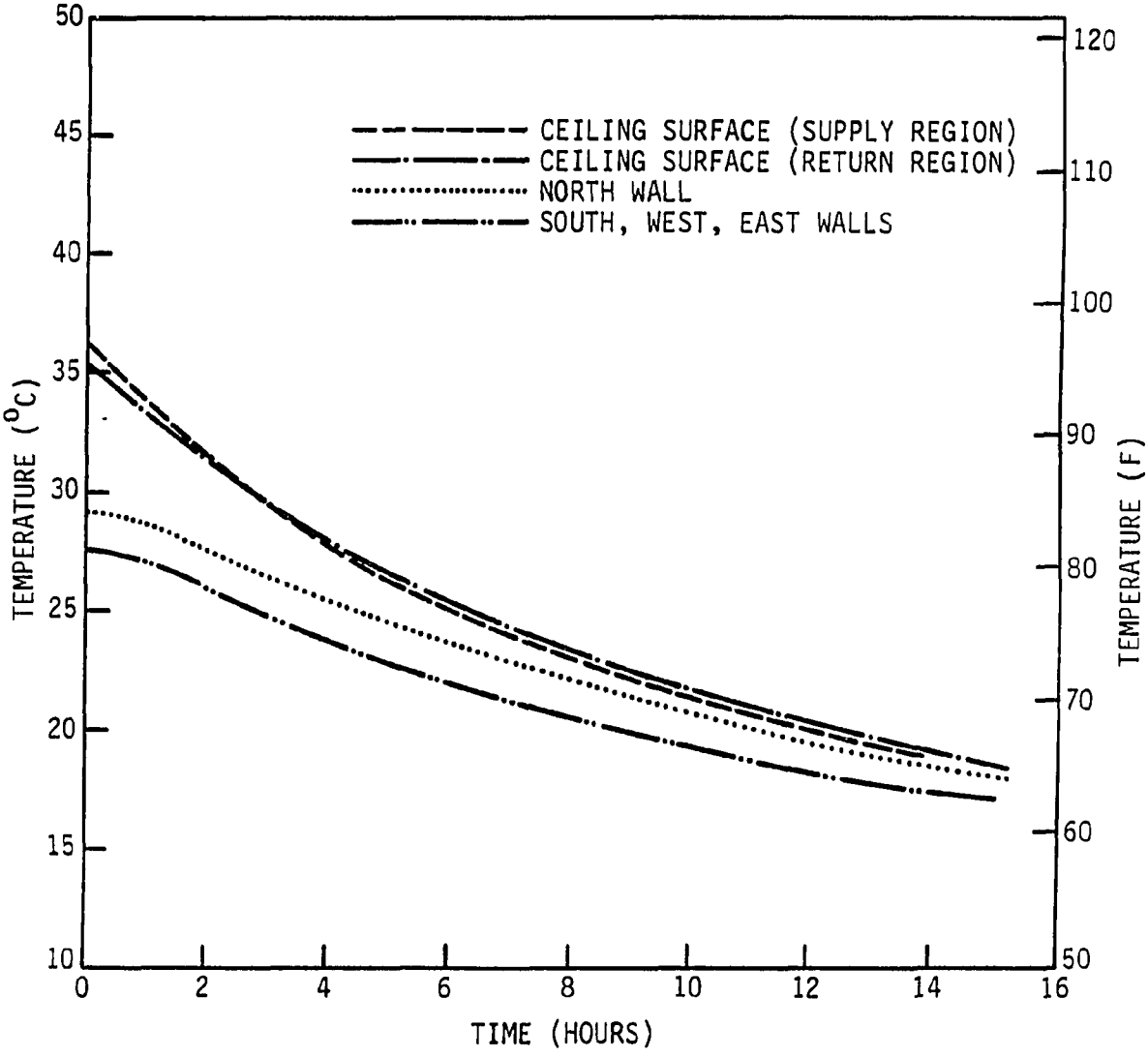

FIGURE 3.10. Thermal response of enclosure and radiant heating system during cool-off

positional temperature bias was present. However, if the comfort level for occupants can be improved by adopting this type of arrangement is unknown.

2. The water supply temperature had a large effect on the rate of increase in ceiling surface temperature. In contrast, the local heat-up rate of the ceiling was not a function of the water flow rate through the radiant system. However, the low flow rate results in a lower mean ceiling temperature.
3. Surprisingly, the air temperature in the room was higher than the wall temperature. This suggests that the wall is heated by a combination of radiation heat transfer from the ceiling and convection heat transfer from the air. Even though it could not be verified conclusively, room air appears to be heated by a combination of convection from the floor and the warm ceiling as air moves outward toward the walls along the ceiling.
4. The room air temperature did not lag the wall and floor temperature during a heat-up transient.
5. This study demonstrated that an enclosure can be heated adequately using a low-temperature heat source. At the same time, however, because of the large thermal lag of the ceiling, a sophisticated control system capable of adjusting supply-water temperature might be necessary for comfort if high cost effectiveness is desired.

CHAPTER 4 AN EXPERIMENTAL COMPARISON OF A RADIANT PANEL CEILING AND A FORCED-AIR HEATING SYSTEM

Introduction

Radiant heating systems have been used to provide space heating in a multitude of industrial, commercial, and residential applications. In addition, research has been performed in several studies to evaluate energy requirements as a function of corresponding degree-day data. For example, in a recent study, Buckley (1986) reported that with low-intensity (It may also be classified as medium-intensity, since the temperature range is from 150 to 650°C) radiant systems replacing original forced-air heating systems, the energy savings could amount to 42 to 70%. Earlier, Bailey (1980) performed a detailed study of the energy requirements for space heating of a lab building and a gymnasium, using both radiant and convective heating. The results showed that high-intensity radiant heating was more energy efficient than convective heating. Specifically, radiant heating reduced the energy consumption by 13% in the lab building and by 16% in the gymnasium.

Few attempts have been made, however, to investigate the efficiency of low temperature (i.e., surface temperature is less than 150°C) of low-temperature hydronic radiant systems installed in residential buildings. Therefore, whether the same conclusions that have been made for high- to low-intensity radiant heating systems can

be extended to common residential buildings with low-temperature radiant panels is the main focus of this study.

In this study energy consumptions for space heating using a hydronic radiant system and a forced-air system are compared experimentally for a residential building. This was accomplished by alternately operating the radiant system and the forced-air system in the same house for the same indoor conditions during a winter heating season. Instead of utilizing the degree-day or the variable base degree-day approach, actual indoor and outdoor temperature differences were recorded and the energy consumptions were frequently checked to maximize the data base.

Description of Facilities

The experiment was conducted in the Energy Research House for a ten-week period from mid-January through the end of March, 1986. The ERH, as mentioned before, is a three-story, 223-m^2 (2400-square-feet), well insulated residential house. The average wall thermal resistance is approximately 3.5 $m^2{}^oC/W$ (20 $hr \cdot ft^2 \cdot F/Btu$). The plane view of each floor of the house is shown in Figure 4.1. Most of the ground level is bermed, thus reducing heat transmission losses from the residence. The south wall contains a 24-panel solar collector, which is part of an active solar heating system. In addition, the house was designed with several passive solar heating features. The building was constructed tightly so that the air changes are less than 0.25 times per hour.

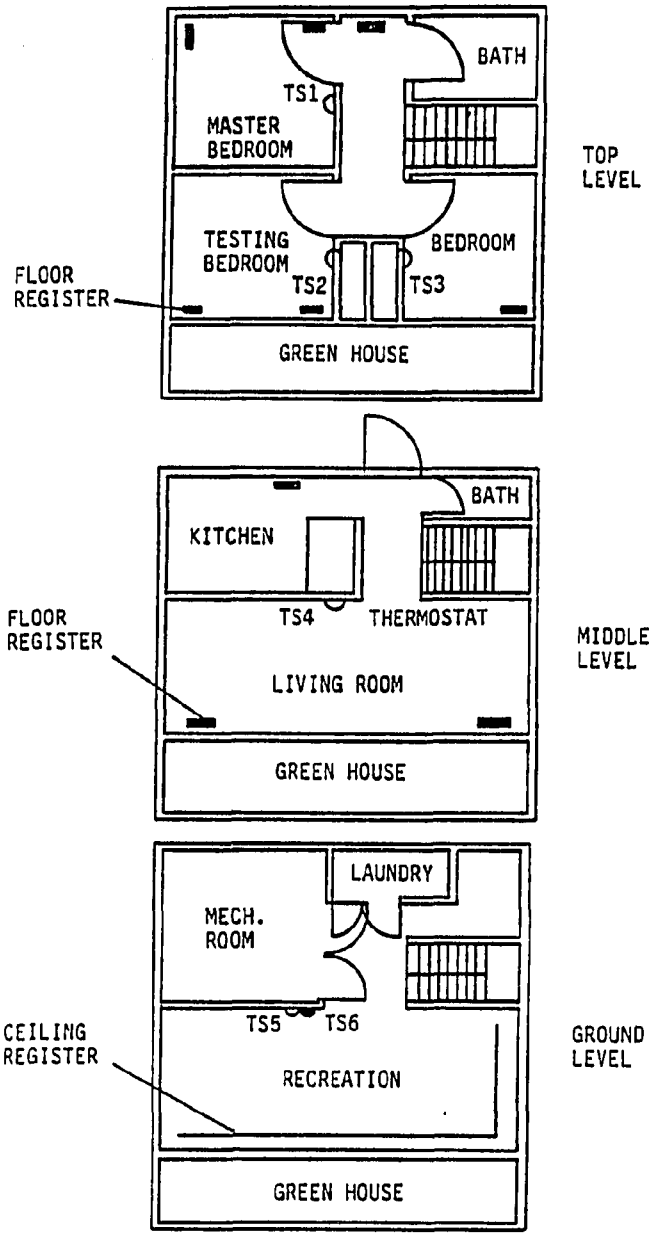

FIGURE 4.1. Plane view of the interior of the Energy Research House

Radiant heating system

The radiant heating system uses hot water flowing through tubes embedded in the ceiling. The panel structure is similar to that recommended in the ASHRAE Handbook (1987). A detailed cross section is shown in Figure 3.1. the copper tubes are spaced 15.2 cm (6.0 in.) apart and covered by approximately 2.54 cm (1.0 in.) of plaster. Each panel covers about 80% of the respective ceiling area.

The radiant heating system consists of eight separate ceiling panels. Specifically, one is located on the ground floor (recreation room), three on the first floor (living room, kitchen, and hallway), and four on the second floor (each bedroom and bathroom). These eight panels are grouped into five separate zones. The hot water flow to each zone is controlled by a motorized valve that in turn is controlled by a thermostat mounted on the wall of each room at a height of 12.7 cm (5 ft) from the floor.

The water flowing through the radiant tubes was heated by an instantaneous, in-line electrical water heater located in the mechanical room. The nominal capacity of the in-line water heater is 9 kW. The output temperature of the heater can be adjusted by a built-in potentiometer.

As hot water passes through the tubes in the ceiling, heat diffuses throughout the ceiling panel, thus elevating the ceiling temperature to an operating level. The warm ceiling exchanges radiant energy with various unheated surfaces in the room and consequently

raises the room air temperature by convection. Simultaneously, the operative temperature is also raised to a comfort level. The complete radiant heating system is the same as the system shown in Figure 3.3 with the exception that the domestic hot-water heater was replaced by the in-line heater.

Forced-air heating system

The forced-air heating system is very similar to those installed in typical residential buildings. Air heating is provided by four electrical resistance heating units, each having a 5.5 kW capacity. These heaters are installed directly in the main duct system just downstream of the fan. After being heated, the air is blown by the fan to the heated spaces through air ducts and floor registers. The location of each register is shown in Figure 4.1.

The indoor air temperature was controlled in the forced-air mode by using a single thermostat located on the ground floor. Even with this control arrangement, the air temperatures were quite uniform throughout the residence. For most of the time during the heating season, only two heating units were required so that the overall capacity was 11 kW, which was comparable to the radiant system's 9 kW. The system diagram is shown in Figure 4.2. It should be noted that the dampers to the outside were kept closed during all tests of the force-air and radiant systems.

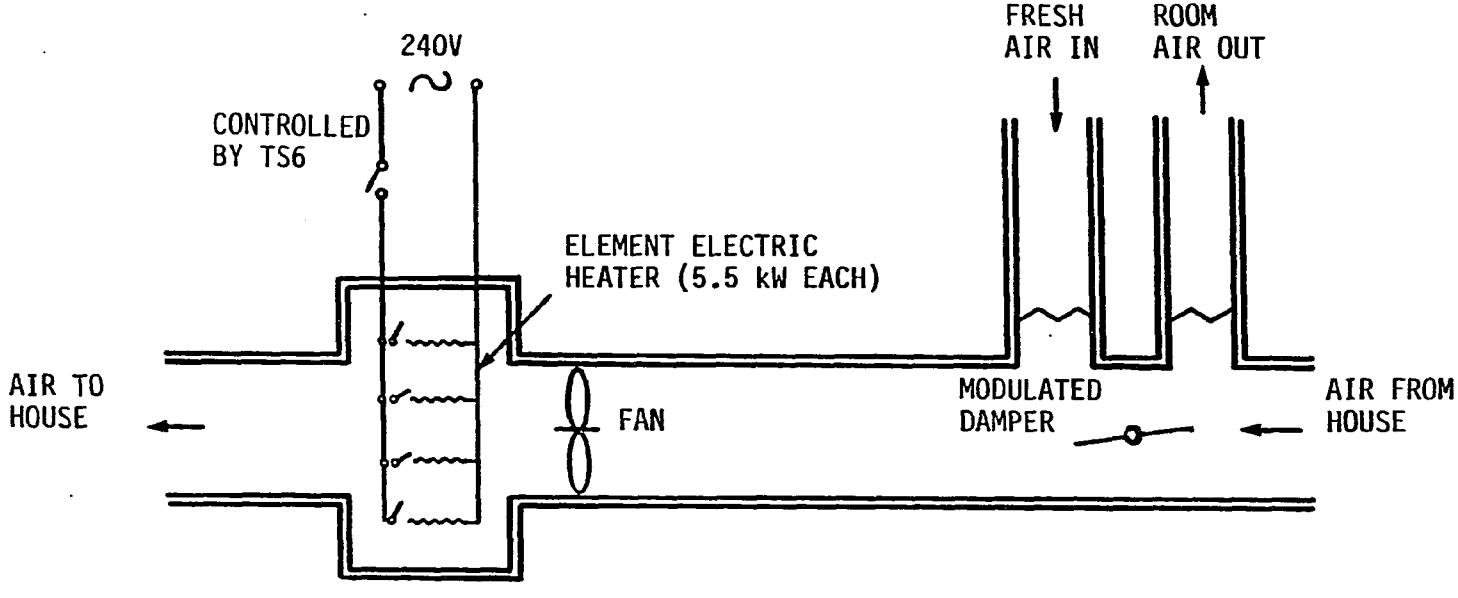

FIGURE 4.2. Schematic of forced-air heating system

Test room

The master bedroom, located on the upper floor, was instrumented for a space condition study. Thermocouples for measuring the air temperatures were located at heights of 0.6, 1.2, 1.8, and 2.3 m (2, 4, 6, and 7.5 ft) from the floor. Thermocouple shielding was not necessary since the radiant panel operated at a temperature only slightly above room air. Specifically, a comparison of thermocouple readings showed that there was no perceivable difference between shielded and unshielded thermocouples at the same location. The globe temperature, which was used to calculate the operative temperature, was measured by a thermocouple placed in a black globe. The outdoor temperature was also recorded. All data were taken at three-hour intervals.

Experimental Procedure

The experimental study consisted of alternate operations of the radiant system and the forced-air system while maintaining the house at approximately the same dry-bulb temperature. The duration of the alternate operations ranged from four to eight days, depending on local weather conditions. Specifically, the shift from one heating mode to the other was frequent enough to expose the heating modes to similar weather conditions. At the same time, however, it was not so frequent that the heat storage residue in the ceiling from the radiant mode would significantly affect the accuracy of the energy consumption calculation.

Both outdoor and indoor temperatures were recorded at three-hour intervals by the Fluke datalogger. The instrumentation uncertainty for temperature measurements was approximately ±0.2°C. The energy consumptions were read daily (with some exceptions) during most of the study. The outdoor and indoor temperatures were averaged over each energy consumption reading period. As a result, a set of data consisting of energy consumptions as a function of indoor and outdoor temperature differences was collected. A regression analysis was then performed so that the house overall heat loss coefficient for each heating mode was determined.

It should be noted that the pump used in the radiant mode and the fan used in the forced-air mode both have a nominal power rating of 0.56 kW (3/4 hp). Since they consumed similar amounts of energy that were only a fraction of the total energy, about 5 to 6%, their energy consumptions were not recorded.

Results and Discussion

The experimental data are presented and analyzed in detail with special emphasis on a comparison of the energy consumption for the two heating modes. A discussion of intermittent occupancy and a comparison of air stratification is also presented.

Energy consumption comparison

Figures 4.3 and 4.4 are plots of energy consumption data for the radiant and forced-air heating modes, respectively, as a function of

the inside and outside air temperature difference. The straight lines were obtained by the least-squares method using all data recorded during the period of study. It can be observed that the radiant heating system resulted in a lower overall heat transfer coefficient for the house than the forced-air system. The resultant linear relations are:

$$Q = 0.311\Delta T - 1.521 \qquad \text{for radiant heating}$$

$$Q = 0.339\Delta T - 1.091 \qquad \text{for forced-air heating}$$

where Q is energy consumption for the residence, in kW, and ΔT is the indoor-outdoor temperature difference, in °C. This means that the radiant heating saves energy by about 21% when both systems are operated with an indoor-outdoor temperature difference of 20°C (36F), and 16% when the temperature difference is 30°C (54F).

It should be noted that the resultant regression lines do not extrapolate to the origin. This is justifiable when we consider the fact that energy is usually not required for heating when the indoor and outdoor temperature difference is lower than a certain value.

Due to the scatters of the experimental data, a statistical analysis was performed to determine the coefficient of the correlation, r. It was found that

$$r^2 = 0.84 \qquad \text{for radiant data}$$

$$r^2 = 0.75 \qquad \text{for forced-air data}$$

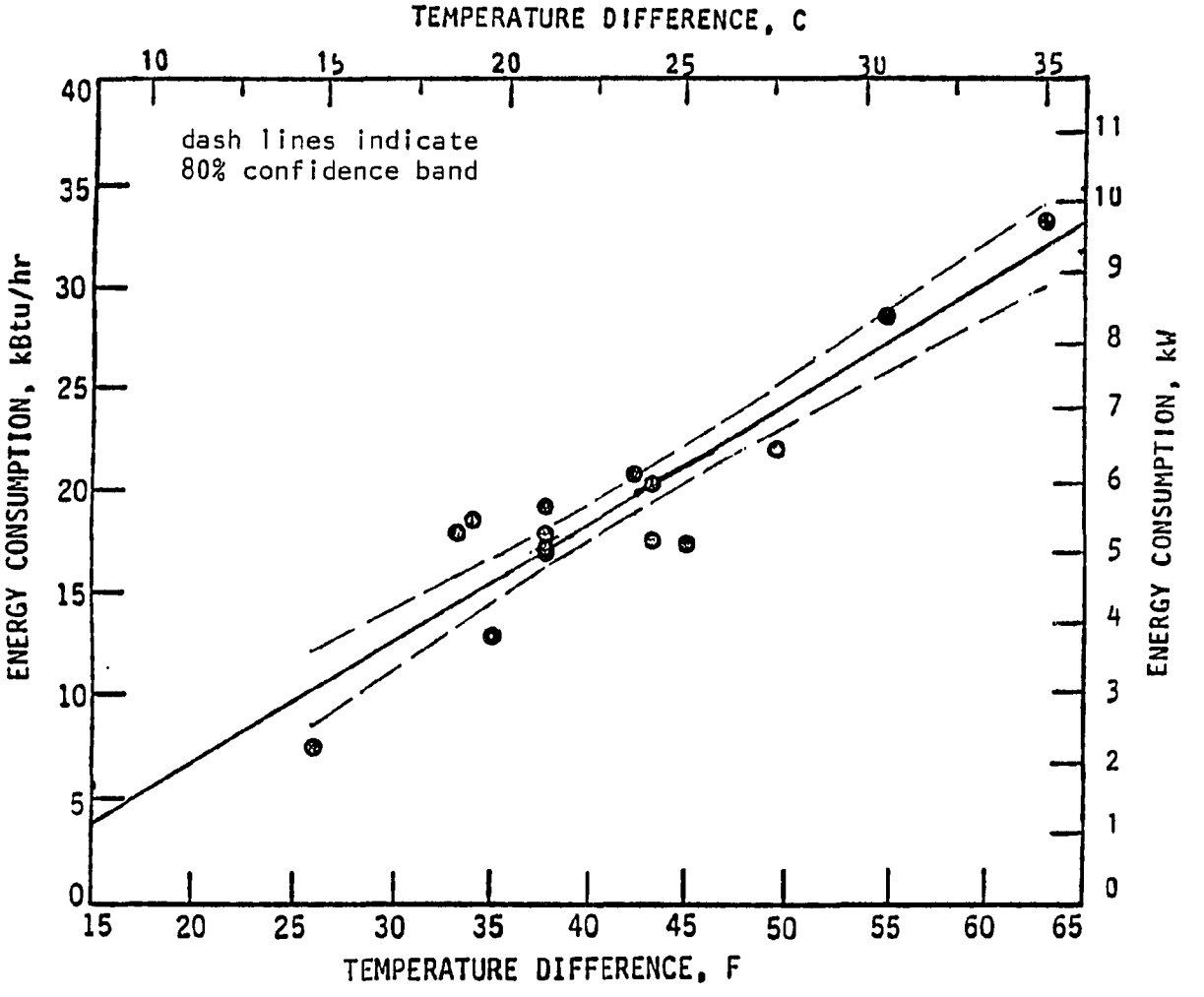

FIGURE 4.3. Energy consumption for radiant heating mode

These values are significant, since they indicate that about 84% (75%) of the total variation in the radiant (forced-air) data can be accounted for by this linear correlation and only 16% (25%) of the total variation in the radiant (forced-air) data are due to random variation.

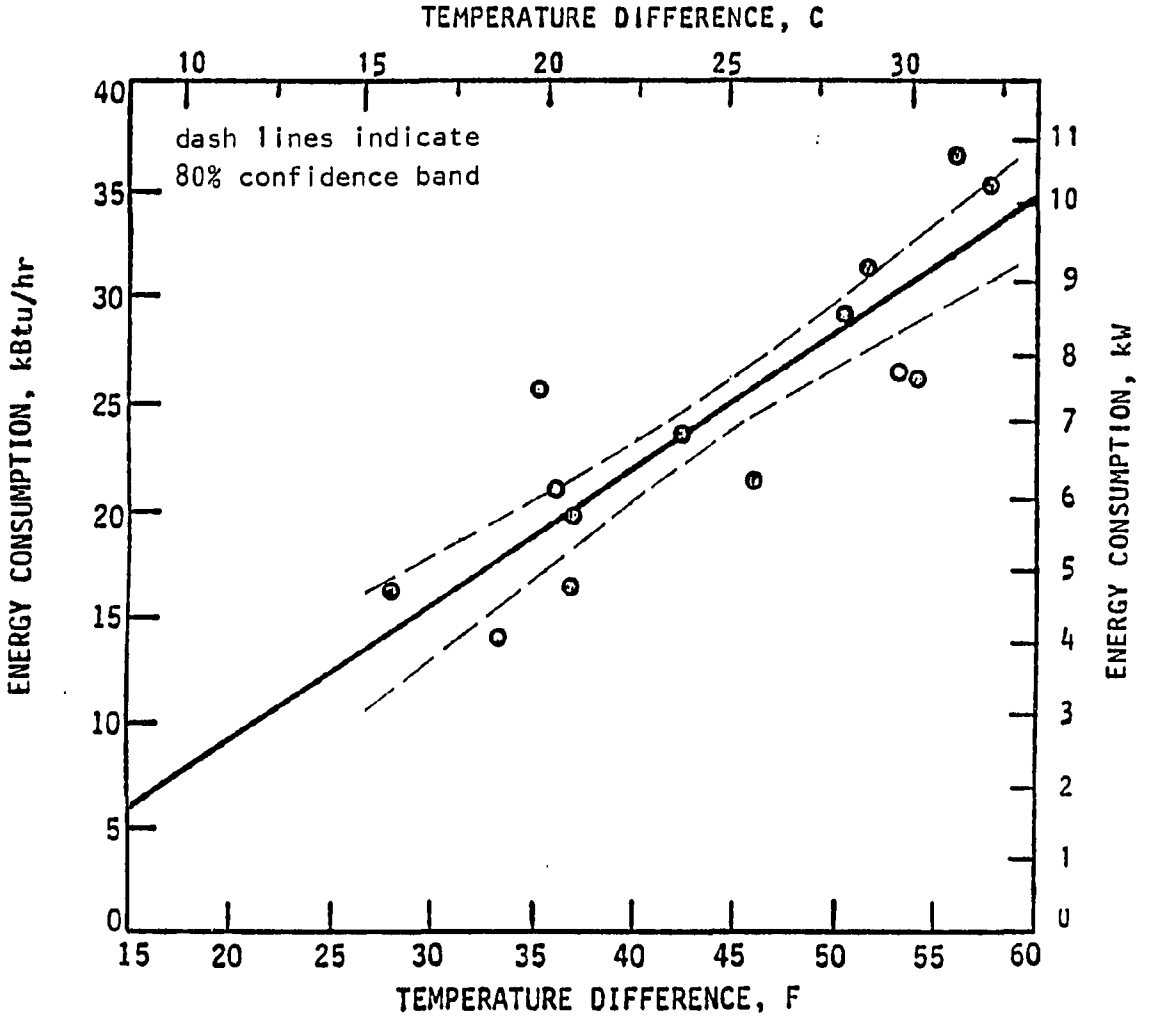

FIGURE 4.4. Energy consumption for forced-air heating mode

An 80% confidence band was also constructed around this regression line in both Figures 4.3 and 4.4. Superimposition of these two figures indicate that within the range of about 20 to 35°C (36 to 63F) temperature difference, these two bands are exclusive of one another.

words, within this range, the regression results are conclusive to at least 80% confidence.

Another approach, based on the following equation, is to have the regression lines pass through the origin.

$$Q = UA \cdot \Delta T$$

where UA is the overall heat transfer coefficient for the residence. This approach results in lower UA values for both heating systems. For example, with the least-squares method, the resulting UA is 248 W/°C (470 Btu/hr·F) for radiant heating versus 301 W/°C (570 Btu/hr·F) for forced-air heating. The potential energy savings when the radiant heating system is used is thus 17%.

If we reject the most eccentric data point, specifically, the one for the forced-air mode at ΔT = 20°C (36F), the savings will be reduced to 15%. If we further reject the second most eccentric data point at ΔT = 14.5°C (26F) for the radiant mode, the UA values will be 251 W/°C (475 Btu/hr·F) for the radiant mode and 290 W/°C (550 Btu/hr·F) for the forced-air mode, representing a 14% savings. The resulting linear curves for this last case are shown in Figure 4.5 Therefore, the low-temperature radiant system in this study has been demonstrated to be more than 14% more energy efficient than the forced-air system, even after the most unfavorable data point for forced-air heating and the most favorable data point for radiant heating are rejected. Table 4.1 summarizes the results of the regression analyses.

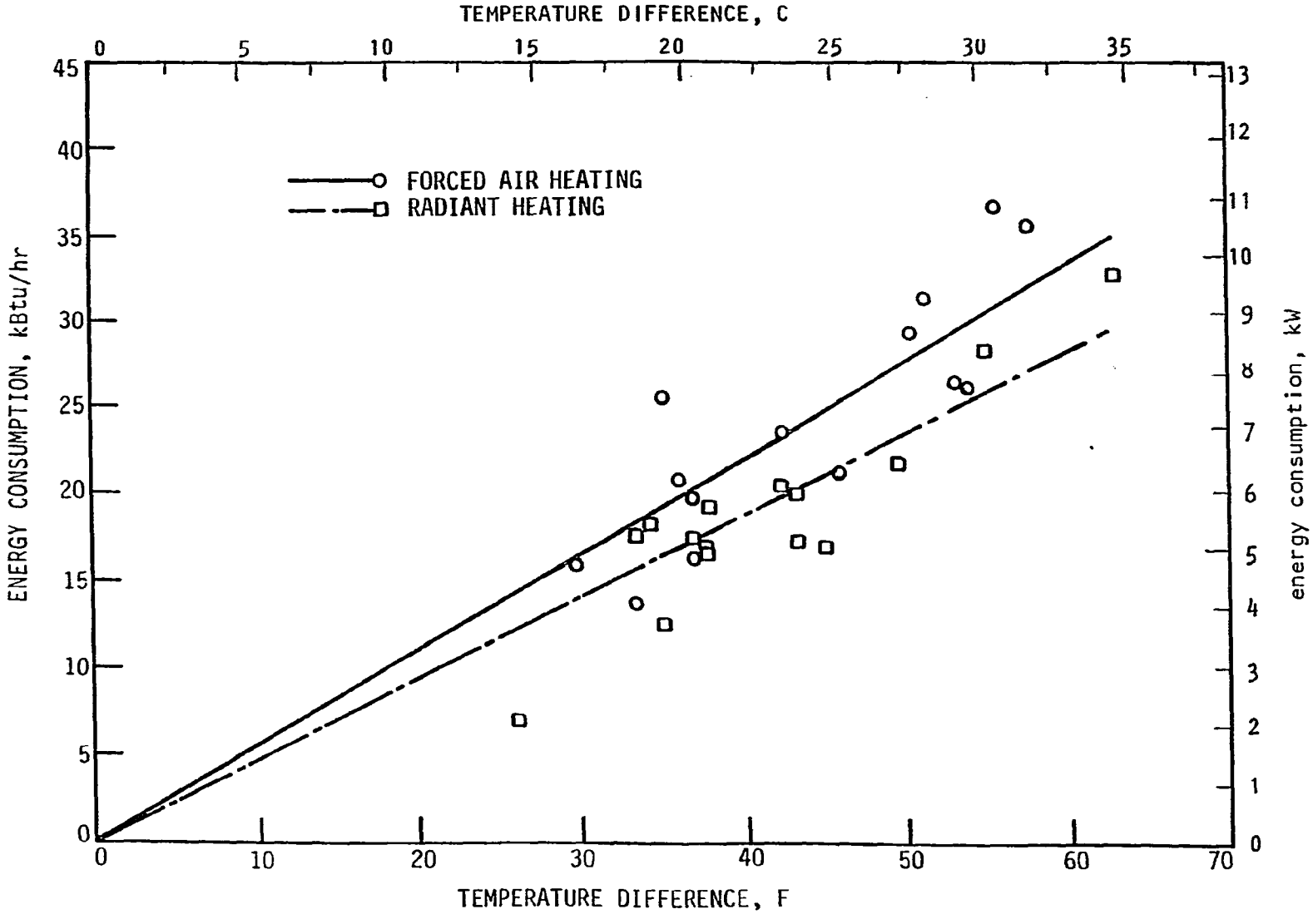

FIGURE 4.5. A comparison between energy consumption for radiant and forced-air heating system

TABLE 4.1. Regression Results

Type	Forced-air Heating		Radiant Heating		Energy Savings
	UA-W/°C (Btu/hrF)	ΔT_0°C (F)	UA-W/°C (Btu/hrF)	ΔT_0°C (F)	
2-constant[a] all data	340 (643)	3.2 (5.8)	310 (590)	4.9 (8.8)	20%[b]
1-constant[c] all data	301 (570)	0	248 (470)	0	17%
1-constant reject 1 pt.	290 (550)	0	248 (470)	0	15%
1-constant reject 2 pts.	290 (550)	0	251 (475)	0	14%

[a]Equation for 2-constant is $q = UA \cdot \Delta T + b$ (ΔT_0 is the value of ΔT when $q = 0$, so $\Delta T_0 = -b/UA$).

[b]This value is obtained by using $\Delta T = 20$°C. When ΔT increases, the savings reduce toward its lowest limit at about 9% for the 2-constant approach.

[c]Equation for 1-constant is $q = UA \cdot \Delta T$; so $\Delta T_0 \equiv 0$.

Additional energy savings

It is important to note that the energy savings described above for the radiant heating system are conservative, and in actuality, additional savings may be possible. There are basically two reasons:

Firstly, for the same comfort level (i.e., the same operative temperature), radiant operation requires a lower room temperature than does forced-air heating operation. The definition of operative

temperature is given by ASHRAE Standard (55-81) as follows: "The uniform temperature of an enclosure in which an occupant would exchange the same amount of heat by radiation plus convection as in the actual non-uniform environment." Numerically, the operative temperature is the average of the room temperature and the mean radiant temperature (MRT) weighted by respective heat transfer coefficients, h_r and h_c. Since the mean radiant temperature for a radiant system is higher than that for a forced-air system, the same operative temperature for a radiant system requires a lower room temperature.

For low-temperature radiant heating, the operative temperature is only slightly higher than that for a convective heating system. Specifically, for our experiment, the difference was generally less than 1°C (2F). As insignificant this number may appear, if the indoor dry-bulb temperature is reduced by 1°C (2F), the result would be about (1/ΔT)% of additional savings. For example, for a 25°C (45F) temperature difference, 7.2 kW (24.6 kBtu/hr) of heating energy is required for the forced-air system, while to maintain the same operative temperature, only 5.9 kW (20.0 kBtu/hr) of heating energy is required for the radiant heating system. This represents a 17.4% savings, compared to the 14% savings when the same dry-bulb temperature was maintained for both systems. In summary, a reduction in the dry-bulb temperature in the radiant mode can result in an additional energy savings of 3.4%.

Secondly, each time the radiant mode was shifted to the forced-air mode, the energy stored in the warm ceiling contributed to meeting a small fraction of the heating load for the forced-air operation. In addition, each time the forced-air mode was shifted to the radiant mode, additional energy was required to elevate the radiant ceiling to its operative temperature. This ceiling temperature was usually 8° to 10 °C (14 to 18F) higher than when the forced-air system was in operation. The additional energy, which was required to elevate all five ceiling panels to a 8°C (15F) higher temperature, was estimated at approximately 10 kW-hr (34.1 kBtu). It is obvious that without this alternating operation, the energy consumption for the radiant heating system would be even less than was recorded. If this effect is taken into account, the energy savings for the radiant system could be increased by about an additional 4%.

It should be pointed out that there were a few factors which were not taken into account during the experiment. First, the wind speed and direction on each day were observed but not accounted for. These effects are minimum because the house is very tight with very insignificant infiltration (about 0.25 air change per hour). Second, the solar gain on each day was not accounted for. Third, it has been noticed that the indoor temperatures for a few radiant testing periods were only about 18.5°C (65F) while that for a couple of forced-air testing periods were about 23.5°C (74F), a few degrees departing from the normal 20 to 22°C (68 to 72F) range. Although the experimental

data were entirely based on the indoor-out temperature difference, the variation of indoor temperature during each test may have some subtle effect on the overall results.

Intermittent occupancy and heat-up rate

While it can be concluded to 80% confidence that a radiant system is more energy efficient for the House where the indoor comfort condition is maintained on a continuous basis, the same conclusion may not necessarily be true for residences that have intermittent occupancy. Specifically, heat storage and diffusion is an undesirable feature of a hydronic radiant system when it is operated intermittently. In contrast, a forced-air system does not require energy for elevating the ceiling panel temperature.

Another disadvantage of a hydronic radiant heating for intermittent occupancy is its slow thermal response. Although some researchers have found that infrared radiant heaters can quickly increase the space's mean radiant temperature and thus bring the operative temperature to a comfortable level within minutes (Berglund et al. 1982), this is not the case for the low-temperature, hydronic radiant ceiling panel discussed herein. As reported in Chapter 3, the transient response of the air temperature is very slow in response to a step increase in supply water temperature; frequently, more than one hour is needed for the room temperature to increase from 15.5 to 21°C (60F to 70F).

Stratification

The air stratification was also measured in this study. The floor diffuser arrangement did not result in significant air stratification in the room during the forced-air heating mode. In fact, the air stratification for the radiant ceiling heating was slightly greater than that for the forced-air heating as illustrated in Figure 4.6. It can thus be concluded that the energy savings for the radiant system in this study was not due to reduced air stratification as has been reported in other radiant heating studies (Diamant 1984; discussions on Bryan 1981). However, it can be deduced that if a ceiling diffuser is used in large rooms with greater ceiling heights, then the radiant heating system might save even more energy than indicated by this study, the reason being that the reduced thermal stratification for radiant heating compared to a ceiling diffuser will work to the radiant system's advantage. This possibly explains why the study by Buckley (1986) on medium-temperature radiant systems showed much higher savings than what is indicated in this research.

Although the energy efficient mechanisms for a radiant system are unclear, the heat energy distribution is probably a contributing factor. For radiant panel heating, the air temperature is not as uniform throughout the space as it is for a forced-air system. Specifically, cold spots exist in both the air and wall surfaces in those regions that are not directly exposed to the radiant ceiling panel. These cold spots may have reduced the conduction heat losses and air infiltration heat losses.

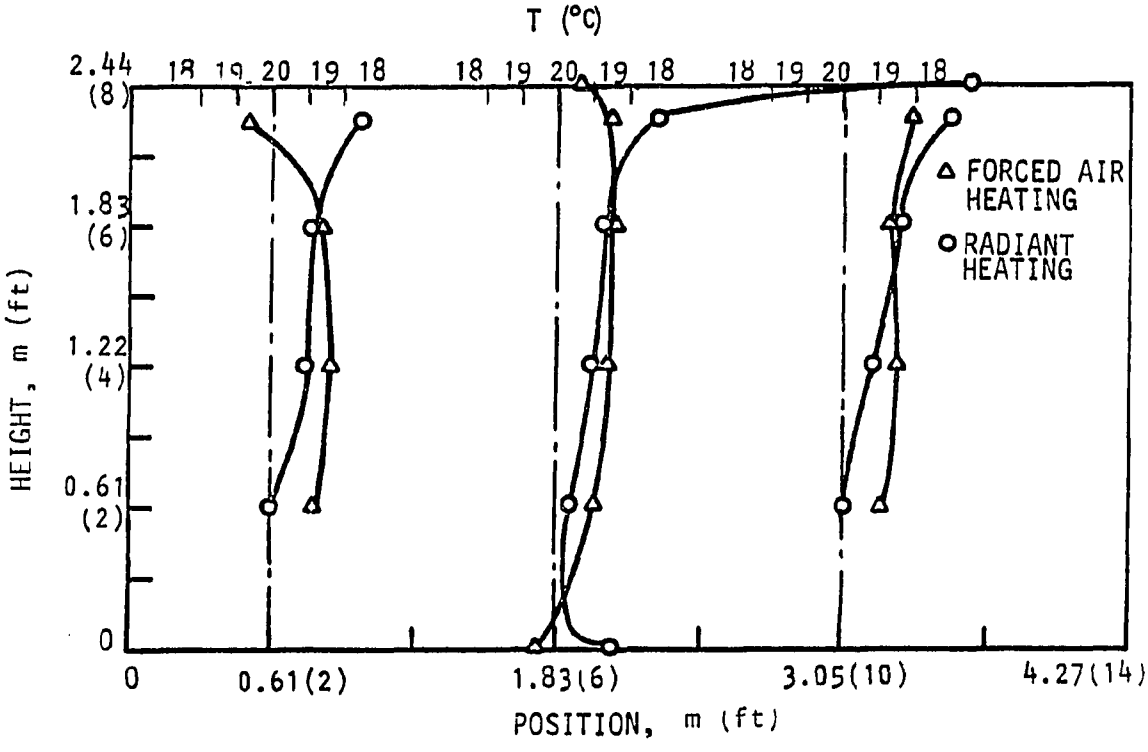

FIGURE 4.6. A comparison of room air stratification

Conclusion

This study showed that for the house studied herein, a radiant heating system can result in an energy savings of about 14% to 20% over a forced-air heating system, depending on which regression curve is being used. The regression analysis leads to an overall heat loss coefficient of 251 W/°C (475 Btu/hr·F) for the radiant system and 290 W/°C (550 Btu/hr·F) for the forced-air system, even after eccentric data points that are favorable to the radiant system are rejected.

The actual energy savings for the radiant system could be even higher (up to 7.4% higher) for several reasons:

- The air temperature for a radiant system can be lower than the air temperature for a forced-air system when the same operative temperature is maintained. Although for the hydronic radiant panel the temperature difference is not very significant, less than 1°C (2F), the corresponding energy savings could increase by 3.4%.
- Because of energy storage effects in the ceiling during a heating mode shift, the energy consumption is overestimated for the radiant system and underestimated for the forced-air system. The amount of additional energy used for shifting is estimated to be 10 kW-hr (34 kBtu), which could increase the energy savings of the radiant system by another 4%.

However, due to the data scattering, the regression results may not be very conclusive. A statistical analysis shows about 80% confidence on the above results.

In addition, an investigation of air stratification showed that the differences in air stratification for the two heating systems were quite small.

CHAPTER 5 A NUMERICAL STUDY OF HEAT TRANSFER IN A HYDRONIC RADIANT CEILING PANEL

Introduction

Heat transfer in a hydronic radiant ceiling panel was modelled using a numerical approach. The specific radiant ceiling panel investigated in this study is shown in Figure 5.1. Hot water is carried through copper tubes embedded in a plaster ceiling, resulting in an elevated temperature on the ceiling surface. Space heating is then provided by radiant heat exchange between the warm ceiling and the unheated surfaces in the room enclosure. In addition, convection heat transfer by either natural or forced-air motion also contributes to the transfer of heat from the ceiling to the room.

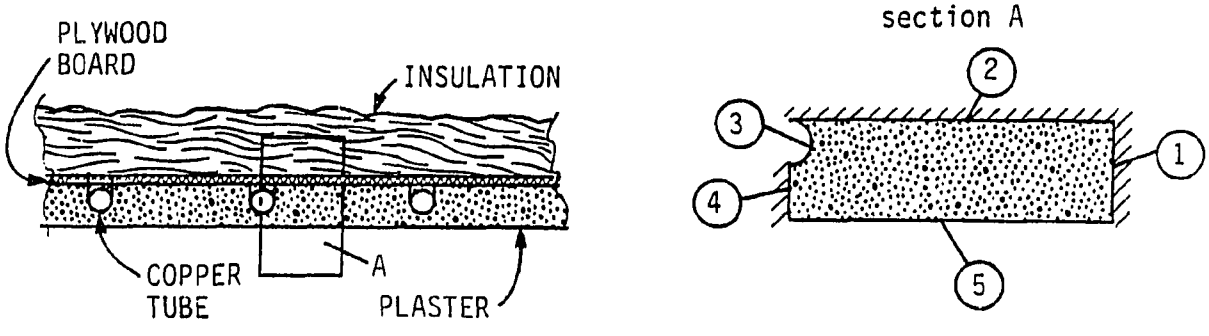

FIGURE 5.1. Modeling of a hydronic radiant ceiling panel

Even though researchers have been active in the area of radiant heating for a long time, only a few studies have been performed in the area of modeling heat transfer from various types of panels. Among these studies is that of Hedgepeth and Sepsy (1972), who presented a thermodynamic simulation for a radiant ceiling panel. However, the panel structure analyzed in their study differed from the standard ceiling panel (ASHRAE 1987) shown in Figure 5.1. For example, in the former the copper tube is finned while in the latter it is not. Although a lumped analysis of a ceiling panel was performed years ago by Schutrum et al.(1953), there is no literature dealing with a detailed study of heat transfer in a standard radiant panel ceiling.

The main objective of this study is the development of a numerical model that can be used to study the heat transfer characteristics of a radiant ceiling panel. Using this numerical model to design radiant heating panels is also illustrated by investigating the effects of tube spacing, plaster thickness, and convection heat transfer coefficient on the ceiling heat flux.

Model Approach

The radiant ceiling panel was modeled by focusing on a typical two-dimensional section that contains half of a copper tube with hot water flowing inside as shown in Figure 5.1. A two-dimensional approximation was possible because the temperature variation in the water flow direction is quite small compared to that on a plane that is

perpendicular to the flow direction. The governing equation for this region is the two-dimensional transient heat equation,

$$\frac{1}{\alpha}\frac{\partial T}{\partial t} = \left(\frac{\partial^2 T}{\partial x^2} + \frac{\partial^2 T}{\partial y^2} \right) \tag{5.1}$$

At steady state, the transient term on the left hand side goes to zero, reducing the equation to the Laplace equation.

The two-dimensional section contains five boundaries as shown in Figure 5.1. Since adjacent tubes are close to the same temperature, an adiabatic boundary can be assumed on side 1, a distance halfway between the tubes. Boundary 2 is assumed to be adiabatic because the top of the ceiling panel is well insulated. Boundary 3, which is semicircular, is assumed to be isothermal at the bulk temperature of the hot water flowing inside the copper tube. This assumption is based on the thermal conductivity of the copper tube being three orders of magnitude greater than that of plaster. Because of symmetry, side 4 is also an adiabatic boundary. Boundary 5 is the ceiling surface that faces the room enclosure. This surface is exposed to both radiation and convection heat transfer as described below.

According to Schutrum et al.(1953), the room temperature, T_a, is approximately equal to the AUST (Average Unheated Surface Temperature) in a room heated by a ceiling panel. Therefore, it is reasonable to assume the AUST to be the same as the average room temperature in this study. As a result, the radiant heat exchange between the ceiling and the other surfaces in the enclosure can be approximated as

$$q_r = \epsilon\sigma(T^4 - T_a^4) \tag{5.2}$$

where we assume the shape factor to be unity.

Although the predominant heat transfer mode for a radiant ceiling panel is radiation, convection due to either natural or forced-air motion may also be an important factor, particularly for a low-temperature radiant panel (ASHRAE 1987 and Jones et al. 1975). As a consequence, the ceiling surface is actually a combined radiation and convection boundary with the convective heat transfer coefficient, h, being in the range of 2 to 10 $W/m^2{}^\circ C$ (Jennings 1978). Therefore, the combined heat flux from the surface can be expressed as

$$q = \epsilon\sigma(T^4 - T_a{}^4) + h(T - T_a) \tag{5.3}$$

Numerical Formulation

The numerical formulation of the ceiling panel model described above requires solving the heat diffusion equation, Eq. (5.1), for irregular and nonlinear boundaries.

Figure 5.2 is the two-dimensional ceiling section divided into a finite number of grids. Because of the semicircular isothermal boundary, curvilinear grids were used at distances less than the tube diameter from the top boundary. Rectangular coordinates were used in the region below the tube. Since the temperature gradient is expected to be higher in the region of the isothermal boundary, nonuniform grids were used, with the finest grid spacing placed closest to the circular tube. With this arrangement, the coordinates of each node were determined by

$$\Delta x_{i,j} = C \cdot \Delta x_{i,j-1} \tag{5.4}$$

and

$$x_{i,j} = x_{i,j-1} + \Delta x_{i,j-1} \tag{5.5}$$

These equations result in a grid size that increases away from the isothermal boundary. The rate of incrementation in the x-direction, C, was fixed at 1.2 in this study. The coordinates of the first node in each row can be expressed as

$$x_{i,1} = \sqrt{2Ry - y^2} \qquad \text{for } y < 2R \tag{5.6}$$

$$x_{i,1} = 0 \qquad \text{for } y \geq 2R \tag{5.7}$$

The first grid size can be determined from the number of x-direction grids, m, as follows:

$$\Delta x_{i,1} = DA_i \left(\sum_{j=1}^{m} (C^j) \right)^{-1} \tag{5.8}$$

A similar grid arrangement exists for the y coordinate system when $y > 2R$ and uniform spacing exists when $y \leq 2R$. The above equations completely define the grid coordinates and grid spacing.

This grid arrangement was preferred over the body fitted rectangular grid method because fewer grids were required to obtain the same order of accuracy. In addition, the semicircular boundary can be much more closely approximated using the grid arrangement presented herein.

In reference to Figure 5.3, the finite difference equations can now be written for each node. Using a nodal energy balance approach, the finite difference equations for the internal nodes are as follows:

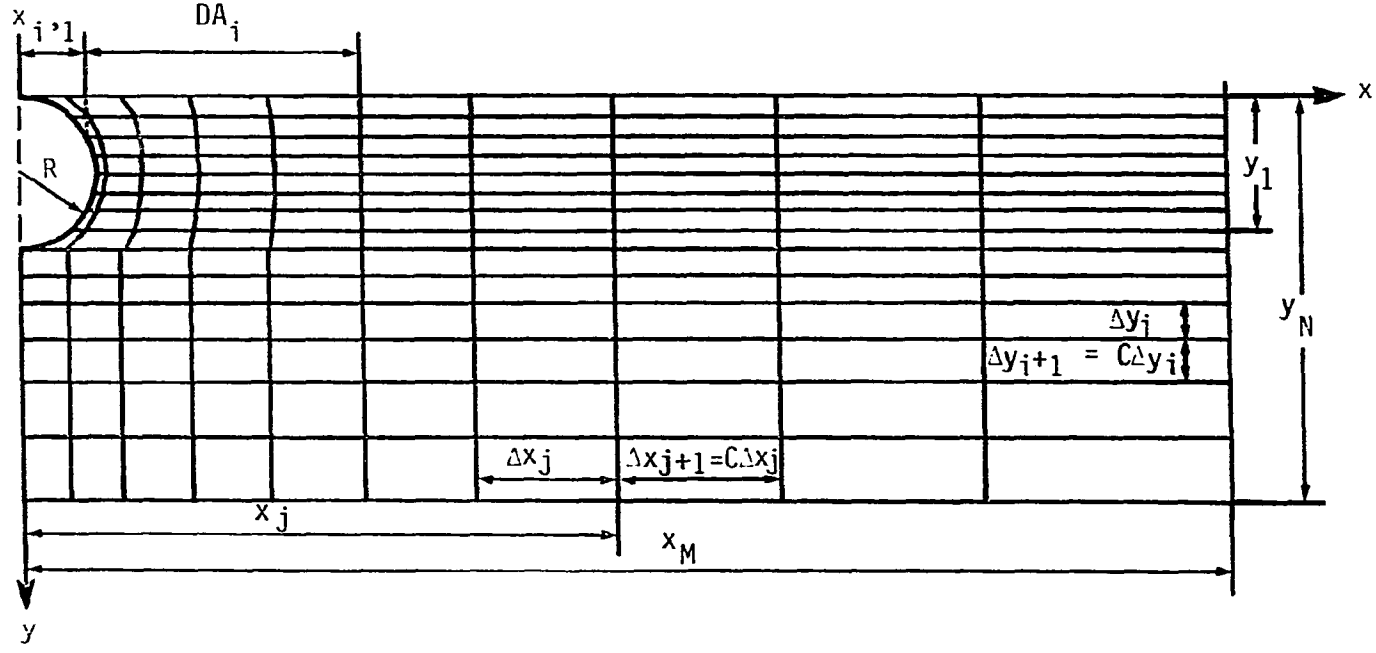

FIGURE 5.2. Grid distribution for the ceiling model

$$\frac{\Delta n_{j-1}}{\Delta x_{i,j}} (T_{i,j-1} - T) + \frac{\Delta n_j}{\Delta x_{i,j+1}} (T_{i,j+1} - T)$$

$$+ \frac{\Delta m_{i-1}}{\Delta l_{i-1,j}} (T_{i-1,j} - T) + \frac{\Delta m_i}{\Delta l_{i,j}} (T_{i+1,j} - T)$$

$$= \frac{\rho C_p}{k} \Delta n_j \Delta m_i \left(\frac{T^{n+1} - T}{\Delta t} \right) \tag{5.9}$$

where

$$\Delta n_j = \Delta l_{i,j}/2, \quad \Delta m_i = (\Delta x_{i,j} + \Delta x_{i,j+1})/2 \tag{5.10}$$

$$\Delta l_{i,j} = \sqrt{(x_{i+1,j} - x_{i,j})^2 + \Delta y^2} \tag{5.11}$$

For those nodes that are adjacent to either an isothermal or an adiabatic boundary, Eq. (5.9) should be modified to fit the individual node.

Prior to formulating the finite difference equations for the nodes in last row, which corresponds to the surface of the ceiling, the nonlinear radiation boundary was linearized. Even though simple methods are available for linearization, the more accurate Newton's linearization was used as follows:

$$(T^{k+1})^4 \cong 4(T^k)^3 T^{k+1} - 3(T^k)^4 \tag{5.12}$$

where the superscript k denotes the iteration number. The resulting finite difference equation is

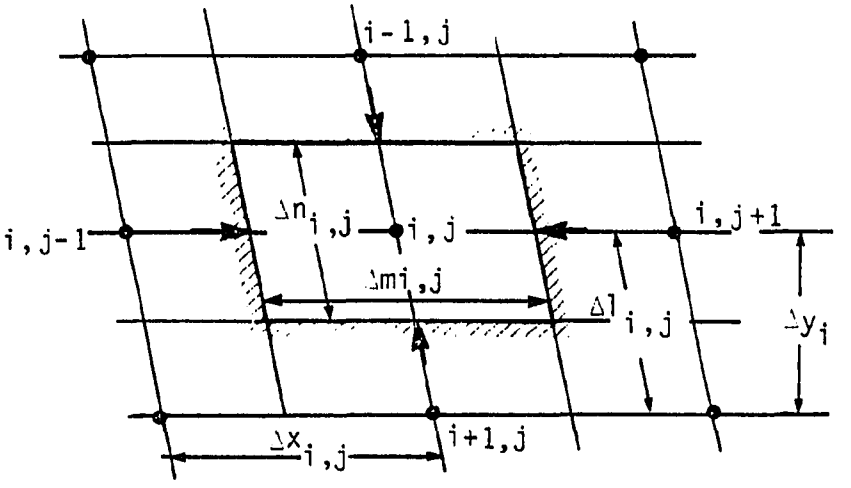

FIGURE 5.3. Nomenclature for finite difference equations set up at grid node(i,j)

$$\frac{\Delta n_{j-1}}{\Delta x_{i,j}}(T_{i,j-1}-T) + \frac{\Delta n_j}{\Delta x_{i,j+1}}(T_{i,j+1}-T) + \frac{\Delta m_{i-1}}{\Delta y_{i-1}}(T_{i-1,j}-T)$$

$$+ \Delta m_i\left[\frac{\epsilon\sigma}{k}T_a^4 + 3(T^k)^4 - 4(T^k)^3 \cdot T + \frac{h}{k}(T_a-T)\right]$$

$$= \frac{\rho C_p}{k}\Delta n_j \cdot \Delta m_i\left(\frac{T^{n+1}-T}{\Delta t}\right) \qquad (5.13)$$

It should be noted that the right hand sides of Eqs. (5.9) and (5.13) reduce to zero at steady state.

Nondimensional Formulation

Nondimensionalizing the above finite difference equations has the advantage of reducing the number of independent variables. As a first step, the following dimensionless variables are introduced with distances scaled by the tube radius, R, and temperature by the tube surface temperature, T_0 (in Kelvin):

$$X = x/R, \quad Y = y/R, \quad \theta = T/T_0$$

$$\Delta L = \frac{\Delta l}{R}, \quad \Delta M = \frac{\Delta m}{R}, \quad \Delta N = \frac{\Delta n}{R} \tag{5.14}$$

The nondimensionalization results in two important dimensionless parameters:

$$Pi = \frac{\epsilon \sigma R}{k} T_0^3 \tag{5.15}$$

$$Bi = \frac{hR}{k} \tag{5.16}$$

The first parameter, arbitrarily designated as Pi, accounts for the radiation effect, while the second parameter, the Biot number, accounts for the convection effect. It is important to note that thermal conductivity, k, is defined for the plaster rather than for the air. The heat flux of the ceiling surface, q, can also be expressed nondimensionally as

$$Q = ql/(k \cdot T_0) \tag{5.17}$$

Note that ql is in W/m per element of the ceiling surface. After making the above transformation, Eqs. (5.9) and (5.13) can be rewritten as follows:

$$\frac{\Delta N_{j-1}}{\Delta x_{i,j}} (\theta_{i,j-1} - \theta) + \frac{\Delta N_j}{\Delta x_{i,j+1}} (\theta_{i,j+1} - \theta)$$

$$+ \frac{\Delta M_{i-1}}{\Delta L_{i-1,j}} (\theta_{i-1,j} - \theta) + \frac{\Delta M_i}{\Delta L_{i,j}} (\theta_{i+1,j} - \theta)$$

$$= \frac{\Delta N_j \Delta M_i}{Fo} \qquad \text{for internal nodes} \tag{5.18}$$

$$\frac{\Delta N_{j-1}}{\Delta X_{i,j}}(\theta_{i,j-1} - \theta) + \frac{\Delta N_j}{\Delta X_{i,j+1}}(\theta_{i,j+1} - \theta) + \frac{\Delta M_{i-1}}{\Delta Y_{i-1}}(\theta_{i-1,j} - \theta)$$

$$+ \Delta M_i \cdot Pi[1 + 3(\theta^k)^4 - 4(\theta^k)^3 \cdot \theta] + \Delta M_i \cdot Bi(1 - \theta)$$

$$= \frac{\Delta N_j \Delta M_i}{Fo} \qquad \text{for the nodes in the last row} \tag{5.19}$$

where

$$Fo = \frac{k\Delta t}{\rho C_p R^2} = \frac{a\Delta t}{R^2} \tag{5.20}$$

takes the same form as the Fourier number, although it does not have the same physical implication.

The nondimensional form has a significant advantage in that the ceiling-unit heat output, ql, which is the most important output of the numerical model, can be expressed as

$$Q = f(Pi, Bi, \theta_a) \tag{5.21}$$

for a given geometry. The independent variables are thus reduced from the original five (k, ϵ, h, T_0, T_a) to three (Pi, Bi, θ_a).

Numerical Solution Schemes

Both steady state and transient state were solved using different numerical solution schemes.

Steady state solution

A steady state heat diffusion solution is desirable in order to establish the relationship between the ceiling heat output and supply water temperature, ceiling panel geometry, and panel material under normal operating conditions.

Rewriting Eqs. (5.18) and (5.19) by collecting the same θ terms and by setting the right hand side to zero, we have

$$A\theta + B\theta_{i,j-1} + C\theta_{i,j+1} + D\theta_{i-1,j} + E\theta_{i+1,j} = P \qquad (5.22)$$

where A, B, C, D, E, and P (with subscripts i,j omitted) are all constant.

These simultaneous equations were solved using the Gauss-Siedel iteration method (Patankar 1980). For problems involving a conservative field such as the Laplace equation, this scheme is particularly appealing since the sufficient convergence criterion of this scheme, the Scarborough criterion (Gastinel 1970)

$$|a_{ii}| > \sum_{j=1(j\neq i)}^{m} |a_{ij}| \qquad (5.23)$$

is always satisfied.

The steady state solution was also obtained using the block Gauss-Seidel iteration methods (Anderson et al. 1984). In contrast to the

normal Gauss-Seidel approach, which is a point iteration method, the block method uses a block iterative approach as described below. Starting from a known boundary, such as the top row (which is an adiabatic boundary), a row (or column) sweep can be formulated as illustrated in Figure 5.4. So for the ith row and (k+1)th iteration, the resulting equations are

$$(A\theta_{i,j} + B\theta_{i,j-1} + C\theta_{i,j+1})^{k+1} = Q \tag{5.24}$$

$$Q = P - D\theta^{k+1}_{i-1,j} - E\theta^{k}_{i+1,j} \tag{5.25}$$

where θ^{k+1} is from the previous sweep and θ^{k} is from the previous iteration, so that they are all known quantities. Thus, each equation in the ith row involves only three unknowns and each row forms a three-element tridiagonal matrix, which can now be readily solved by any of the direct methods, such as the Thomas algorithm (Thomas 1949).

The block iteration method, when applied to this particular problem, increased the actual computing time instead of decreasing it. Table 5.1 is a comparison between the point and block Gauss-Seidel iteration methods for various convergence parameters, ϵ. The convergence is checked by

$$\left| \frac{T^{k+1} - T^{k}}{T^{k+1}} \right| \leq \epsilon \tag{5.26}$$

The point and block methods yielded very similar results, as shown in Figure 5.5.

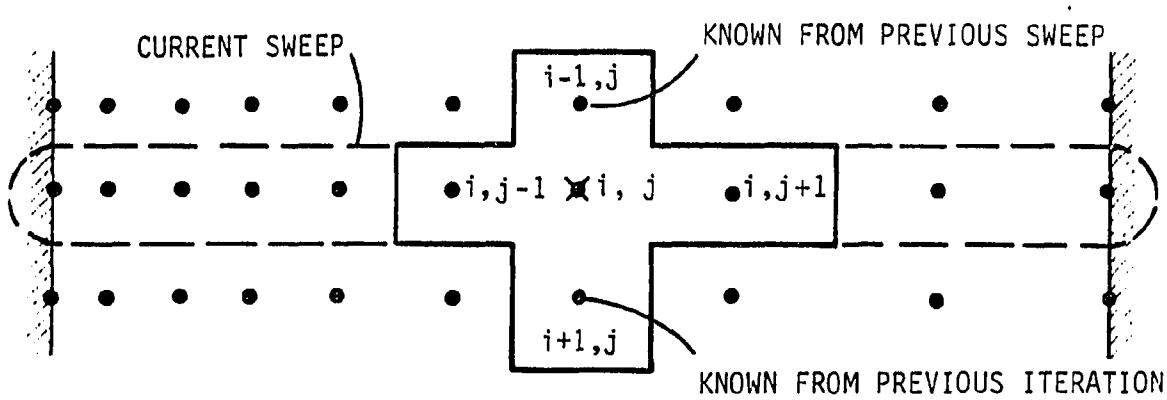

FIGURE 5.4. Illustration of block Gauss-Seidel iteration scheme

It should be noted that the convergence criterion showed a large effect on the final result. For different ϵ, not only the rate of solution was different, the final temperature distribution also converged at slightly different values. This behavior might have been caused by the curvilinear grids near the tube. These grids are not rectangular; therefore, directly applying the Laplace equation without transformation of coordinates for these grids might have resulted in this inconsistency. Nevertheless, these deviations are very small for low ϵ and the accuracy was acceptable.

Transient solution

An actual radiant panel heating system frequently operates in an unsteady state manner. Specifically, the hot water supply stops when

TABLE 5.1. Comparison of Point and Block Iterative Methods

Numerical Scheme	Convergence Criterion	Iteration Number	Execution Time(s)
Point iterative	5×10^{-5}	177	3.81
	1×10^{-5}	732	15.59
	1×10^{-7}	3945	83.75
Block iterative	5×10^{-5}	141	5.10
	1×10^{-5}	629	22.57
	1×10^{-6}	1808	64.67

the room temperature goes above the preset upper limit, and the operation resumes as the temperature drops below the lower limit. The unsteady state problem is also applicable during the start-up of the system.

Although implicit methods are frequently recommended for solving unsteady problems, explicit methods have advantages when applied to heat transfer problems involving radiation boundaries. Specifically, calculations of double iterations, which are required by implicit methods, may be more costly in terms of computation time than restrictions on the time increment caused by the explicit stability criteria. For example, a comparison of steady state calculations using the implicit method shows that the solution for each time increment will only be obtained after n-th iterations, where n is on the order of hundreds. In contrast, the explicit method requires no iterations, even though it does require marching with finer time increments. In

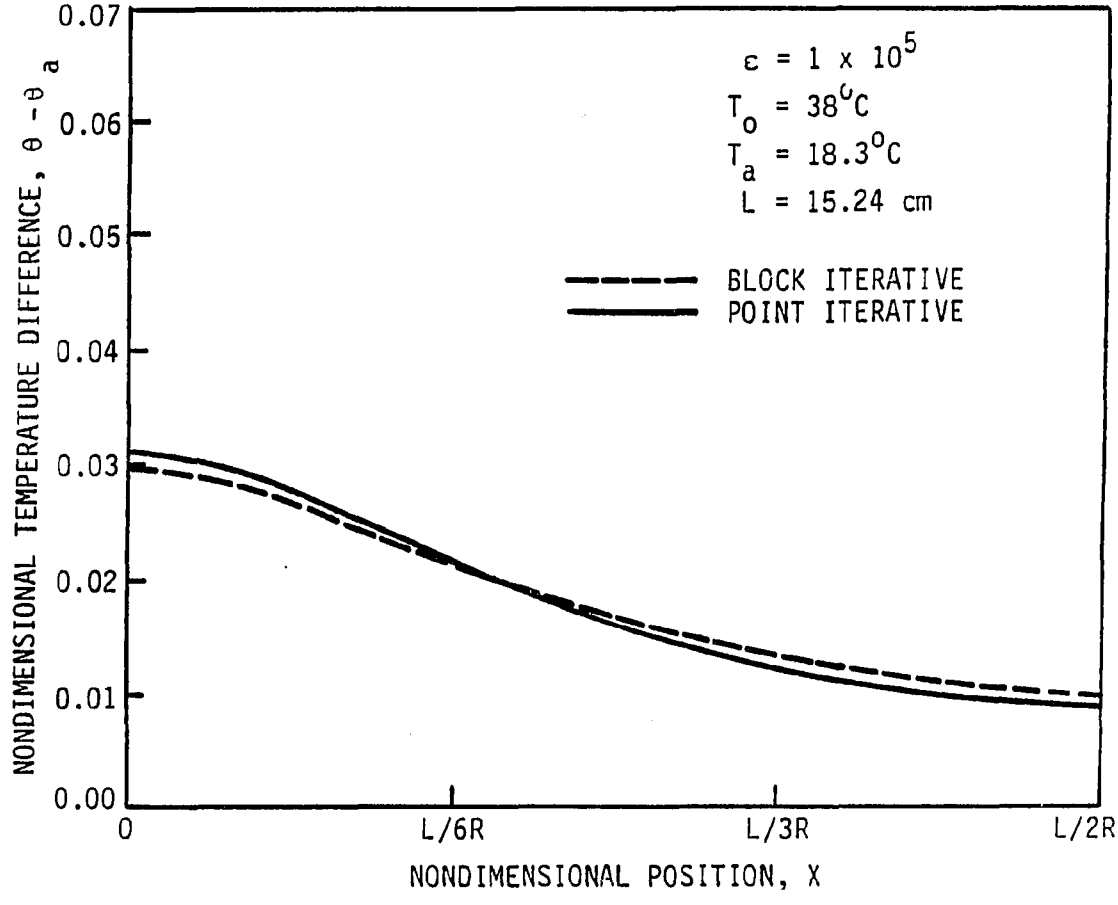

FIGURE 5.5. Nondimensional steady state temperature comparison for point and block iterative methods

other words, with roughly the same CPU time, an explicit method can afford a time increment one hundred or more times finer than an implicit method. Since such small time increments are usually unnecessary, an explicit method can mean less computation time. On the

basis of the above discussions, an explicit method was used to calculate the unsteady radiant heat transfer problem.

In similar fashion to the steady state formulation, by collecting the same θ terms in Eqs. (5.18) and (5.19), we get

$$F\theta^{n+1} = A'Q + B\theta_{i,j-1} + C\theta_{i,j+1} + D\theta_{i-1,j} + E\theta_{i+1,j} - P \quad (5.27)$$

where

$$A' = A + F \quad (5.28)$$

$$F = \frac{\Delta M_i \Delta N_j}{Fo} \quad (5.29)$$

This set of equations can be readily solved by marching from t = 0, assuming that the initial conditions are given. The time increment is restricted by the stability criterion as follows:

$$Fo\left(\frac{1}{(\Delta X)^2} + \frac{1}{(\Delta Y)^2}\right) \leq 1 \quad (5.30)$$

which for a moderate grid size (in this case, 0.254 X 0.127 cm) requires a time increment of about two seconds.

The transient model described above can also be used to calculate the steady state solution by marching to infinity or in practice until the temperature increase is negligible over the time increment. Steady state was generally reached in two to three hours, depending on the supply temperature. The computation time required by this method is comparable to or less than that of the Gauss-Seidel iteration scheme. In addition, this method has a significant advantage over the Gauss-Seidel iteration in that it not only yields the final steady state

solution but also furnishes the entire temperature history during the transient period. A FORTRAN program using this explicit scheme is listed in Appendix B.

Results

Before the results are presented, several comments are required concerning the selection of both physical and numerical parameters. The supply temperatures for radiant hydronic ceilings are usually in the range of 30 to 70°C. The supply temperature used herein is close to the lower temperature range, which is representative of solar collectors and heat pumps. A convection heat transfer coefficient of 5.5 $W/(m^2°C)$ was used because it represents an intermediate value of the 2 to 10 $W/(m^2°C)$ range suggested by Jennings (1978). The panel size is based on the standard radiant ceiling panel design (ASHRAE 1987) where tubes are separated by a distance of 15.24 cm and covered by a 2.54 cm layer of plaster; the hot water is carried in copper tubes having an outer diameter of 0.953 cm. The properties of plaster used in this analysis are (Holman 1981) C_p = 0.84 kJ/kg°C, k = 0.48 W/m°C, ρ = 1440 kg/m^3, and ϵ = 0.91. A grid size of M = 8, N = 12 was selected. Even though the temperature gradients were quite small, a fine grid size was required because of the curvilinear grids near the circular tube.

Temperature distributions along the ceiling surface are presented in Figure 5.6 for different times. The topmost line is the steady

state temperature distribution. The temperature gradients are zero at both ends of the ceiling section as expected for adiabatic boundaries at $x = 0$ and $L/2$. The curves also show that it takes more than 10 minutes for heat to diffuse from the copper tube to the centerline position at $x = L/2$. Of special importance is the observation from Figure 5.6 that it takes approximately two hours for steady state to be reached. This time period agrees qualitatively with experiments that were performed in Chapter 3.

Figure 5.7 compares the steady state temperature distribution obtained by the transient solution marching to infinity and the point-iterative method. The average difference between the point-iterative solution and the transient solution is about 1°C. Since the temperatures calculated by the numerical scheme were normalized by T_0, the percent difference in terms of the nondimensional temperature, using $T_0 = 311$ K, is only 0.0032. Figure 5.7 also shows that the results obtained by the iterative method are dependent on the convergence parameter. The main cause of this discrepancy is yet to be understood. It can be concluded, however, that the iterative method with a large tolerance does not yield reliable results. As the convergence parameter (ϵ) decreases, the surface temperature distribution moves toward the transient solution, although very slowly.

Figure 5.8 plots the heat flux per ceiling unit versus the temperature difference between the tube and the room for different values of the convection heat transfer coefficient, h. These results

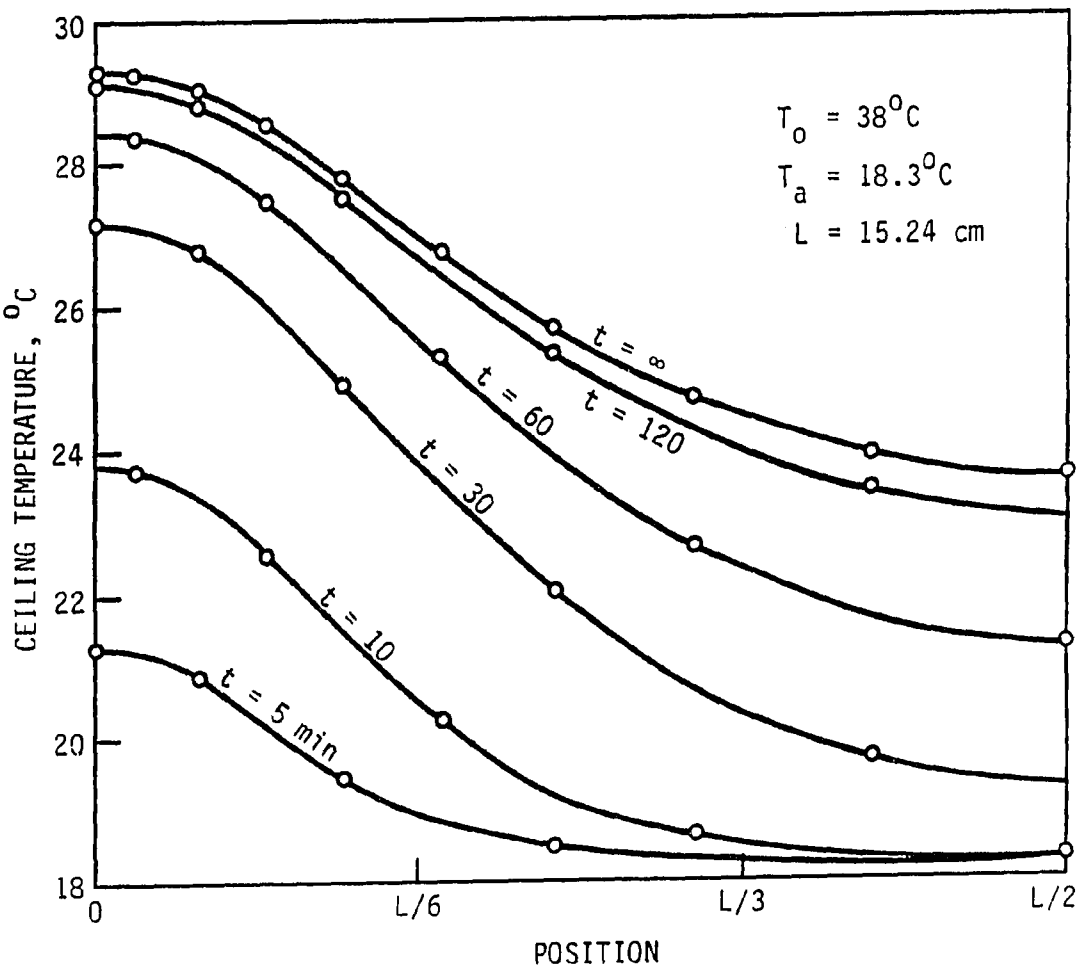

FIGURE 5.6. Ceiling surface temperature distribution at different times

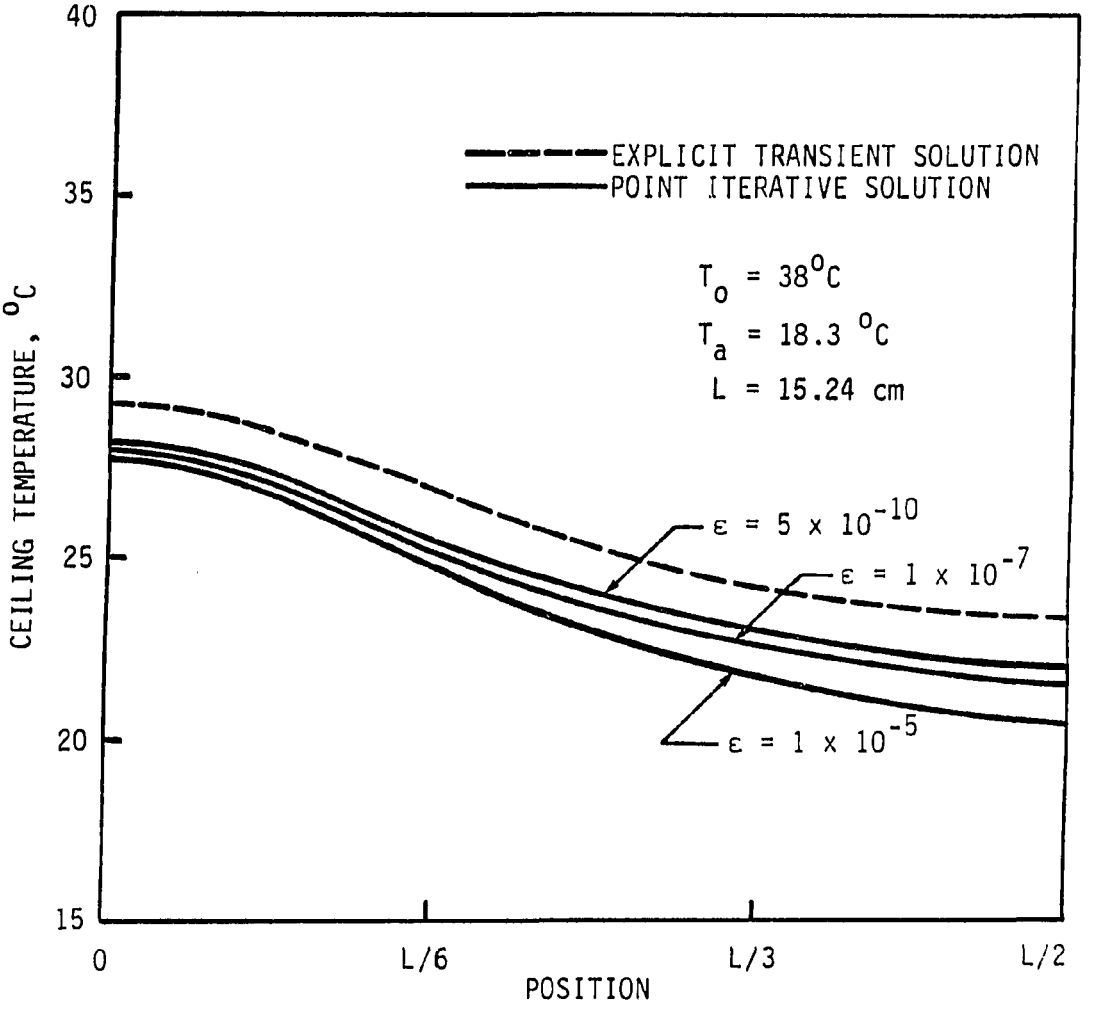

FIGURE 5.7. Steady state temperature comparison for explicit transient method and point iterative method

were obtained using the transient explicit model since this solution is independent of the tolerance parameter, ϵ. The interesting observation is that except for regions very close to the origin, a linear relation can be approximated between the heat flux and the tube temperature. In addition, as h goes to infinity, the heat flux approaches the value that corresponds to what would be obtained if the radiation-convection boundary is replaced by the Dirichlet boundary (i.e., a boundary with temperature specified) at the room temperature. Figure 5.8 shows that convection does not have a significant effect on the ceiling heat output, especially since the h value for a residential space is, as mentioned earlier, around 2 to 10 $W/m^2{}^oC$.

The numerical model's usefulness for radiant ceiling panel design can be demonstrated by observing the effect of tube spacing and plaster thickness on heat transfer. Figure 5.9 shows that increasing the distance between tubes beyond 15 cm does not result in a noticeable increase in heat flux. This result suggests that slight shifts in the adiabatic boundary (boundary 1), caused by slight temperature differences between adjacent tubes, will not change the predicted heat flux. Therefore, the original assumption of a line of symmetry halfway between the adjacent tubes is justified.

In contrast to the tube spacing, the thickness of the plaster has a greater effect on the heat flux. Figure 5.9 shows that the heat output increases with reduced plaster thicknesses. For example, using a supply temperature of 49°C, the heat output per unit length of tube

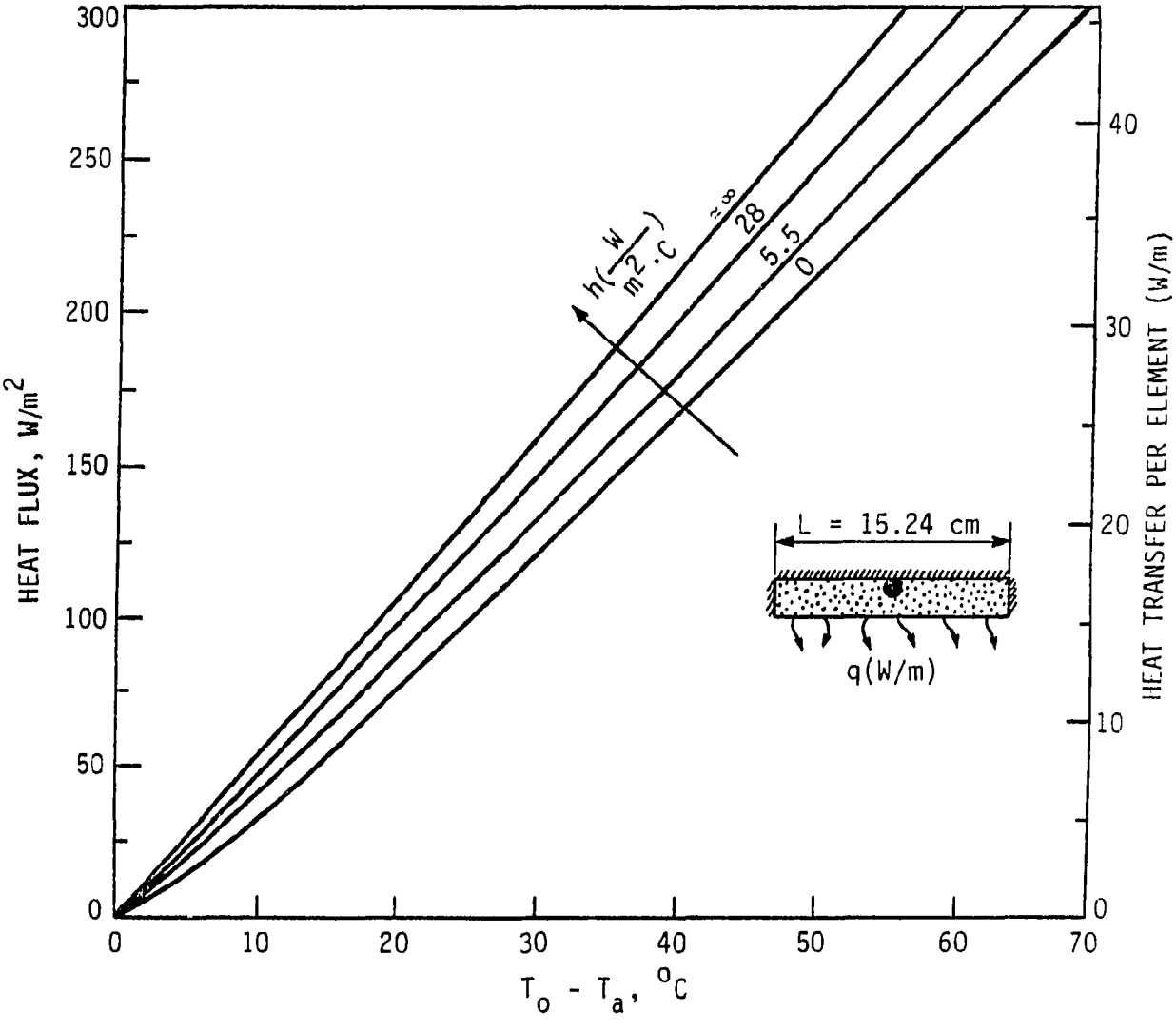

FIGURE 5.8. Ceiling panel heat flux variation with temperature difference under convection effects

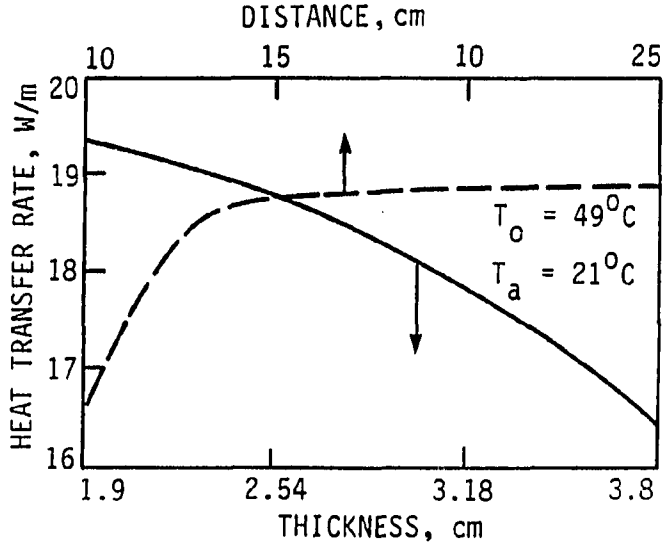

FIGURE 5.9. Effects of plaster thickness and tube spacing on heat output from panel unit

is about 16.7 W/m for a 38 mm thickness in comparison to 18.8 W/m for the standard 25.4 mm thickness. It should be noted that maximizing the heat flux is not the only consideration for determining an optimum plaster thickness. Other factors to be considered are construction convenience, panel heat storage, and surface temperature uniformity.

Figure 5.10 compares temperature distributions for different ceiling plaster thicknesses. As can be observed, increasing the thickness reduces the surface temperature variation. However, it should be noted that during the actual operation of a radiant ceiling panel the temperature distribution is probably more uniform than shown.

This results from an on-off operation, which is a common feature of most heating systems.

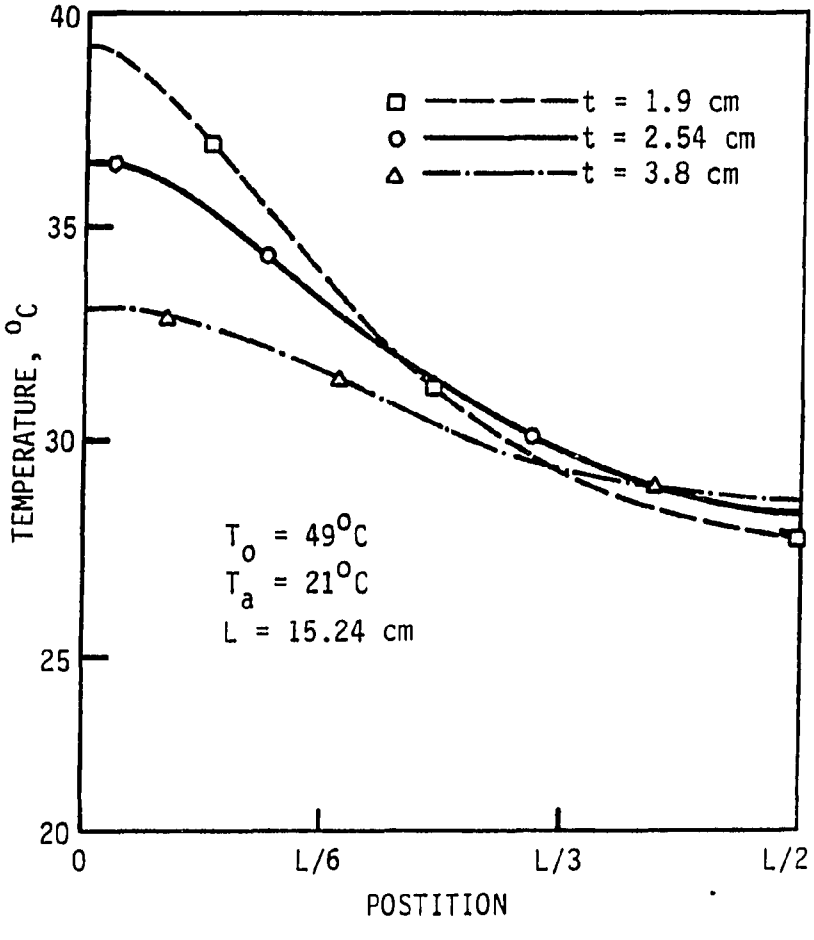

FIGURE 5.10. Effect of plaster thickness on surface temperature distribution

The numerical model can be used in the future to aid the design of a hydronic radiant ceiling and the selection of optimal sizes and

supply water temperature. An additional investigation is the subject of Chapter 7.

Conclusion

A two-dimensional panel unit was isolated for this study. The heat transfer from this unit was predicted using a numerical method. For solving the steady state problem, the point Gauss-Seidel iteration method was more effective than the block iterative method, in terms of both actual CPU time and memory space. This occurred even though the block iteration method had a faster convergence rate. In both methods, the tolerance affected the accuracy of the final results.

Transient state solutions were obtained using an explicit scheme. The advantages of using this scheme outweigh the disadvantages when compared to other schemes. Specifically, the presence of the fourth power of temperature (due to radiation) results in additional iterations for most implicit methods. The steady state can also be obtained from the transient calculation by proceeding to large times.

The output of the transient numerical model was the surface temperature distribution and panel unit heat transfer as functions of the tube temperature. Since there is no exact solution to this problem, it was difficult to evaluate the relative errors associated with the numerical methods. However, the results agrees qualitatively with experiments performed in Chapter 3.

In the future, the numerical model developed in this study can be used for designing and sizing radiant panel ceilings. In addition, the overall system performance can be related to controllable parameters such as the inlet water temperature, mass flow rate, total tube length, tube spacing, and plaster thickness.

CHAPTER 6 A SEMI-ANALYTICAL FORMULATION FOR HEAT TRANSFER FROM STRUCTURES WITH EMBEDDED TUBES

Introduction

The objective of this chapter is to develop a working correlation which can be used for design. This correlation relates the heat output from the hydronic radiant panel to the tube diameter, tube separation length, material covering the tubes, thickness of the covering, surface conditions (i.e., reflectivity and emissivity), surface orientation (i.e., ceiling or floor panel), temperature of the water flowing in the tubes, and room air temperature. It was formulated by examining cases for which an exact solution exists and then combining these analytical solutions to form a general correlation. Correction factors were added to the correlation in order to improve the agreement between the correlation and the results obtained by a finite-element solution for the same problem.

The heat-output correlation developed in this study has the advantage over numerical methods in that the interrelationships between various variables are explicit and the solution for a wide range of conditions is available immediately from a single equation. Therefore, the design process can be greatly simplified. In addition, this correlation is simple, easy to use, and unlike many empirical equations, it is also physically sound and dimensionally consistent.

Formulation of Physical Model

A typical panel section, consisting of a single tube in a two-dimension domain, is illustrated in Figure 6.1. The only difference between this panel unit and that studied in Chapter 5 is that this unit is twice of that unit. In addition, this unit is not confined to a ceiling panel. It may as well be part of a floor panel. A two-dimensional approximation is applicable because the temperature gradient in the axial direction of the tube is much smaller than the gradient in the perpendicular direction. The wall of the tube can be approximated as a constant temperature boundary equal to the water temperature for two reasons: First, the thermal conductivity of the tube wall is considerably higher than that of the solid material surrounding the tube; second, the thermal resistance between the tube wall and room air is several orders of magnitude greater than the convection resistance inside the tube. The side of the panel opposite to the space being heated is assumed to be an adiabatic boundary since it is generally well insulated in practice. Even though the tubes adjacent to the tube embedded in the panel section of interest may have a slightly different temperature, this temperature difference is assumed to have a negligible effect on heat transfer. Therefore, geometric symmetry leads to an approximation of adiabatic side boundaries. All of the heat exchange with ambient (i.e., adjoining air space) is assumed to take place at the panel surface by a combination of radiation and convection heat transfer.

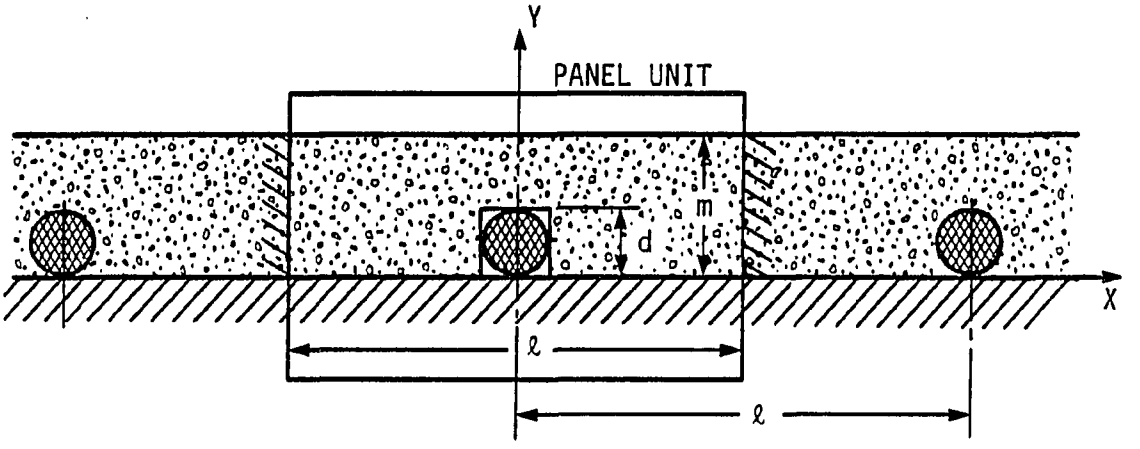

FIGURE 6.1. A typical heating panel unit isolated from the overall panel

Only homogeneous and isotropic conducting material is considered. The governing equation for the steady-state heat conduction is the Laplace equation

$$\frac{\partial^2 T}{\partial x^2} + \frac{\partial^2 T}{\partial y^2} = 0 \tag{6.1}$$

which is subjected to the following boundary conditions for those reasons mentioned above:

$$x = 1/2, \quad \frac{\partial T}{\partial x} = 0 \tag{6.2}$$

$$\text{at tube}, \quad T = T_0 \tag{6.3}$$

$$y = 0, \quad \frac{\partial T}{\partial y} = 0 \tag{6.4}$$

$$y = m, \quad \frac{\partial T}{\partial y} = -[\frac{h}{k}(T - T_\infty) + \frac{\epsilon\sigma F}{k}(T^4 - T_\infty^4)] \tag{6.5}$$

For moderate temperature differences between the surrounding air and embedded tube, the radiation term in Eq. (6.5) can be linearized by the following approximation:

$$T^4 - T_\infty^4 \cong 4\left(\frac{T + T_\infty}{2}\right)^3 (T - T_\infty) \tag{6.6}$$

Several nondimensional variables can be introduced for the purposes of reducing the number of variables required to define the problem. These variables are

$$Pi = \frac{\epsilon\sigma Fd}{k} T_0^3 \tag{6.7}$$

$$Bi = \frac{hd}{k} \tag{6.8}$$

$$Ti = T_\infty/T_0 \tag{6.9}$$

where Pi is the conduction-radiation parameter, Bi the conduction-convection parameter or the Biot number, and Ti the sink-source temperature ratio. Eq. (6.5) can be rewritten in a linear form

$$y = m, \quad \frac{\partial T}{\partial y} = -\frac{Hi}{d}(T - T_\infty) \tag{6.10}$$

where Hi is an equivalent heat transfer coefficient in the nondimensional form defined by

$$Hi = Bi + 4Pi(Ti_a)^3 \tag{6.11}$$

and Ti_a is a nondimensional average of the panel surface and ambient temperature defined by

$$Ti_a = \left(\frac{T + T_\infty}{2T_0}\right) \tag{6.12}$$

When the temperature difference between T_0 and T_∞ is moderate, then T can be approximated as the average of T_0 and T_∞ such that

$$T \cong \frac{(T_0 + T_\infty)}{2} \tag{6.13}$$

which leads

$$Ti_a = (\frac{1 + 3Ti}{4}) \tag{6.14}$$

Solution and Semi-Analytical Formulation

The solution to the above equations is greatly simplified if the round tube can be approximated as a square tube. This approximation is valid if the cross-sectional area of the panel is large relative to that of the tube, in which case the edge effects are dampened out as heat diffuses through the conducting medium. For other cases, a factor must be introduced to account for edge effects.

The solution can also be expressed in the nondimensional form by introducing two nondimensional length variables

$$L = (l - d)/d \tag{6.15}$$

$$M = (m - d)/d \tag{6.16}$$

These nondimensional numbers have specific geometric implications: L represents the normalized distance between tube edges and M the normalized thickness of the cover layer on top of the tube.

In order to obtain a correlation with physical justifications, it is necessary to examine those cases for which an analytical or exact solution is possible.

Solution as $L \to 0$

As L approaches zero, then l approaches d, which corresponds to the case where the hot tubes are packed together as shown in Figure 6.2. When the round tube is approximated as a square tube, then a simple one-dimensional heat conduction problem with the prescribed boundary conditions results. A solution for this simple case is easily obtained using the electric circuit analogy. Considering heat transfer as a combined series and parallel loop, the equivalent thermal resistance is

$$R = \frac{m - d}{k} + \left(h + 4\epsilon\sigma F \left(\frac{T + T_\infty}{2} \right)^3 \right)^{-1} \tag{6.17}$$

which can be expressed in terms of the nondimensional numbers as follows:

$$Ri = \frac{Rk}{m - d} = \frac{HiM + 1}{HiM} \tag{6.18}$$

The heat flux is then

$$q = \frac{T_0 - T_\infty}{R} = \frac{k(T_0 - T_\infty)}{m - d} \left(\frac{HiM}{HiM + 1} \right) \tag{6.19}$$

If the nondimensional heat output Qi is defined by

$$Qi = \frac{ql}{k(T_0 - T_\infty)} \tag{6.20}$$

then

$$Qi = \frac{Hi}{HiM + 1} \tag{6.21}$$

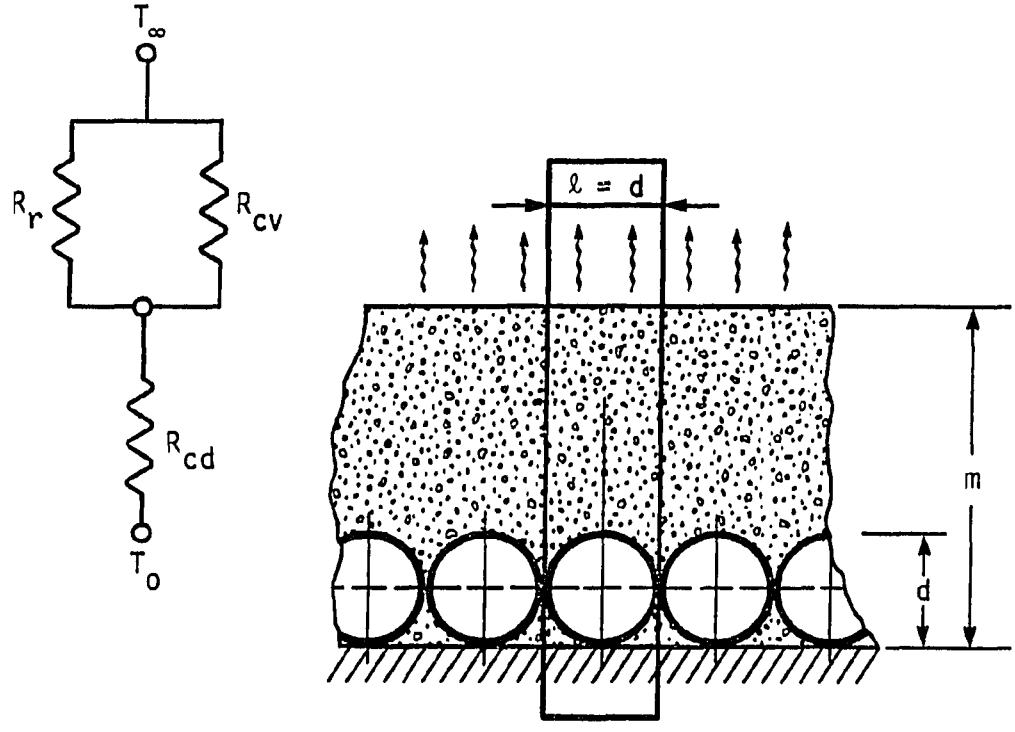

FIGURE 6.2. A heating panel model for the extreme case of L=0

Eq. (6.21) is accurate if M is sufficiently large, but errors may result if M is small. An alternative solution, which is developed below, takes into account the round tube geometry while neglecting heat flow in the x direction. Heat output from a differential increment of the tube surface is

$$dq = \frac{(T_0 - T_\infty)}{(y/k + 1/\bar{h})}\, dx \qquad (6.22)$$

where y is the distance between tube surface and panel surface as shown in Figure 6.2:

$$y = (m - d) + \left(\frac{d}{2} - \sqrt{\left(\frac{d}{2}\right)^2 - x^2} \right) \tag{6.23}$$

and $\bar{h}$ is the equivalent heat transfer coefficient

$$\bar{h} = h + 4\epsilon\sigma F \cdot T_0^3 \cdot Ti_a^3 \tag{6.24}$$

The heat output from the unit can be obtained by integrating Eq. (6.22) over the surface as follows:

$$ql = qd = 2 \int_0^{d/2} \frac{k(T_0 - T_\infty)\, dx}{(m - d) + \left(\frac{d}{2} - \sqrt{\left(\frac{d}{2}\right)^2 - x^2} \right) + k/\bar{h}} \tag{6.25}$$

The nondimensional form of the heat output equation is then

$$Qi = 2 \int_0^1 \frac{du}{(1 - \sqrt{1 - u^2} + 2/Ui)} \tag{6.26}$$

where

$$u = x/\left(\frac{d}{2}\right) \tag{6.27}$$

and

$$Ui = \frac{Hi}{HiM + 1} \tag{6.28}$$

The parameter, Ui, can be interpreted as a nondimensional thermal transmittance for the case where Eq. (6.21) is applicable. Eq. (6.26) was integrated using Simpson's rule with Ui as an influencing parameter. Nondimensional heat output, Qi, is plotted versus Ui in Figure 6.3 for Eqs. (21) and (26). The large difference between the

two equations in the high Ui region is due to geometry effects, which become stronger as Hi increases and M decreases.

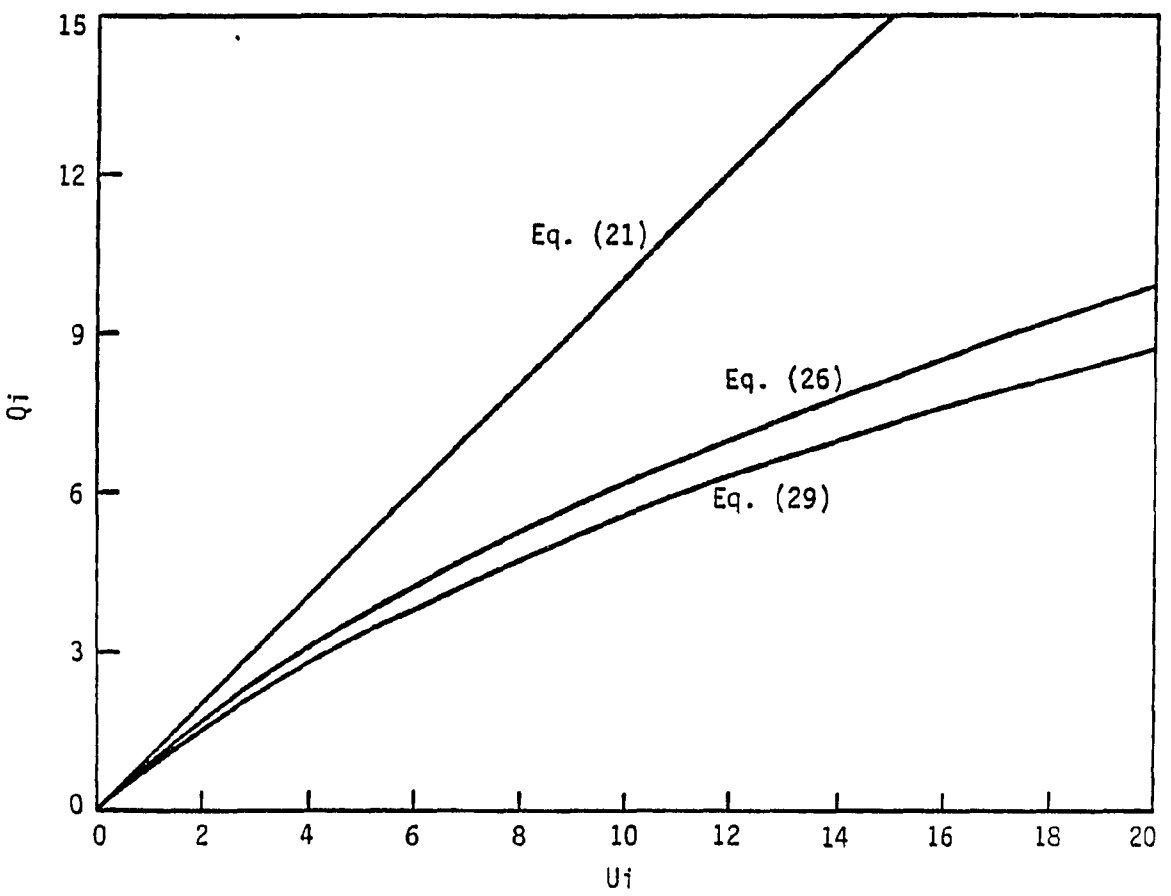

FIGURE 6.3. Comparison of heat outputs obtained by different equations

Using the numerical results as a close approximation of the exact solution, a correction factor was introduced into Eq. (6.21) by trial and error so that the resulting equation will be equivalent to Eq. (6.26). The resulting correlation for heat output is

$$Qi = \tanh[(2/Ui)^{1/3}]\cdot Ui \tag{6.29}$$

or

$$qd = k(T_0 - T_\infty)\cdot\tanh[(2/Ui)^{1/3}]\cdot Ui \tag{6.30}$$

As Ui gets smaller, Eq. (6.29) approaches Eq. (6.21). This behavior is physically justified since Ui decreases with increasing M and decreasing Hi, which also corresponds to a condition which dampens out geometric effects. Eq. (6.29) is also plotted in Figure 6.3. Although Eq. (6.26) can be more accurately represented by a polynomial equation, Eq. (6.29) has the advantage of being simple and physically sound in that it satisfies several extreme conditions.

Solution as M → 0

As M approaches zero, m approaches d. This corresponds to a condition where the structure does not extend out beyond the diameter of the tubes as shown in Figure 6.4. The panel unit in Figure 6.4 can be divided into three regions with regions 1 and 3 being mirrors of each other and region 2 representing the tube region. The heat transfer characteristics of regions 1 and 3 are similar to those of an adiabatic end fin, if the round tube is, again, approximated as a square one. For symmetry, only region 1 of the panel section needs to

be analyzed. The governing equation can be derived by applying the conservation of energy to a differential element so that the resulting equation is (Arpaci 1966)

$$\frac{d^2T}{dx^2} - \frac{h}{kd}(T - T_\infty) - \frac{\epsilon\sigma F}{kd}(T^4 - T_\infty^4) = 0 \tag{6.31}$$

which is subject to the following two boundary conditions:

$$x = 0, \quad \frac{dT}{dx} = 0 \tag{6.32}$$

and

$$x = (1 - d)/2, \quad T = T_0 \tag{6.33}$$

These equations can be normalized by introducing

$$\theta = T/T_0, \qquad X = x/d, \qquad \phi = \theta - \theta_\infty \tag{6.34}$$

and then linearizing the radiation term by Eq. (6.6). Eqs. (6.31) through (6.33) can be rewritten as

$$\frac{d^2\phi}{dX^2} - Hi\phi = 0 \tag{6.35}$$

and

$$X = 0, \quad \frac{d\phi}{dX} = 0 \tag{6.36}$$

$$X = L/2, \quad \phi = 1 - \theta_\infty \tag{6.37}$$

where Hi is defined by Eq. (6.11).

The solution to the governing differential equation, Eq. (6.35), subject to the boundary conditions in Eqs. (6.36) and (6.37), is

$$\phi = (1 - \theta_\infty)\frac{\cosh(\sqrt{Hi}\cdot X)}{\cosh(\sqrt{Hi}\cdot L/2)} \tag{6.38}$$

The heat output from region 1 is equal to the heat leaving the tube through conduction, which is analogous to heat transfer out of the base of a fin, so that

$$q(\frac{1 - d}{2}) = k(T_0 - T_\infty)\cdot\sqrt{Hi}\cdot\tanh(\sqrt{Hi}\cdot L/2) \tag{6.39}$$

The heat output directly from the embedded tube (i.e., region 2) is

$$qd = k(T_0 - T_\infty)Hi \tag{6.40}$$

The total heat output from a panel section is obtained by summing the heat outputs from the three regions

$$q1 = k(T_0 - T_\infty)[2\sqrt{Hi}\cdot\tanh(\sqrt{Hi}\cdot L/2) + Hi] \tag{6.41}$$

or in the nondimensional form

$$Qi = 2\sqrt{Hi}\cdot\tanh(\sqrt{Hi}\cdot L/2) + Hi \tag{6.42}$$

As L approaches infinity (i.e., the distance between tubes greatly increases), $\tanh(\sqrt{Hi}L/2)$ approaches unity, so that the heat output approaches a maximum value of

$$Qi_{max} = 2\sqrt{Hi} + Hi \tag{6.43}$$

General solution

A general case, which represents a typical heating panel with embedded tubes, can be obtained by adding a conducting layer of thickness (m-d) to the structure in Figure 6.5. Using an approximation similar to that for Eq. (6.31) used in the previous section, the following governing differential equation can be obtained for region 1:

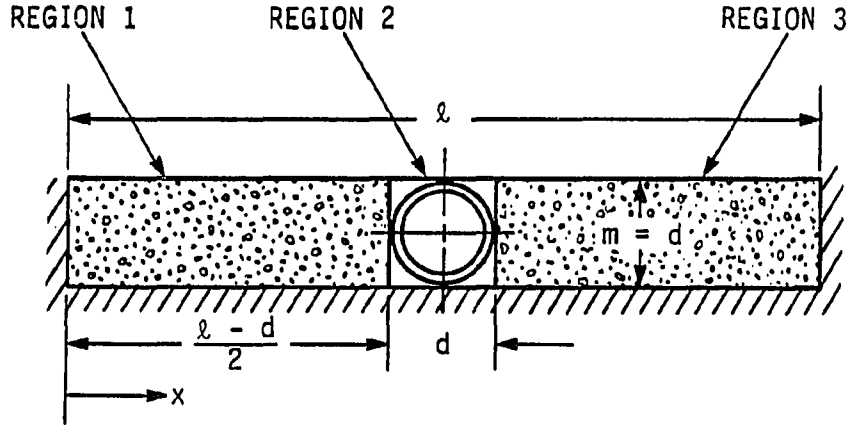

FIGURE 6.4. A heating panel model for the extreme case of M=0

$$\frac{d^2\phi}{dx^2} - Ui\phi = 0 \tag{6.44}$$

Recalling the solution that was obtained for Eq. (6.35), the solution to Eq. (6.44) is

$$\phi = (1 - \theta_\infty)\frac{\cosh(\sqrt{Ui}\cdot X)}{\cosh(\sqrt{Ui}\cdot L/2)} \tag{6.45}$$

where Ui is defined by Eq. (6.28).

Since this is an approximate solution, a correction term should be added to obtain a final solution which more closely agrees with the results obtained by a numerical method approach. Therefore, the heat output from region 1 with the correction term represented by CT is

$$q(1 - d)/2 = k(T_0 - T_\infty)\cdot\sqrt{Ui}\cdot\tanh(\sqrt{Ui}\cdot L/2) + CT/2 \tag{6.46}$$

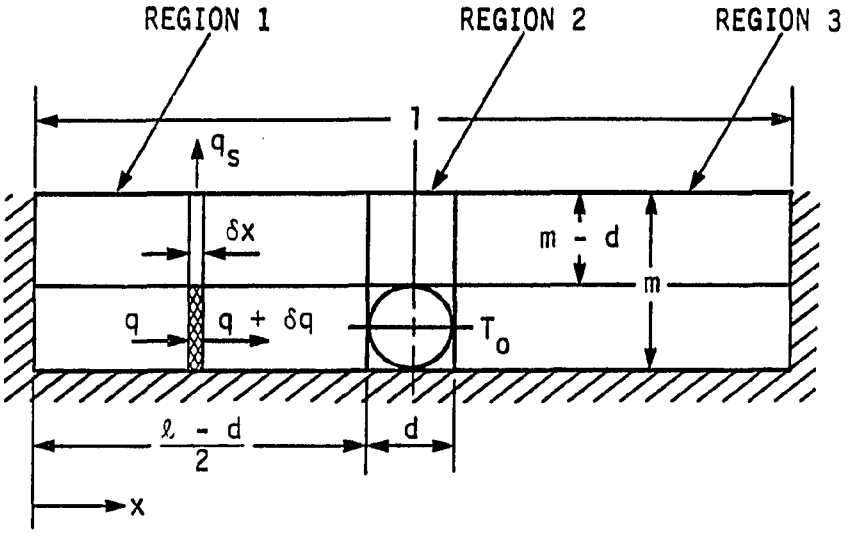

FIGURE 6.5. A heating panel model for the general case of L≠0, M≠0

The heat output from region 2 is approximately the same as that from Eq. (6.30). Therefore, in terms of nondimensional parameters, the heat output from a complete panel section is twice Eq. (6.46) plus Eq. (6.30):

$$Qi = 2\sqrt{Ui}\cdot\tanh(\sqrt{Ui}\cdot L/2) + CT + Ui\cdot\tanh[(2/Ui)^{1/3}] \qquad (6.47)$$

where the correction term, CT, accounts for all the effects that may occur in the approximations, namely, neglecting X direction heat flow and approximating the round tube as a square tube when calculating heat transfer from regions 1 and 3. Even though the first and third terms in Eq. (6.47) were derived using an analytical approach, the correction

term was obtained by a trial-and-error method. Specifically, a correction term was derived that minimizes the difference between Qi values obtained from Eq. (6.47) and those calculated using a numerical method, which more closely approximates an exact solution. The numerical method used was a canned finite-element package called ADINAT (1980). A commanding module for executing this code and a FORTRAN program creating the input data for the ADINAT are listed in Appendix C. The optimal correction term that minimizes errors from Eq. (6.47) is:

$$CT = 0.2\left(\frac{M}{M + Hi}\right)\left(1 - e^{-\beta L^2}\right) \tag{6.48}$$

where

$$\beta = 0.015\left(1 - e^{-1.5M^2}\right) \tag{6.49}$$

In summary, the general expression for nondimensional heat output from a complete panel section is give by Eq. (6.47) with the correction term defined by Eqs. (6.48) and (6.49).

Discussion

The semi-analytical formula, Eq. (6.47), approximately satisfies most extreme cases. These extreme cases are as follows:

1. $L = 0$. The structure resembles one-dimensional heat conduction with an essential and a mixed boundary condition.
2. $L = 0$ and $M \to \infty$. The heat flux leaving the structure is zero.

3. $M = 0$. The structure resembles a fin with an adiabatic tip for which there is an exact solution available.
4. $M = 0$ and $L \to \infty$. The structure resembles an infinite fin for which there is also an exact solution available.
5. $Bi \to \infty$. The mixed boundary approaches an essential boundary with T_∞ imposed on it.

The agreement between the general semi-analytical solutions that exist for several of the above extreme cases supports the physical soundness of this formulation. However, for the case when both Bi and $Pi = 0$, a physically unsound situation is encountered, i.e., a constant temperature source enclosed by adiabatic boundaries. Even so, the applicability of the semi-analytical method is not jeopardized, since the Bi and Pi parameters do not approach zero for practical applications.

The semi-analytical formula, Eq. (6.47), may not be valid when applied to certain cases that violate the various assumptions that were made in deriving the equation. One example is when the embedded tube or piping system carries very hot fluids (e.g., hot gases) so that the tube temperature is much greater than the ambient temperature. Under these circumstances the linearization of the radiation term may introduce large errors so that Eq. (6.47) becomes invalid.

Another example, which concerns geometrical extremes, is when the tubes are very closely packed or when the tubes are only slightly covered so that edge effects become very pronounced. Although a factor

has been incorporated into Eq. (6.47) to account for edge effects, errors could still occur. Finally, when the convective heat transfer coefficient, h, approaches infinity (i.e., the ambient temperature approaches the panel surface temperature) and M = 0, the solution based on the square tube approximation will have a line of singularity. Even though this has been eliminated by introducing a round tube approximation in Eq. (6.29), the results are likely to deviate.

For nearly all practical applications, the special conditions discussed above are unrealistic so that Eq. (6.47) is generally valid for analyzing heat transfer from embedded tubes. For most practical cases, the differences between the numerical and the correlational results are less than 5%. For the application of a hydronic radiant panel ceiling, the correlation predicts the heat output to within 1.5% of the numerical solutions. These differences are shown in Table 6.1 for a wide range of Hi, L, and M which are the nondimensional numbers that influence the total heat output from the panel section.

Figures 6.6 and 6.7 show explicitly the relationship between Qi and the Hi, L, and M. As shown in Figure 6.6, the heat output, Qi, increases with L, which represents the tube separation distance and thus the panel surface area, until a maximum value is approached. This maximum value increases with Hi, the nondimensional heat transfer coefficient, and decreases with increasing M, the thickness of the tube cover. The effect of M on Qi is shown in Figure 6.7.

TABLE 6.1. Comparison of Qi from Eq. (6.47) and Qi from finite-element solution

M	L	Hi	Qi, Eq.(6.47)	Qi, f.e.	Error(%)
1.8		1.0	0.8305	0.8619	3.6
	15	0.5	0.7178	0.7546	4.9
		0.1	0.4278	0.4502	5.0
		1.0	0.8281	0.8592	3.6
	8	0.5	0.7146	0.7483	4.5
		0.1	0.4173	0.4076	-2.4
		1.0	0.6037	0.5796	-4.2
	2	0.5	0.4686	0.4494	-4.2
		0.1	0.1736	0.1606	-8.1
0.6		1.0	1.1092	1.0830	-2.4
	15	0.5	0.8551	0.8477	-0.9
		0.1	0.4391	0.4107	-6.9
		1.0	1.1002	1.0819	-1.7
	8	0.5	0.8419	0.8463	-0.5
		0.1	0.4126	0.3934	-4.9
		1.0	0.9390	0.8852	-6.1
	2	0.5	0.6368	0.6115	-4.1
		0.1	0.1838	0.1772	-3.7
1.2[a]	15	0.1	0.4353	0.4375	0.5

[a]Represents a typical radiant ceiling panel.

Conclusion

A semi-analytical formula, Eq. (6.47), was obtained which expresses a nondimensional heat output, Qi, from a panel structure with embedded tubes in terms of three nondimensional parameters (L, M, and

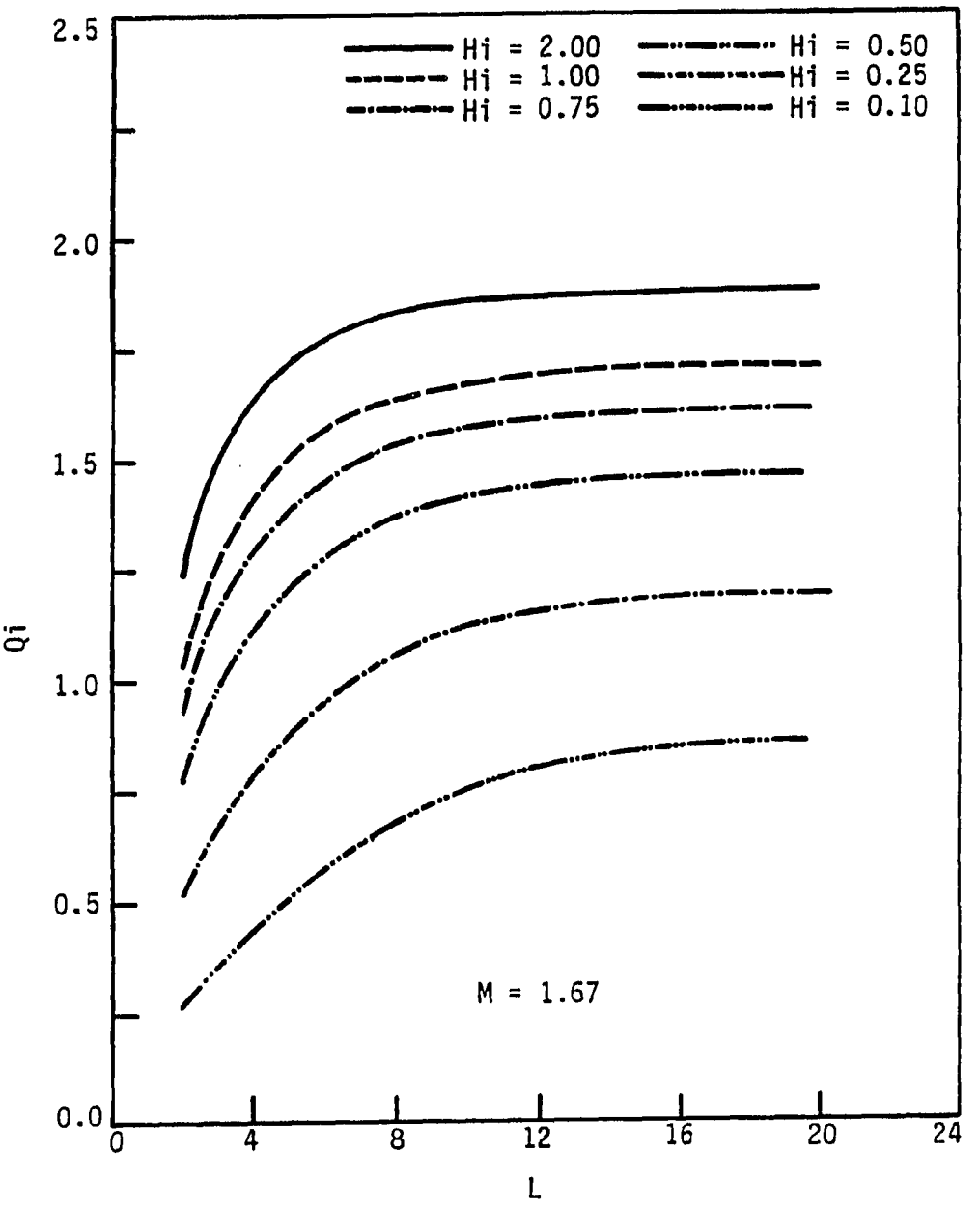

FIGURE 6.6. Heat output Qi as a function of tube separation distance L and equivalent heat transfer coefficient Hi

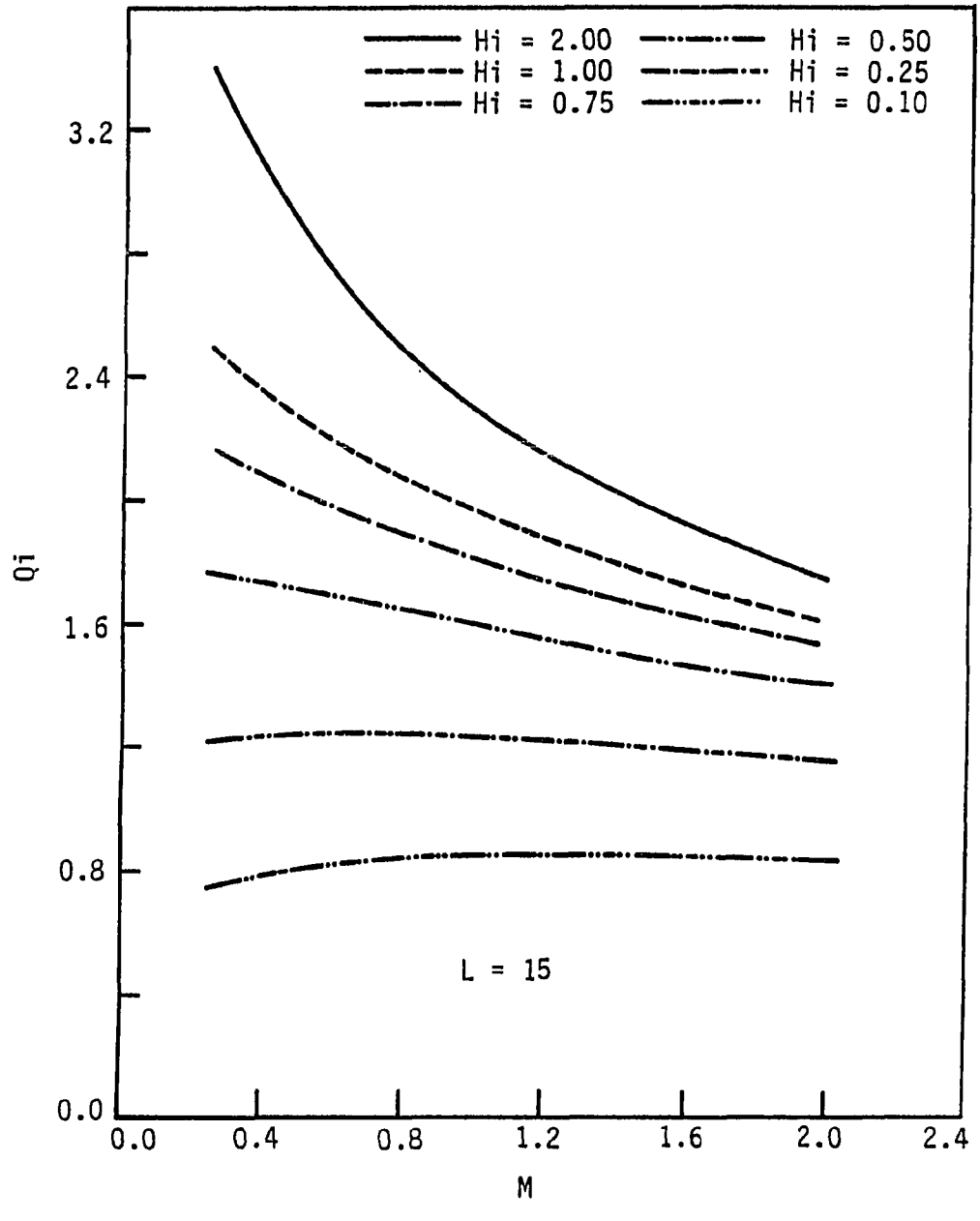

FIGURE 6.7. Heat output Qi as a function of cover thickness M and equivalent heat transfer coefficient Hi

Hi). This correlation was developed by solving the heat diffusion equations for several extreme cases where analytical solutions exist and then combining these solutions along with a correction term so that the resulting equation approximately describes the heat transfer from the panel surface. The correction term was derived by using a trial-and-error approach which minimized the differences between the correlation and a finite-element solution. The agreement between the semi-analytical correlation and the finite-element solution was generally within 5% for a wide range of conditions representing practical cases.

The semi-analytical formula has advantages in that it explicitly relates the heat output from the structure to the various physical and geometrical parameters. In addition, this heat output can be easily calculated using a single equation. As a result, the thermal design of structures that contain embedded tubes for heating is greatly simplified.

CHAPTER 7 A NEW METHOD FOR DESIGNING A HYDRONIC HEATING PANEL

Introduction

A detailed procedure for designing a hydronic radiant panel is presented in the ASHRAE Handbook (1987). A weakness in one of the design methods presented by ASHRAE is that the panel surface temperature is the fundamental design parameter even though it is neither easily controllable nor directly known during the actual operation of a panel system. Another complication of using panel surface temperatures as a design parameter is that these temperatures are not uniform during operation, because the spot directly beneath the embedded tube is always warmer than the neighboring area. Depending on the tube arrangement, the ceiling panel as a whole may also show a global temperature variation. Therefore, it may not be practical to refer to the panel temperature without first specifying the method for averaging these temperatures.

ASHRAE (1987) also presents two very useful charts for estimating the heat output from both ceiling panels and floor panels. In order to use these charts, the equivalent thermal resistance for a panel of interest must be determined. The values of thermal resistance for most practical panel structures are listed in Table 1 through Table 3 in Chapter 7 of the ASHRAE Handbook (1987).

One drawback of the ASHRAE method is that it does not take into account the possible variations of convective heat transfer coefficient

and surface emissivity from system to system. However, for common panels and enclosure conditions where the ranges of these two parameters are small, these variations are insignificant and the ASHRAE method is widely applicable. Another drawback of the ASHRAE method, as presented in the Handbook, is that it is graphic oriented, which makes it difficult to incorporate the method into a computer system simulation for heating panel systems.

The design methodology presented herein relates the supply water temperature, panel heat output, and physical characteristics of the panel to each other. Also the design method focuses on the panel heat output as a function of supply water temperature rather than panel surface temperature. An example of a typical design calculation is that for a specific panel structure, panel material, and supply water temperature, the minimum panel size can be determined. Another example is that if the panel size is given, then the minimum water supply temperature or flow rate can be determined for a precalculated heating load. In either case, the design calculation can be performed without knowing the panel surface temperatures.

This design procedure is relevant to hydronic radiant panels which occupy large surface areas of a ceiling, and thus operate at low-temperature, that is, at surface temperatures slightly higher than the room air temperature. For this situation, the operative temperature (defined as the uniform temperature of an enclosure in which an occupant would exchange the same amount of heat by radiation plus

convection as in the actual non-uniform environment) is very close to the room air temperature so that the knowledge of the panel surface temperature is not required for calculating the operative temperature (defined in Chapter 4). For example, with a mean panel surface temperature of 32°C (90F) and a typical room air temperature of 24°C (75F), the operative temperature is only 24.8°C (76.6F) which is close to the room temperature.

Even though the new method presented herein was developed for the purpose of designing hydronic radiant ceiling panels that are used for space heating, it is also applicable for designing wall and floor heating panels provided that one side of the panel is well insulated. The difference between a ceiling panel and a floor panel is that combined radiation and convection is the major mode for heat transfer from the surface for a ceiling panel while free convection is dominant for a floor panel. This new design method utilizes the semi-analytical correlation, developed in the last Chapter, to approximate the heat output from a panel. Therefore, the work presented herein is a continuation of this previous study with special emphasis on demonstrating heating panel design.

Fundamental Relations

The fundamental relationships between local panel heat output per unit length of the embedded tube and various physical and geometrical parameters were developed in Chapter 6. These parameters include the

thermal conductivity of the panel material (k), the panel surface emissivity (ϵ), the average convective heat transfer coefficient (h), the shape factor (F), the tube diameter (d), the tube spacing (l), the tube cover thickness (m), the room air temperature or AUST(Average Unheated Surface Temperature, T_∞), which was shown to approximate room air temperature (Schutrum et al. 1953), and the local water temperature (T). In order to reduce the number of independent variables, these parameters were grouped in Chapter 6 to form five dimensionless parameters: L, M, Bi, Pi, and Ti, with L representing the dimensionless tube spacing, M the dimensionless cover thickness, Bi the conduction-convection number, Pi the conduction-radiation number, and Ti the source-sink temperature ratio. The heat output per unit length of embedded tube, was also nondimensionally represented by Qi, which stands for the heat transfer from a panel unit including a tube site. For practical purposes the number of parameters can be further reduced by combining Bi, Pi, and Ti into a single dimensionless parameter, Hi, which represents the nondimensional combined radiation and convection heat transfer coefficient. All these numbers are defined in Chapter 6. A semi-analytical formula was developed in Chapter 6 which explicitly describes Qi as a function of L, M, and Hi for low-temperature radiant panels. This correlation, Eq. (6.47) is based on assumptions that one side of the panel is well insulated and the supply temperature is less than 90°C (195F) so that the non-linear effects are not significant. This relation was compared with the results of a finite-element analysis and good agreement was found.

Figures 7.1 through 7.4 are radiant heat flux charts plotted using this formula. With these charts, the heat output per unit length of embedded tube of a radiant panel can be readily determined, thus greatly simplifying the calculation procedure.

It should be emphasized that in order to obtain Bi, the convective heat transfer coefficient, h, should be known. There are a variety of approaches to obtaining h, depending on the panel orientation and whether the air motion is forced due to ventilation, natural due to buoyancy, or a combination of the two effects. Convection in panel systems is usually considered to be free convection caused by air motion due to induced buoyancy. However, some panel systems also incorporate mechanical ventilation, and convection for this case can be combined forced and free convection. Convection values are very difficult to establish, and many factors are involved in the calculation. ASHRAE Handbook (1987) presents the following equations for calculating convection heat transfer due to natural causes:

$$q_c = 0.041(T_p - T_\infty)^{1.25}/D_e^{0.25} \qquad \text{for ceiling panel}$$

$$q_c = 0.390(T_p - T_\infty)^{1.31}/D_e^{0.08} \qquad \text{for floor panel}$$

$$q_c = 0.290(T_p - T_\infty)^{1.32}/D_e^{0.05} \qquad \text{for wall panel}$$

where q_c is heat flux from the panel, T_p is panel mean surface temperature, T_∞ is the ambient temperature, D_e is the panel characteristic dimension (equivalent diameter), and H is the height of

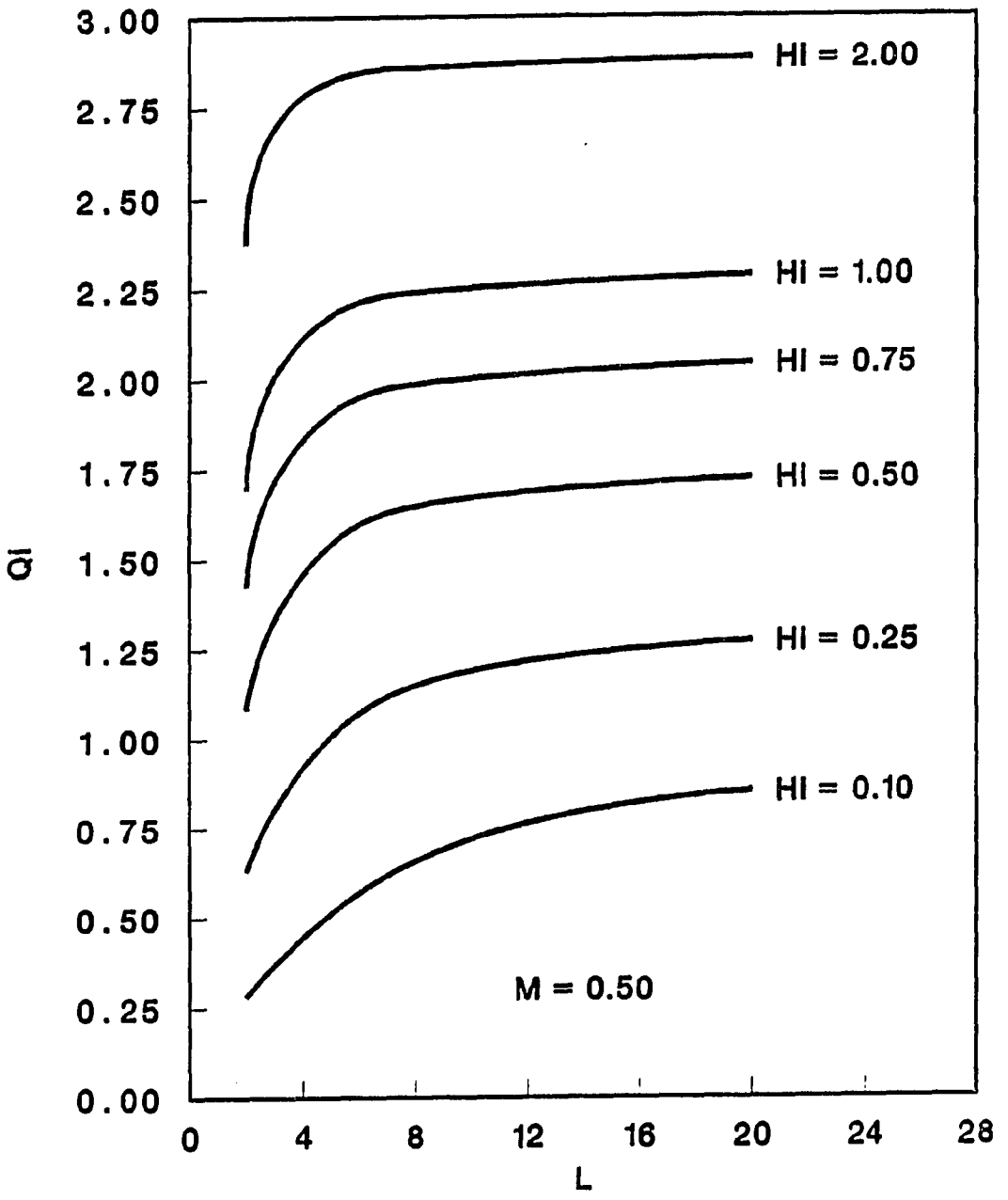

FIGURE 7.1. Radiant heat flux chart, M = 0.5

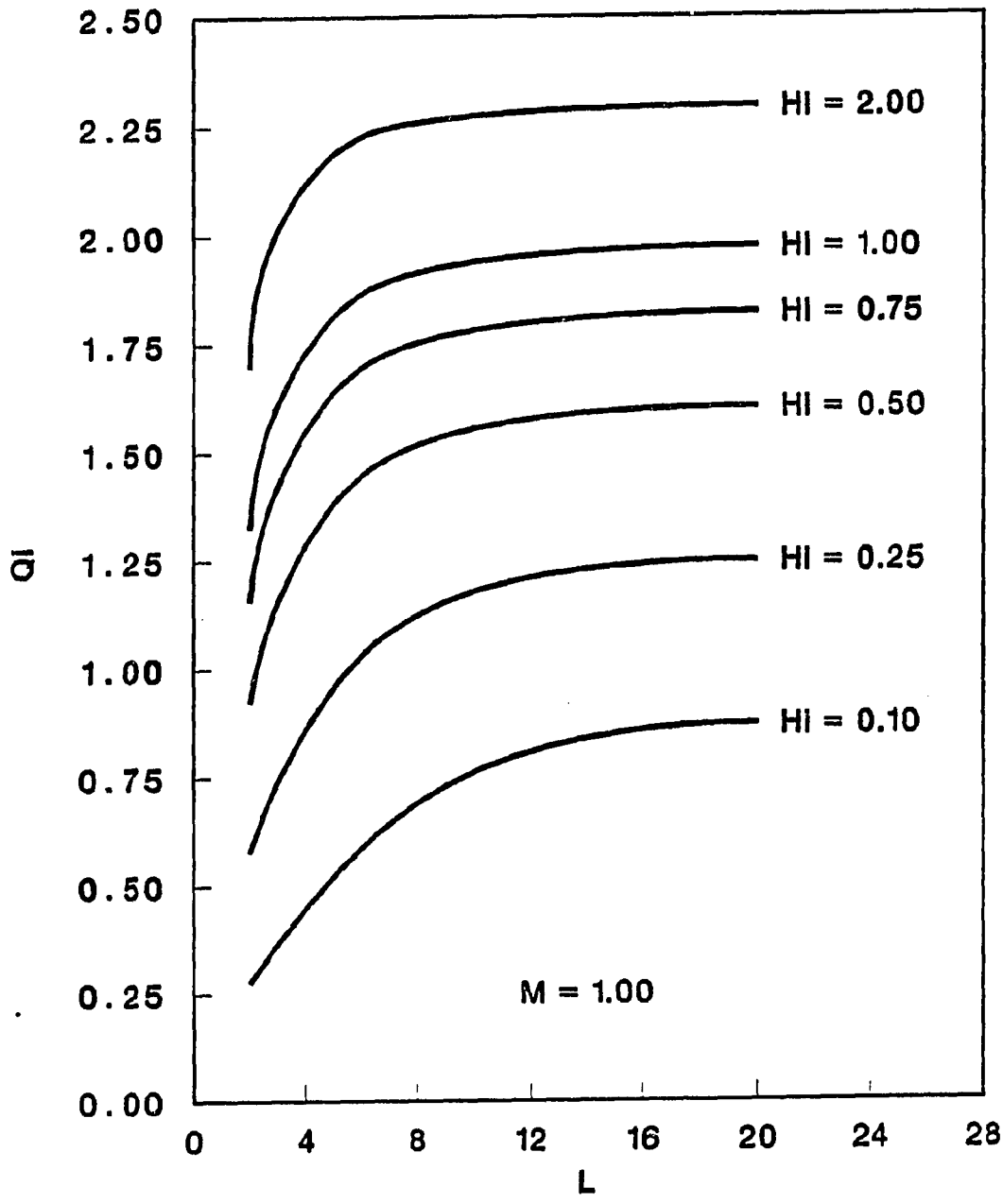

FIGURE 7.2. Radiant heat flux chart, M = 1.0

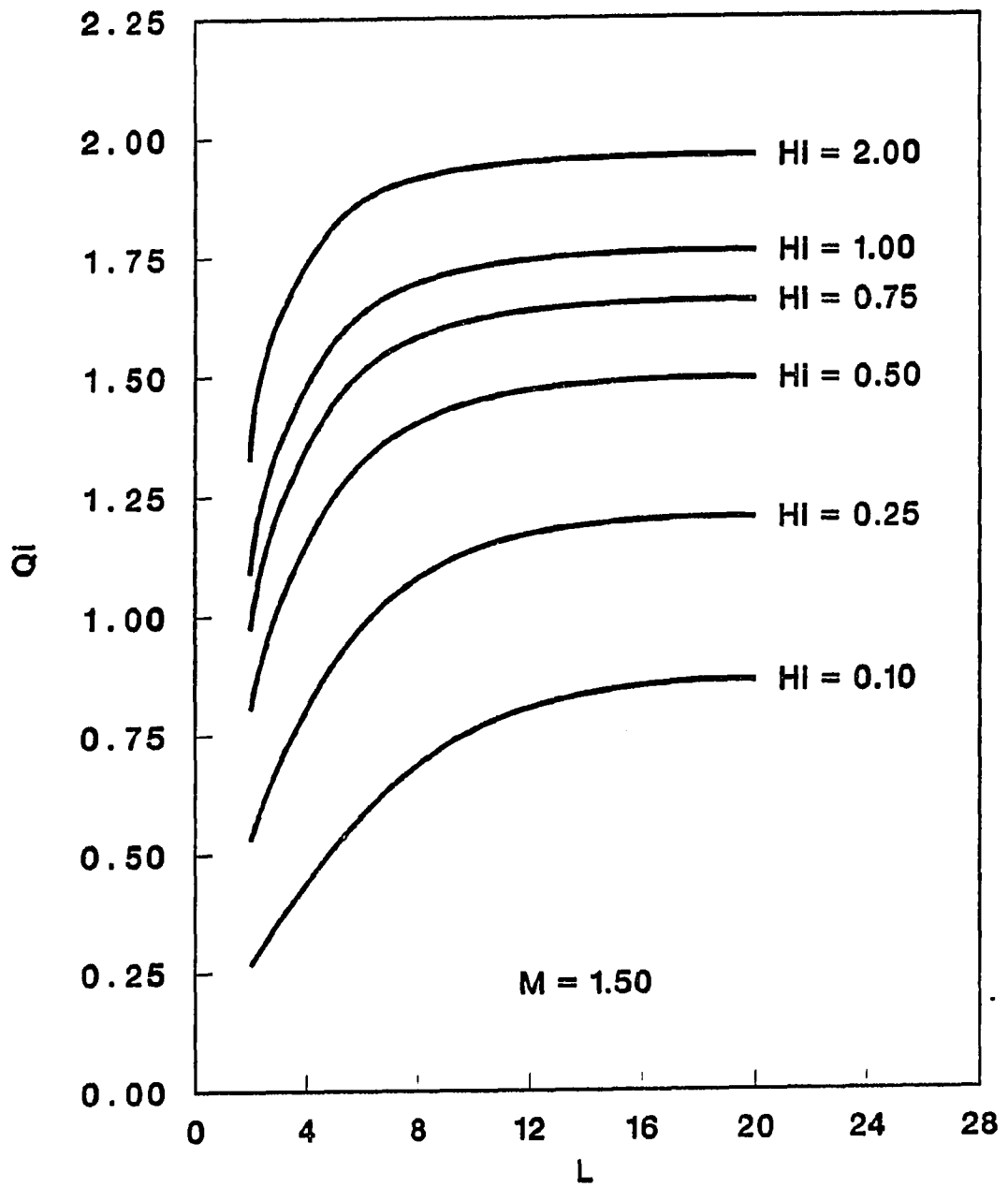

FIGURE 7.3. Radiant heat flux chart, M = 1.5

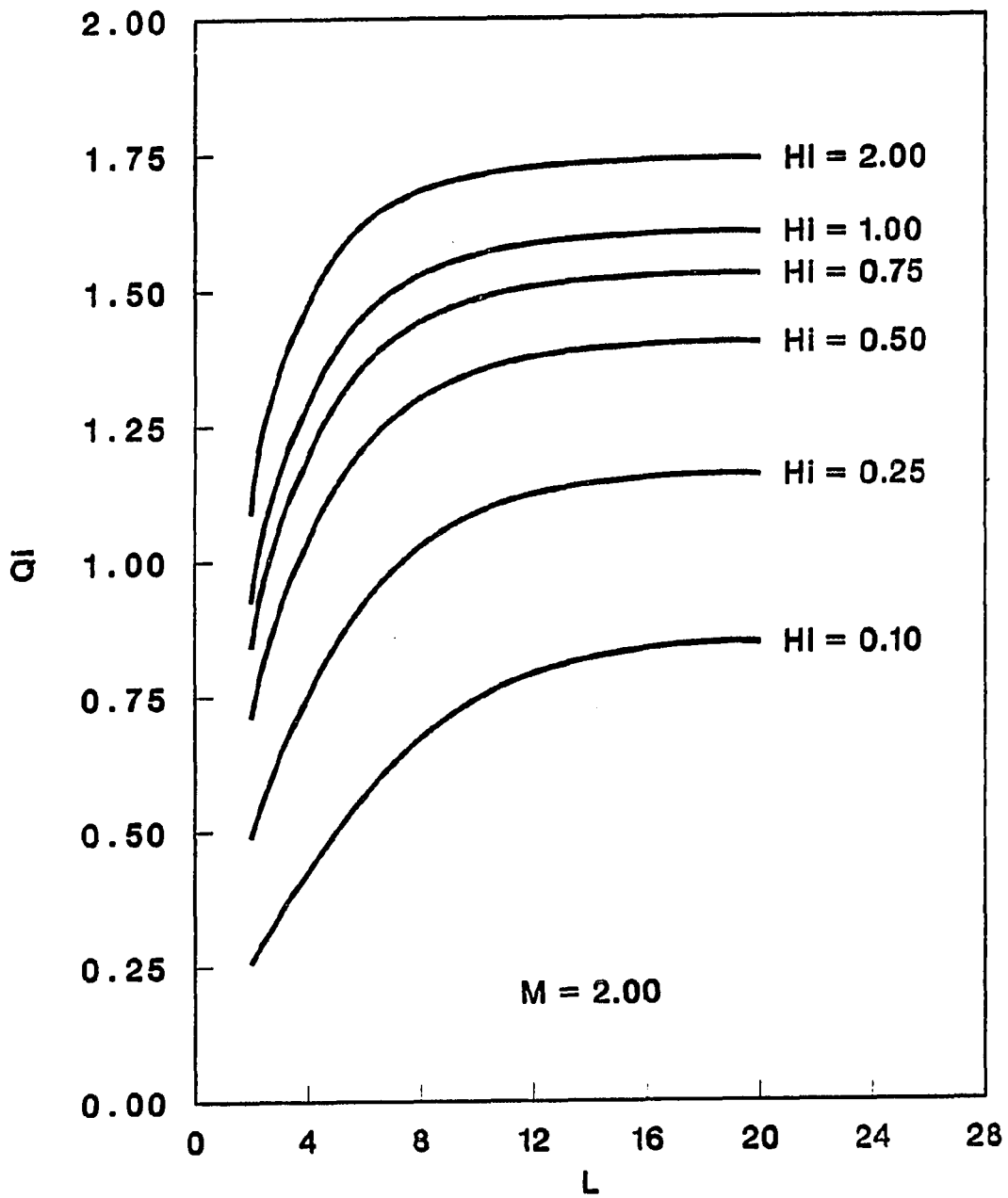

FIGURE 7.4. Radiant heat flux chart, M = 2.0

the wall. These correlations attempt to relate the heat flux to the panel size and room configuration, while other references ignore the size effect. For example, Jennings (1978) suggested the following equations:

$$q_c = 0.81(T_p - T_\infty)^{1.12} \qquad \text{for floor panel}$$

$$q_c = 0.22(T_p - T_\infty)^{1.25} \qquad \text{for ceiling panel}$$

The heat transfer coefficient for free convection can also be calculated from the fundamental convective heat transfer theory. Using the analysis given in most of fundamental heat transfer texts (e.g., Holman 1981), the value of h for surface temperatures around 30 to 40°C (see Appendix D) is estimated to be 4 to 5 $W/m^2°C$ for floor panels.

The temperature dependence of the convective heat transfer coefficient can be reduced if there is mechanical ventilation, since the forced-convection heat transfer coefficients are basically temperature independent. In reality, surface temperature dependence can be ignored when estimating h, and then Bi, at least for the narrow range of temperatures encountered in low-temperature panel heating. Also, as mentioned earlier in Chapter 5, small deviations in h values have insignificant effects on the overall heat output, since the predominant thermal resistance is from the panel medium.

Development of the New Method

The heat transfer equation presented in the above analysis is based on a panel unit consisting of a single tube, so that applying this equation to the design of a panel heating system requires that the whole panel be considered. As shown previously, a single panel unit is treated as a two-dimensional domain perpendicular to the flow direction with the assumption that the temperature gradient along the flow direction is much smaller. Thus, the heat output from the two-dimensional surface, $q \cdot l$, has units of energy rate per unit length of imbedded tube and can be related to the local water temperature through Eq. (6.47). The local water temperature (approximated as an isothermal boundary temperature in the panel unit) is not the same as the supply water temperature since the temperature of hot water decreases as it flows downstream through the tubes. To be able to relate the overall heat output of the radiant panel to the panel inlet or supply temperature, an additional analysis is required.

Figure 7.5 is a plane view of a typical heating panel. Neglecting the effects of the slight temperature difference between adjacent tubes and the effects of corners and elbows, the complete panel can be considered as consisting of infinite number of the infinitesmal control volumes whose projected area is $l \cdot dx$ (shaded area in Figure 7.5).

Figure 7.6 illustrates the energy balance for the control volume. The depth of the volume is the length of the panel unit, l. If the conduction loss through the insulated side of the control volume is

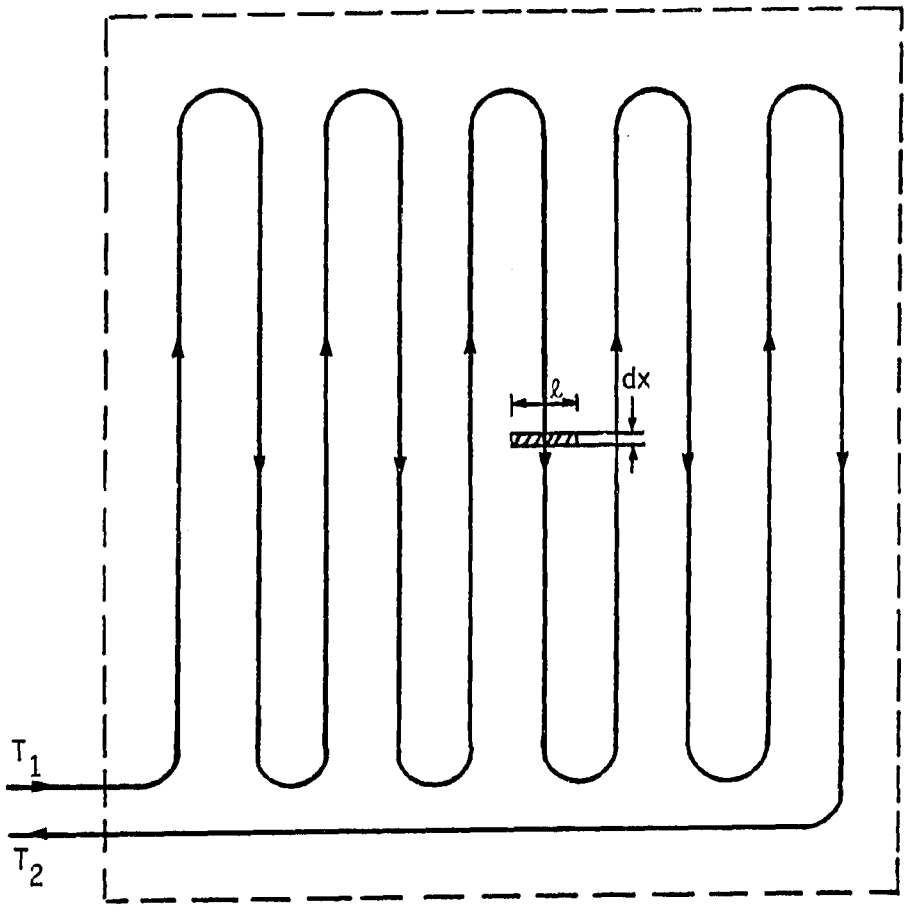

FIGURE 7.5. Plane view of a typical tube arrangement for a whole heating panel

negligible, then an energy balance on the control volume can be expressed as

$$i \cdot \dot{m} = (i + \Delta i)\dot{m} + (q \cdot 1)\Delta x \qquad (7.1)$$

where i is the enthalpy, and $\dot{m}$ is the mass flow rate of water, and q·l is the heat output from the two-dimensional surface of the panel unit or control volume.

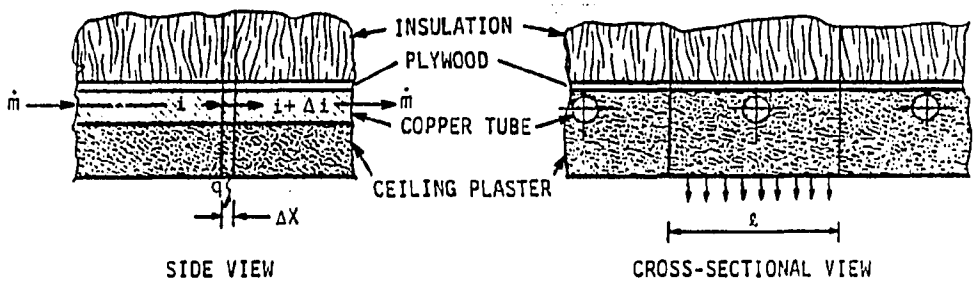

FIGURE 7.6. Illustration of the energy balance for a control volume

Recalling Eq. (6.20), the heat output per unit length of embedded tube (q·l) can be obtained from

$$q \cdot l = Qi \cdot k(T - T_{\infty}) \tag{7.2}$$

where Qi can be determined from the radiant charts or directly calculated by Eq. (6.47). Regardless of which approach is taken, the three nondimensional parameters must be determined. Specifically, L and M are fixed for any particular tube size, tube spacing, and panel thickness while the third parameter, Hi, depends on Bi, Pi, and Ti, which are dependent on panel material and room enclosure conditions.

Although Pi and Ti all depend on T, the local water temperature, this dependence is weak and can be ignored. As a result, Hi can be approximated as temperature independent. Therefore, Qi is also temperature independent and consequently Eq. (7.2) is a linear function of the local water temperature, T.

By rearrangement and application of $di = c \cdot dT$ and Eq. (7.2), Eq. (7.1) can be rewritten as

$$-c \cdot \dot{m} \cdot dT = Qi \cdot k(T - T_\infty)dx \tag{7.3}$$

where c is specific heat for water. Equation (7.3) is a first order differential equation, with the boundary condition

$$x = 0, \quad T = T_1 \tag{7.4}$$

where T_1 is the inlet water temperature. Assuming the total stretched tube length is S, so that the temperature of the water outlet from the panel, T_2, can be determined by simply integrating each side of Eq. (7.3) over respective ranges,

$$\int_{T_1}^{T_2} \frac{dT}{(T-T_\infty)} = -\int_0^S \frac{Qi \cdot k}{c \cdot \dot{m}} dx \tag{7.5}$$

Thus the outlet temperature and the total heat output from the panel can be determined, assuming that all the heat transferred from the water contributes to the heat output from the radiant panel surface. The temperature of the water leaving the heating panel and, thus, returning to the heat source is

$$T_2 = T_\infty + (T_1 - T_\infty) \cdot \exp(-Qi \cdot k \cdot S/c \cdot \dot{m}) \tag{7.6}$$

while the total heat output from the panel surface of area A is

The temperature of the water leaving the heating panel and, thus, returning to the heat source is

$$T_2 = T_\infty + (T_1 - T_\infty)\cdot\exp(-Qi\cdot k\cdot S/c\cdot\dot{m}) \tag{7.6}$$

while the total heat output from the panel surface of area A is

$$(q\cdot A) = c\cdot\dot{m}(T_1 - T_2) \tag{7.7}$$

Discussion

This new method provides an alternate approach to estimating the heat output from a heating panel. Moreover, it establishes a correlation between various parameters involved in the heating panel design, which can then be incorporated into a computer simulation. However, this method is limited in its practical applications for several reasons. Specifically, heat losses through the top insulation and edges of the panel were not taken into account in developing this method. These losses vary with individual panels. Also, the heat transfer between adjacent tubes was neglected in this analysis. Nevertheless, as discussed in Chapter 5, this effect is negligible for most tube spacing arrangements greater than 10 cm apart.

Due to their complexity, this study did not account for the effects of the metal lath on the thermal behavior of a typical radiant ceiling panel. Experiences have shown that if a metal lath is installed in the plaster ceiling, as for most ceiling panels, then the predicted heat output from the ceiling can be less than the actual heat

output from such a ceiling. The reason for this difference in heat output is that the assumption of a homogeneous medium is violated.

An experimental test of the radiant ceiling panel at the ISU Energy Research House was performed during the winter season of 1984 to 1985 (see Chapter 3). The theoretical prediction of panel heat output by the design method described herein, which neglects the metal lath effect, is within 16% of the experimental results. However, taking into account the metal lath and using an equivalent thermal conductivity approach, the discrepancy reduces to 5%. An illustration of this comparison can be seen in Appendix E.

The design methodology presented above can be used for several applications. Specifically, it can be used to determine:

1. The heat output rate from an existing heating panel, provided the ambient air condition is given;
2. heating panel size for a given heating load and supply water condition;
3. water flow rate or inlet water temperature for a particular size and type of heating panel in order to meet a certain heating load;
4. optimal cover thickness when the ambient condition is given.

Two of these applications are illustrated in Appendix E.

It should be noted that because of the various assumptions that were used in developing the semi-analytical correlation, this methodology may not be applicable to some situations which may be

encountered in heating panel design. For example, butyl rubber tubes and plastic tubes are replacing copper tubes in modern applications; whether or not this method can be applicable to those cases in which rubber or plastic tubing are used remains to be investigated. It is likely, however, that this method will still be applicable if the thin tube wall is treated as part of the conducting media surrounding the tube. Therefore, the inner tube diameter instead of outer tube diameter would be used in the calculations for this special case. For many floor panels, only perimeter insulation instead of complete bottom insulation is used. In this case, the adiabatic boundary condition used in the model will be violated and a certain deviation from actual thermal behavior of a panel will likely occur.

Conclusion

This chapter is a continuation of the theoretical study performed in Chapter 6 dealing with heat transfer from structures with embedded tubes, particularly heating panels. In this previous study, a semi-analytical correlation was developed between heat output per unit length of embedded tube and other factors, including tube cover thickness, tube spacing, thermal properties of panel materials, and ambient air. The study presented herein investigates a complete heating panel with tubes. For example, a typical heating panel might completely cover the ceiling or floor space of a room. The analysis can be used to calculate the overall heat output from such a structure as a function of the above mentioned factors.

This methodology is applicable to the design of those panels that have low-temperature heat sources with one side of the panel well insulated. Two specific applications are illustrated in Appendix B. The method was compared with experimental results obtained from a field study of a radiant ceiling panel. Reasonable agreements of 16% for the case treating panel as homogeneous medium and 5% for the case taking an equivalent thermal conductivity of the panel were found. Again, it is important to note that the model may not be applicable to those structures which deviate from the assumptions that were made during the model development.

CHAPTER 8 CONCLUSIONS AND SUGGESTIONS

Conclusions

The study presented herein covers both experimental and theoretical aspects of a hydronic radiant ceiling panel heating system. Except for Chapter 1 which is the Introduction and Chapters 6 and 7 which preserve continuity, each chapter is by and large independent, covering a different aspect of the heating system..

In Chapter 2 the radiant ceiling panel heating system was evaluated in conjunction with an active solar heating system using field test data collected during the months of March and April, 1985. Each component of the combined system, including the flat-plate solar collectors, the storage tank, the solar-to-radiant heat exchanger, and the radiant ceiling panel-room enclosure, was studied and examined.

An evaluation of the thermal performance of each component showed that the flat-plate collector used in this study can be expected to have an efficiency of 40% in a mild winter month and that the storage tank heat losses are significant when the tank mean temperature reaches 35°C and above. A performance evaluation of the solar-to-radiant heat exchanger showed that about 85% of useful solar energy can be provided for radiant heating via a solar-to-radiant heat exchanger. It was estimated that radiation constitutes about two-thirds and convection about one-third of the energy transferred to the enclosure from the ceiling panel. It was also estimated that 50% of the house heating

load can be supplied by solar energy using a radiant heating system during mild winter months (assuming 0°C outdoor temperature). The final conclusion is that despite the low temperature of the energy source, the combined systems worked well in providing space heating.

An extensive test was performed in Chapter 3 to further the understanding of the transient response of the radiant panel ceiling and enclosure. Several interesting points were observed through this test: First, the coil arrangement for the ceiling panel helps achieve high temperature uniformity of the ceiling surface; second, the water supply temperature has a large effect on the heat-up rate while the water flow rate has only a marginal effect; third, the test results suggest that the wall is heated by a combination of radiation from the ceiling and convection from the air; fourth, the room air temperature does not lag the wall and floor temperature during a heat-up transient; fifth, the slow response of the enclosure due to its large mass may require a sophisticated control system in order to make the system cost effective, particularly for intermittent occupancy. Finally, this study provided both the grounds for building a theoretical model and useful data which could be compared to the theoretical predictions using the model.

Another experimental test was performed from January through March, 1986 with the results being reported in Chapter 4. The purpose of this study was to compare the energy requirements for a forced-air heating system and the radiant ceiling panel heating system. This

study showed that for the Research House, a radiant heating system can result in an energy savings of about 14 to 20% over the forced-air heating system, depending on how the experimental data are interpreted and analyzed. A regression analysis leads to an overall heat loss coefficient of 251 W/°C (475 Btu/hr·F) for the radiant system and 290 W/°C (550 Btu/hr·F) for the forced-air system.

The actual energy savings for the radiant system could be even higher (up to 7.4% higher) for several reasons: First, the air temperature for a radiant system can be lower than the air temperature for a forced-air system when the same operative temperature is maintained. Second, because of energy storage effects in the ceiling during a heating mode shift, the energy consumption is overestimated for the radiant system and underestimated for the forced-air system.

Chapter 5 reports a numerical study of heat transfer in a ceiling panel unit that is isolated from the whole panel. The heat diffusion equation is used to solve both the steady and transient state problems. The Gauss-Siedel method is applied to the steady state problem. The point Gauss-Seidel iteration method is found to be more effective than the block iterative method, even though the block iteration method has a faster convergence rate. In both methods, the tolerance affected the accuracy of the final results.

Transient state solutions are obtained using an explicit scheme. The advantages of using this scheme outweigh the disadvantages when compared to other schemes. The steady state can also be obtained from the transient calculation by proceeding to large times.

Based on the numerical results, the relationships between heat output from the panel unit and various factors such as tube spacing, tube cover thickness, and convective heat transfer coefficient are also examined in Chapter 5. This heat transfer coefficient does not have a significant effect on the heat output from the ceiling as suggested by this study.

In Chapter 6, a different approach is taken to relate the heat output from the radiant panel unit to various factors. A semi-analytical formula, Eq. (6.47), is obtained which expresses a nondimensional heat output, Qi, from a panel structure with embedded tubes in terms of three nondimensional parameters (L, M, and Hi). This correlation is developed by solving the heat diffusion equations for several extreme cases where analytical solutions exist and then combining these solutions along with a correction term so that the resulting equation approximately describes the heat transfer from the panel surface. The correction term is derived by using a trial-and-error approach which minimized the differences between the correlation and a finite-element solution. The agreement between the semi-analytical correlation and the finite-element solution was generally within 5% for a wide range of conditions representing practical cases.

The semi-analytical formula has advantages in that it explicitly relates the heat output from the structure to the various physical and geometrical parameters. In addition, this heat output can be easily calculated using a single equation. As a result, the thermal design of

structures that contain embedded tubes for heating is greatly simplified. Although this correlation is developed for many structures with embedded pipes or tubes, the application of this formula to the radiant panels are emphasized.

Chapter 7 is a continuation of Chapter 6. It applies the correlation developed in Chapter 6 to a complete heating panel by integrating the heat output from the panel unit along the entire tube length. The analysis can be used to calculate the overall heat output from such a structure under any specified conditions.

This methodology is applicable to the design of those panels that have low-temperature heat sources with one side of the panel well insulated. Two specific applications are illustrated in Appendix B. The method was compared with experimental results obtained from a field study of a radiant ceiling panel and reasonable agreement (16% for the case treating panel as homogeneous medium and 4% for the case taking an equivalent thermal conductivity of the panel) was found.

The advantage of this new approach over the well established ASHRAE method is that it can better fit into a computer simulation for a radiant heating system.

Suggestions

Due to time constraints, this study did not cover several other aspects of the radiant system. The following are suggested for further studies:

A numerical study taking into account the metal lath effect

Since a metal lath is an integral part of a plaster radiant ceiling panel, and its effect on heat transfer is significant, this study will be very useful in accurately predicting the thermal behavior of a ceiling panel. In addition, a more accurate estimation of the equivalent ceiling thermal conductivity can be made based on the results of this study.

A PC controlled radiant heating system

One of the outstanding features of a radiant ceiling panel is its extended heat transfer surface which makes it possible to use low temperature heat sources. A personal computer controlled radiant system monitoring inlet temperature instead of operating on the on-off basis would be a very interesting study. This study can confirm whether or not a sophisticated control can greatly improve the cost-effectiveness of a radiant heating system by keeping the supply water at minimum necessary temperature.

Acoustic aspect of a radiant ceiling panel

It has been observed throughout the experiments performed in the ERH that a considerable amount of noise occasionally propagates through the whole ceiling panel when the system was operating, particularly during the start-up periods. To study this phenomenon and to understand the cause of this noise would be an interesting research

project. This research would lead to a better understanding of the acoustic nature of a radiant ceiling panel and help prevent system failures.

APPENDIX A : A DETERMINATION OF CONFIDENCE BAND OF REGRESSION RESULTS

Due to the scattering of the data collected during the experiments reported in Chapter 4, it is necessary to perform a statistical analysis on the regression results in order to to determine the confidence band of at least a regression curve. The calculations presented herein focus on an analysis of the regression results using all data, two-variable mode. The confidence band of the regression curve for the radiant system is determined such that the regression curve for the forced-air system is completely excluded from the band.

First, all data collected are used to determine the regression curves for both the radiant system and the forced-air system. The least-squares method is applied. The relation between the energy consumption and the difference between outdoor and indoor temperatures is assumed to be:

$$Q = b \cdot \Delta T + a$$

The constants a and b can be determined by

$$a = \frac{\Sigma x^2 \Sigma y - \Sigma x \Sigma xy}{n\Sigma x^2 - (\Sigma x)^2}$$

and

$$b = \frac{n\Sigma xy - \Sigma x \Sigma y}{n\Sigma x^2 - (\Sigma x)^2}$$

where x stands for the recorded temperature differences, y for the recorded energy consumption, and n for the number of tests for each mode. It should be noted that the subscript i that denotes the test

number is omitted from the above equations. Using all data for the radiant mode and the forced-air mode results in the following equations

$$Q_r = 0.31063 \cdot \Delta T - 1.5210$$

$$Q_c = 0.33936 \cdot \Delta T - 1.0914$$

for the radiant and the forced-air system, respectively (where Q is in kW and ΔT is in °C).

These regression results show that the radiant system is more energy efficient, since both the coefficient and the intersect for the radiant curve are smaller than that of the forced-air curve. However, in order to determine the degree of confidence that this conclusion can be drawn from the data collected, a further statistical analysis is required.

First, the correlation coefficient, r, can be computed using the following equation:

$$r = b \cdot s_x / s_y$$

where

$$s = \sqrt{\frac{S(x-\bar{x})^2}{n-1}} \quad , \qquad s = \sqrt{\frac{S(y-\bar{y})^2}{n-1}}$$

Using the experimental data and the above equations, r^2 can be determined for both the radiant and the forced-air testings. It is found that

$r^2 = 0.8368$ for radiant data

$r^2 = 0.7475$ for forced-air data

The values of r^2 are significant; they indicate that for the radiant testing, physical variation is about 84% and random variation is 16%, while for the forced-air testing, physical variation is about 75% and random variation is 25%.

However, only 50% confidence can be associated with this conclusion. Hence, for higher confidence, a band around this line must be constructed. This can be accomplished by the following equations:

$$\bar{y}_x - A_1 \leq \mu_{y.x} \leq \bar{y}_x + A_1$$

$$A_1 = t_{\alpha/2.(n-2)} s_{y.x} \sqrt{\frac{1}{n} + \frac{(x-\bar{x})^2}{(n-1)s_x^2}}$$

where $s_{y.x}$ is called the standard error of estimate and can be expressed as

$$s_{y.x} = \sqrt{\frac{n-1}{n-2}(s_y^2 - a^2 s_x^2)}$$

and $\bar{x}$ is the average temperature difference and s is the sample standard deviation.

Using the experimental data and the above equations, an 80% confidence band is plotted in Figures 4.3 and 4.4.

APPENDIX B : COMPUTER PROGRAM (EXPLICIT METHOD) FOR CHAPTER 5

```
CCCCCCCCCCCCCCCCCCCCCCCCCCCCCCCCCCCCCCCCCCCCCCCCCCCCCCCCCCCCCCCCCCCCCCC
C                                                                      C
C                          PROGRAM TR1TEM                              C
C                                                                      C
C      THIS PROGRAM IS A MODIFIED DIMENSIONLESS VERSION OF A           C
C   CODE THAT AIMS AT SOLVING THE HEAT DIFFUSION EQUATION              C
C   WITH THE EXPLICIT METHOD WITHOUT ITERATION.  THE STEADY            C
C   STATE CAN BE REACHED AS TIME APPROACHES A CERTAIN VALUE            C
C   SUCH THAT THE TEMPERATURE DIFFERENCE BETWEEN CURRENT               C
C   STEP AND PREVIOUS STEP IS NEGLIGIBLE.  THE RESULTS ARE             C
C   ARE GIVEN IN BOTH TEMPERATURE DISTRIBUTION AND HISTORY.            C
C   THE HEAT OUTPUT IS ALSO CALCULATED BY INTEGRATING THE              C
C   SURFACE TEMPERATURES.                                              C
C      THE FOLLOWING ARE THE NOTATION OF THE VARIABLES:                 C
C   AH --- CONVECTION HEAT TRANSFER COEFFICIENT                        C
C   AK --- PANEL THERMAL CONDUCTIVITY                                  C
C   CC --- GRID SIZE GROWTH RATE                                       C
C   CP --- PANEL SPECIFIC HEAT                                         C
C   DE --- PANEL DENSITY                                               C
C   DT --- TIME INCREMENT                                              C
C   EP --- PANEL SURFACE GRAY EMISSIVITY                               C
C   EPS -- CONVERGENCE CRITERION                                       C
C   NX --- GRID NUMBER ALONG X DIRECTION                               C
C   NY1 -- GRID NUMBER ALONG Y DIRECTION AND IN TUBE REGION            C
C   NY2 -- GRID NUMBER ALONG Y DIRECTION AND IN Y>R REGION             C
C   PTM1 - TIME INTERVAL FOR PRINTING SURFACE TEMPERATURES             C
C   PTM2 - TIME INTERVAL FOR PRINTING BODY TEMPERATURES                C
C   RR --- TUBE RADIUS                                                 C
C   TH --- HOT WATER/ISOTHERMAL BOUNDARY TEMPERATURE                   C
C   TINF - AMBIENT/ROOM AIR TEMPERATURE                                C
C   TMX -- MAXIMUM TIME                                                C
C   XX --- HALF LENGTH OF THE TUBE SPACING                             C
C   YY --- PANEL THICKNESS                                             C
C      ALL ABOVE INPUT VARIABLES ARE IN ENGLISH UNITS                  C
C                                                                      C
CCCCCCCCCCCCCCCCCCCCCCCCCCCCCCCCCCCCCCCCCCCCCCCCCCCCCCCCCCCCCCCCCCCCCCC
C
      DIMENSION T(15,15),TP(15,15),X(15,15),Y(15),AA(15,15),
     +          DX(15,15),DL(15,15),X0(15),DL0(15),
     +          B(15,15),C(15,15),D(15,15),E(15,15),
     +          A(15,15),P(15,15),DXN(15),DYN(15),JP(10),
     +          TST(10,15,15),TR(10),T0(15),XR(10)
      READ(5,*)  DE, CP, EP, AK, AH, TH, TINF, EPS
      READ(5,*)  TMX, DT, RR, XX, YY, CC, NX, NY1, NY2, PTM1, PTM2
C
C ---------------------------------------
```

```
C   SPECIFICATIONS(FIXED.VARIABLES ARE IN READ(5,*))
        MARK = 0
        Q0 = 0.
        DT = DT/3600.
        MAX = TMX/DT+.1
        INT1 = PTM1/60./DT+.1
        INT2 = PTM2/60./DT+.1
        N = NY1+NY2+1
        M = NX
        MM = M-1
        MT = M+1
        R = RR/12.
        SIGMA = 0.1714E-8
        TIB = TINF/TH
        PI = EP*SIGMA/AK*R*TH**3
        BI = AH*R/AK
        AF = AK/(DE*CP)
        FO = AF*DT/R**2
C
C ----------------------------------------
C   OBTAIN THE GRIDS AND X, Y
        XB = XX/RR
        YB = YY/RR
        DY = 2./FLOAT(NY1)
        CT = 0.
        DO 50 J = 1, M
 50     CT = CT + CC**(J-1)
        CS = 0.
        DO 52 I = 1, NY2
 52     CS = CS+CC**(I-1)
        NIF = NY1+1
        NI = NIF+1
        NY  = NY1+NY2
        DYN(NIF) = (YB-2.)/CS
        DXN(1) = XB/CT
        DO 56 I = 1, NIF
          Y(I) = DY*(I-1)
          X0(I) = SQRT(2.*Y(I)-Y(I)**2)
          DA = XB-X0(I)
          DX(I,1) = DA/CT
          X(I,1) = X0(I)+DX(I,1)
          DO 56 J = 2, M
          DX(I,J) = CC*DX(I,J-1)
          X(I,J) = X(I,J-1)+DX(I,J)
 56     CONTINUE
          DO 57 I = 1, NY1
          DO 55 J = 1, M
 55       DL(I,J) = SQRT((X(I+1,J)-X(I,J))**2+DY**2)
 57       DL0(I) = SQRT((X0(I+1)-X0(I))**2+DY**2)
        DO 58 I = NI, N
```

```
          Y(I) = Y(I-1)+DYN(I-1)
          DYN(I) = CC*DYN(I-1)
          XO(I) = 0.
          X(I,1) = XO(I)+DXN(1)
          DO 58 J = 2, M
          DXN(J) = CC*DXN(J-1)
          X(I,J) = X(I,J-1)+DXN(J)
  58    CONTINUE
C
CC   ASSIGN INITIAL TEMPERATURE
       DO 100 I = 1, N
       DO 100 J = 1, M
 100   TP(I,J) = TIB
C
CC   ASSIGN COEF'S OF THE FIRST ROW
       DO 110 J = 1, M
         B(1,J) = 0.
         IF(J.GT.1) B(1,J) = DL(1,J-1)/DX(1,J)
         C(1,J) = 0.
         IF(J.LT.M) C(1,J) = DL(1,J)/DX(1,J+1)
         E(1,J) = DX(1,J)/DL(1,J)
         IF(J.LT.M) E(1,J) = (DX(1,J)+DX(1,J+1))/DL(1,J)
         AA(1,J) = 1./(2.*FO)*DL(1,J)*
     +             E(1,J)*DL(1,J)
         A(1,J) = AA(1,J)-(B(1,J)+C(1,J)+E(1,J))
         P(1,J) = 0.
 110   CONTINUE
         A(1,1) = A(1,1)-DLO(1)/DX(1,1)
         P(1,1) = DLO(1)/DX(1,1)
C
CC   ASSIGN COEF'S OF THE MIDDLE ROWS(UPPER PORTION)
       DO 120 I = 2, NY1
       DO 125 J = 1, M
         B(I,J) = 0.
         IF(J.GT.1)
     +   B(I,J) = (DL(I-1,J-1)+DL(I,J-1))/DX(I,J)
         C(I,J) = 0.
         IF(J.LT.M)
     +   C(I,J) = (DL(I-1,J)+DL(I,J))/DX(I,J+1)
         D(I,J) = DX(I-1,J)/DL(I-1,J)
         IF(J.LT.M)
     +   D(I,J) = (DX(I-1,J)+DX(I-1,J+1))/DL(I-1,J)
         E(I,J) = DX(I,J)/DL(I,J)
         IF(J.LT.M)
     +   E(I,J) = (DX(I,J)+DX(I,J+1))/DL(I,J)
         AA(I,J) = 1./(2.*FO)*(DL(I-1,J)+DL(I,J))*
     +             E(I,J)*DL(I,J)
         A(I,J) = AA(I,J)-(B(I,J)+C(I,J)+D(I,J)+E(I,J))
 125     P(I,J) = 0.
         A(I,1) = A(I,1)-(DLO(I-1)+DLO(I))/DX(I,1)
```

```
          P(I,1) = (DLO(I-1)+DLO(I))/DX(I,1)
 120    CONTINUE
C
CC   ASSIGN COEF'S OF THE INTERFACE ROW
       DO 140 J = 1, M
         B(NIF,J) = 0.
         IF(J.GT.1)
     +   B(NIF,J) = (DL(NIF-1,J-1)+DYN(NIF))/DX(NIF,J)
         C(NIF,J) = 0.
         IF(J.LT.M)
     +   C(NIF,J) = (DL(NIF-1,J)+DYN(NIF))/DX(NIF,J+1)
         D(NIF,J) = DX(NIF-1,J)/DL(NIF-1,J)
         IF(J.LT.M)
     +   D(NIF,J) = (DX(NIF-1,J)+DX(NIF-1,J+1))/DL(NIF-1,J)
         E(NIF,J) = DXN(J)/DYN(NIF)
         IF(J.LT.M)
     +   E(NIF,J) = (DXN(J)+DXN(J+1))/DYN(NIF)
         AA(NIF,J) = 1./(2.*FO)*(DL(NIF-1,J)+DYN(NIF))*
     +             E(NIF,J)*DYN(NIF)
         A(NIF,J) = AA(NIF,J)-(B(NIF,J)+C(NIF,J)+D(NIF,J)+E(NIF,J))
 140     P(NIF,J) = 0.
         A(NIF,1) = A(NIF,1)-DLO(NIF-1)/DX(NIF,1)
         P(NIF,1) = DLO(NIF-1)/DX(NIF,1)
C
CC   ASSIGN COEF'S OF THE MIDDYNE ROWS(LOW PORTION)
       DO 160 I = NI, NY
       DO 160 J = 1, M
         B(I,J) = 0.
         IF(J.GT.1)
     +   B(I,J) = (DYN(I-1)+DYN(I))/DXN(J)
         C(I,J) = 0.
         IF(J.LT.M)
     +   C(I,J) = (DYN(I-1)+DYN(I))/DXN(J+1)
         D(I,J) = DXN(J)/DYN(I-1)
         IF(J.LT.M)
     +   D(I,J) = (DXN(J)+DXN(J+1))/DYN(I-1)
         E(I,J) = DXN(J)/DYN(I)
         IF(J.LT.M)
     +   E(I,J) = (DXN(J)+DXN(J+1))/DYN(I)
         AA(I,J) = 1./(2.*FO)*(DYN(I-1)+DYN(I))*
     +             E(I,J)*DYN(I)
         A(I,J) = AA(I,J)-(B(I,J)+C(I,J)+D(I,J)+E(I,J))
         P(I,J) = 0.
 160    CONTINUE
C
CC   ASSIGN COEF'S OF THE LAST ROW
       DO 130 J = 1, M
         B(N,J) = 0.
         IF(J.GT.1) B(N,J) = DYN(N-1)/DXN(J)
         C(N,J) = 0.
```

```
            IF(J.LT.M) C(N,J) = DYN(N-1)/DXN(J+1)
            D(N,J) = DXN(J)/DYN(N-1)
            IF(J.LT.M)
     +      D(N,J) = (DXN(J)+DXN(J+1))/DYN(N-1)
            E(N,J) = DXN(J)
            IF(J.LT.M) E(N,J) = (DXN(J)+DXN(J+1))
            AA(N,J) = 1./(2.*FO)*DYN(N-1)*E(N,J)
            A(N,J) = AA(N,J)-(B(N,J)+C(N,J)+D(N,J)+E(N,J)
     +               *(PI*TP(N,J)**3+BI))
            P(N,J) = E(N,J)*(PI*TIB**4+BI*TIB)
 130     CONTINUE
C
CC    CHECK SCHEME STABILITY CONSTRAINT
         DO 315 I = 1, N
         DO 315 J = 1, M
 315     IF(A(I,J).LT.0.) GOTO 313
         DO 725 J = 1, 6
 725     JP(J) = FLOAT(M*J)/6.+.1
         WRITE(6,600) TH,TINF,2.*XX,YY,2.*RR,DE,CP,AK,EP,AH,
     +                PI,BI,AF,FO
         DO 345 J = 1, 6
          K = JP(J)
 345     XR(J) = X(N,K)*RR
         WRITE(6,676) XO(N)*RR,(XR(J),J=1,6)
C
C ----------------------------------------
C    START TO CALCULATE--BY TIME ACCUMULATION WITHOUT ITERATION
         DO 500 IT = 1, MAX
         TIME = IT*DT*60.
C
CC    CALCULATE T'S
C
CC    FIRST ROW
         T(1,1) = (P(1,1)+C(1,1)*TP(1,2)+E(1,1)*TP(2,1)
     +           +A(1,1)*TP(1,1))/AA(1,1)
         DO 10 J = 2, MM
  10     T(1,J) = (P(1,J)+B(1,J)*TP(1,J-1)+C(1,J)*TP(1,J+1)
     +           +E(1,J)*TP(2,J)+A(1,J)*TP(1,J))/AA(1,J)
         T(1,M) = (P(1,M)+B(1,M)*TP(1,M-1)+E(1,M)*TP(2,M)
     +           +A(1,M)*TP(1,M))/AA(1,M)
         TO(1) = TH
C
CC    MIDDLE ROWS
         DO 20 I = 2, NY
         T(I,1) = (P(I,1)+C(I,1)*TP(I,2)+D(I,1)*TP(I-1,1)
     +           +E(I,1)*TP(I+1,1)+A(I,1)*TP(I,1))/AA(I,1)
         DO 22 J = 2, MM
  22     T(I,J) = (P(I,J)+B(I,J)*TP(I,J-1)+C(I,J)*TP(I,J+1)
     +           +D(I,J)*TP(I-1,J)+E(I,J)*TP(I+1,J)
     +           +A(I,J)*TP(I,J))/AA(I,J)
```

```
          T(I,M) = (P(I,M)+B(I,M)*TP(I,M-1)+D(I,M)*TP(I-1,M)
     +             +E(I,M)*TP(I+1,M)+A(I,M)*TP(I,M))/AA(I,M)
          TO(I) = TH
   20     IF(I.GT.NIF) TO(I) = T(I,1)*TH
C
CC    LAST ROW
          T(N,1) = (P(N,1)+C(N,1)*TP(N,2)+D(N,1)*TP(N-1,1)
     +             +A(N,1)*TP(N,1))/AA(N,1)
          DO 30 J = 2, MM
   30     T(N,J) = (P(N,J)+B(N,J)*TP(N,J-1)+C(N,J)*TP(N,J+1)
     +             +D(N,J)*TP(N-1,J)+A(N,J)*TP(N,J))/AA(N,J)
          T(N,M) = (P(N,M)+B(N,M)*TP(N,M-1)+D(N,M)*TP(N-1,M)
     +             +A(N,M)*TP(N,M))/AA(N,M)
          TO(N) = T(N,1)*TH
C
C -----------------------------------------
C    OUTPUT
          IF(MOD(IT,INT1).NE.0) GOTO 460
          IF(MOD(IT,INT2).NE.0) GOTO 455
          KTIME = IT/INT2
          DO 450 I = 1, N
          TST(KTIME,I,1) = TO(I)
          DO 450 J = 1, M
  450     TST(KTIME,I,J+1) = T(I,J)*TH
  455     DO 425 J = 1, 6
           K = JP(J)
  425     TR(J) = T(N,K)*TH
C
CC    CALCULATE THE HEAT FLUX
          QB = (PI*(T(N,1)**4-TIB**4)+BI*(T(N,1)-TIB))*DXN(1)/2.
          DO 760 J = 1, MM
  760     QB = QB+(PI*(T(N,J)**4-TIB**4)+BI*(T(N,J)-TIB))
     +         *(DXN(J)+DXN(J+1))/2.
          QB = QB+(PI*(T(N,M)**4-TIB**4)+BI*(T(N,M)-TIB))*DXN(M)/2.
          Q = QB*AK*TH
          WRITE(6,680) TIME,Q,MARK,TO(N),(TR(J),J=1,6)
          IF(ABS(Q-Q0).LE.EPS) GOTO 501
          Q0 = Q
C
  460     DO 70 I = 1, N
          DO 70 J = 1, M
   70     TP(I,J) = T(I,J)
  500    CONTINUE
  501     WRITE(6,605)
          WRITE(6,630)
          DO 310 I = 1, N
  310     WRITE(6,655) Y(I)*RR, XO(I)*RR, (X(I,J)*RR, J = 1, M)
C
CC    OUTPUT THE WHOLE TEMP. DISTRIBUTION IN EVERY HR
          KEND = IT/INT2
```

```
      IF(KEND.EQ.0) STOP
      DO 410 KTIME = 1, KEND
      WRITE(6,610) KTIME
      DO 410 I = 1, N
 410  WRITE(6,620) (TST(KTIME,I,J),J=1,MT)
      STOP
 313  WRITE(6,613) DT*3600
      STOP
C
C ----------------------------------------
 600  FORMAT(/,/,/,'   THE FOLLOWING ARE THE TEMPERATURE AND HEAT',
     + ' FLUX HISTORY OF THE CEILING UNIT UNDER:',
     + /,'  TEMP. OF SUPPLY     ',F10.2,' R',
     + /,'  TEMP. AT INFINITE = ',F10.2,' R',
     + /,'  PIPES ARE SEPARATED ',F10.4,' INCHES APART',
     + /,'  PLASTER THICKNESS IS',F10.4,' INCHES',
     + /,'  PIPE DIAMETER IS    ',F10.4,' INCHES',
     + /,'  PLASTER PROPERTIES:',
     + /,'    DE -- DENSITY          ',E10.4,'  LBM/FT**3',
     + /,'    CP -- SPECIFIC HEAT    ',E10.4,'  BTU/(LBM*R)',
     + /,'    AK -- THER. CONDUCTIV.',E10.4,'  BTU/(HR*FT*R)',
     + /,'    EP -- GRAY EMISSIVITY ',E10.4,
     + /,'  COEFFICIENT OF H.T.(AH) ',E10.4,'  BTU/(HR*FT**2*R)',
     + /,'  MAJOR NON-DIMENSIONAL PARAMETERS:',
     + /,'  PI(RAD.)   BI(CONV.)  AF(DIF.)   FO(TRA.)',/,4E11.4,/,/)
 605  FORMAT(/,'-------------------------------------------------',
     + '-------------------------------------------------',/,
     + ' TIME(MIN.)     Q(BTU/(HR.FT**2)     TEMP.(R)',/,/,
     + '   THE FOLLOWING ARE THE COMPLETE DISTRIBUTION OF TEMP.',
     + ' IN THE UNIT EVERY HOUR',/)
 610  FORMAT(/,'    AT HOUR ',I5)
 613  FORMAT(/,'   DT = ',F4.1,' SEC. IS TOO SMALL TO BE STABLE.')
 620  FORMAT(1X,'   T(R)=      ', 13F9.2)
 630  FORMAT(/,/,1X,' THE FOLLOWING SHOWS HOW GRIDS ARE ARRANGED',
     + /,'  Y(IN.)',20X,' X(IN.)',/,' ---------------------------',
     +       '-------------------------------------------------')
 655  FORMAT(1X, F4.2, 8X, 13F9.2)
 676  FORMAT(1X,'TIME   Q     X ', 9F10.3,/,' ------------------',
     + '-------------------------------------------------',
     + '--------------------------------')
 680  FORMAT(1X,F4.0,F7.2,I4,1X,7F10.2)
      END
```

APPENDIX C : COMPUTER PROGRAMS FOR USING FINITE-ELEMENT METHOD

The canned finite-element program ADINAT was used for the analysis in Chapter 6 to establish heat output data for comparison. In order to use this canned program appropriately, a data set should be created in a form that is compatible to the program. A program is written to generate such data set, and listed below:

```
CCCCCCCCCCCCCCCCCCCCCCCCCCCCCCCCCCCCCCCCCCCCCCCCCCCCCCCCCCCCCCCCCCCC
C                                                                     C
C        A PROGRAM TO CREATE A DATA FILE FOR ADINAT                   C
C                                                                     C
C      INPUT VARIABLES FOR THE SUBROUTINE ADTDT ARE:                   C
C   XT --- HALF LENGTH OF THE TUBE SPACING                            C
C   YT --- PANEL THICKNESS                                            C
C   HEQ -- EQUIVALENT HEAT TRANSFER COEFFICIENT                       C
C   TINF - AMBIENT TEMPERATURE                                        C
C      ALL ABOVE PARAMETERS ARE DIMENSIONLESS                         C
C                                                                     C
CCCCCCCCCCCCCCCCCCCCCCCCCCCCCCCCCCCCCCCCCCCCCCCCCCCCCCCCCCCCCCCCCCCCC
C
C
      SUBROUTINE ADTDT(XT,YT,HEQ,TINF)
      DIMENSION XDT(5),YDT(5),X(1000),Y(1000),
     +          MEL(50,2),NOD1(50,2),NOD2(50,2),NOD3(50,2),NOD4(50,2)
      DATA I0,I1,I2/0, 1, 2/
      DATA R0,R1/0.0, 1.0/
      DATA XDT/0.0, 0.433, 0.5, 0.433, 0.0/
      DATA YDT/0.0, 0.250, 0.5, 0.750, 1.0/
C   I.
      WRITE(7,600)
 600  FORMAT('FINITE ELEMENT SOLUTION FOR RADIANT PANEL PROBLEM')
C
C   II.1
      DX1 = 0.3
      DY1 = 0.3
      XTT = 0.0
      YTT = 0.0
      C = 1.2
      DO 10 I=1,30
        XTT = XTT+C**(I-1)
        IF(XTT.LE.XT/DX1) GOTO 10
        N = I
        GOTO 15
```

```
   10   CONTINUE
        STOP
   15   DO 20 I=1,30
          YTT = YTT+C**(I-1)
          IF(YTT.LE.(YT-1.0)/DY1) GOTO 20
          M = I
          GOTO 25
   20   CONTINUE
        STOP
   25   N1 = N+1
        M1 = M+1
        NUMNP = N1*(5+M)
        WRITE(7,601) NUMNP,I2,I0,I1,I1,R0,I0,I0
  601   FORMAT(5I5,F10.4,2I5)
C
C  II.2
        WRITE(7,602) I0,I0,I0
  602   FORMAT(3I5)
C
C  II.3
        WRITE(7,603) I0
  603   FORMAT(I5)
C
C  II.4
        WRITE(7,604) I0,I0,I0,R0
  604   FORMAT(3I5,E10.4)
C
C  II.5
        WRITE(7,605) I0,R0
  605   FORMAT(I10,F10.4)
C
C  II.6
        WRITE(7,606) I1,I0
  606   FORMAT(2I5)
C
C  II.7
        IPND1 = NUMNP-N
        IPND2 = NUMNP
        WRITE(7,607) IPND1,IPND2
  607   FORMAT(16I5)
C
C  III.A AND B
        WRITE(7,607) I1
        WRITE(7,608) R1
  608   FORMAT(8F10.4)
C
C  IV.
        DO 100 I=1,5
          IT = (I-1)*N1+1
          DX1 = (XT-XDT(I))/XTT
```

```
          X(IT) = XDT(I)
          Y(IT) = YDT(I)
          DO 100 J=1,N
          IT = (I-1)*N1+J+1
          X(IT) = X(IT-1)+C**(J-1)*DX1
          Y(IT) = YDT(I)
  100   CONTINUE
        IT0 = IT
        DY1 = (YT-1.0)/YTT
        DO 200 I=1,M
          IT = IT0+(I-1)*N1+1
          X(IT) = 0.0
          Y(IT) = Y(IT-N1)+C**(I-1)*DY1
          YY = Y(IT)
          DO 200 J=1,N
          IT = IT0+(I-1)*N1+J+1
          X(IT) = X(IT-1)+C**(J-1)*DX1
          Y(IT) = YY
  200   CONTINUE
        DO 300 IT=1,NUMNP
  300   WRITE(7,609) IT,I0,R0,X(IT),Y(IT),I0
  609   FORMAT(1X,I4,'C',I4,3F10.4,I5)
C
C  SKIP V.
C
C  VI.A(SKIP B)
        WRITE(7,606) I0,I0
C
C  VII.1
        NTEMP = 5
        WRITE(7,610) I2,I2,I1,NTEMP,N1,I0,I0,I0,I0,I0,I0
  610   FORMAT(11I5)
C
C  SKIP VII.2
C
C  VIII.A AND B
        DO 50 I=1,2
          WRITE(7,606) I,I2
   50   WRITE(7,608) R0,R1,R1,R1
C
C  IX.1
        NODE2 = 1+4*N1
        WRITE(7,611) I1,I1,R1,R0,N1
        WRITE(7,611) NODE2,I1,R1,R0,I0
  611   FORMAT(2I5,2F10.4,I5)
C
C  IX.2
        WRITE(7,611) IPND1,I2,TINF,R0,I1
        WRITE(7,611) IPND2,I2,TINF,R0,I0
C
```

```
C  SKIP IX.3,4,5,6 AND 7
C  SKIP X.
C
C  XI.1
       NPAR2 = N*(4+M)
       NPAR7 = 4
       WRITE(7,612) I2,NPAR2,I0,I0,I1,NPAR7,I0,I0,I1,I0,I0,I0
 612   FORMAT(5I4,I8,2I12,I8,3I4)
C
C  XI.2.A AND C, SKIP B
       WRITE(7,603) I1
       WRITE(7,613) R1
       WRITE(7,613) R1
 613   FORMAT(F10.4)
C
C  SKIP XI.3
C
C  XI.4.1 AND 2
       MM = 4+M
       DO 70 I=1,MM
         MEL(I,1) = (I-1)*N+1
         NOD1(I,1) = I*N1+2
         NOD2(I,1) = I*N1+1
         NOD3(I,1) = (I-1)*N1+1
         NOD4(I,1) = (I-1)*N1+2
         MEL(I,2) = I*N
         NOD1(I,2) = (I+1)*N1
         NOD2(I,2) = (I+1)*N1-1
         NOD3(I,2) = I*N1-1
         NOD4(I,2) = I*N1
         DO 70 J=1,2
         WRITE(7,614) MEL(I,J),I0,I0,I1,I1,R0,R1,R0
         WRITE(7,615) NOD1(I,J),NOD2(I,J),NOD3(I,J),NOD4(I,J)
     +               ,I0,I0,I0,I0
  70   CONTINUE
 614   FORMAT(5I5,3F10.4)
 615   FORMAT(8I5)
C
C  SKIP XII.
C
C  XIII.1
       NPAR1 = 4
       WRITE(7,616) NPAR1,I0,I0,I0,N,I0,I1,I1,I0,I0
 616   FORMAT(I4,I8,4I4,I8,I24,2I4)
C
C  XIII.2
       WRITE(7,617) I1,HEQ
 617   FORMAT(I5,F10.4)
C
C  XIII.3.B, SKIP A AND C
```

```
      NODC11 = NUMNP-N+1
      NODC21 = NODC11-1
      NODC12 = NUMNP
      NODC22 = NODC12-1
      WRITE(7,618) I1,NODC11,NODC21,I0,I1,I1,R1,R0
      WRITE(7,618) N,NODC12,NODC22,I0,I1,I0,R1,R0
618   FORMAT(6I5,2F10.4)
      WRITE(7,619)
619   FORMAT('STOP')
      RETURN
      END
```

The following is a commanding module used to execute ADINAT.

```
1. //FERP JOB I3531,A4.MAP
2. /*JOBPROC DSN=PROG.ADINA.PROCLIB
3. //STEPNAME EXEC ADINAT
4. //SYSIN DD DSN=M.I3531.FILE01,UNIT=DISK,DISP=SHR
```

where FERP is an arbitrary name for the job, I3531 is the account number, A4.MAP is the user name, and FILE01 is the input data file created by the previous subroutine. (In the actual module the numbering may not be used.)

A main program calling the subroutine with prespecified XT, YT, HEQ, and TINF is needed to create such a file. The JCL (Job Control Language) for this program is listed below:

```
1. // JOB
2. /*JOBPARM LINES=7
3. //STEP0 EXEC SCRUNC,PARM='M.I3531.FILE01'
4. //STEP1 EXEC WATFIV
5. //GO.FT07F001  DD  DSN=M.I3531.file01,DISP=(NEW,CATLG),UNIT=DISK,
6. //          SPACE=(6233,(12,3),RLSE)
7. //GO.SYSIN DD *
8. $JOB           A4.MAP,PAGES=100
```

APPENDIX D : AN ESTIMATE OF FREE CONVECTION COEFFICIENT

Most heat transfer textbooks (e.g., Holman 1981) present the formulations to calculate free convection heat transfer coefficients. As an example, the free convection coefficient for a floor panel (an upper surface of heated plate) is considered. To estimate this h value, the following equation can be used:

$$\bar{Nu}_f = \frac{hx}{k} = 0.15(Gr_f \cdot Pr_f)^{1/3}$$

$$Gr_f = \frac{g\beta(T_s - T_\infty)x^3}{\upsilon^2}$$

For air at low pressure, the ideal gas approximation is applicable so that

$$\beta \cong 1/T_f$$

Assuming the film temperature as T_f = 25°C and the panel surface temperature as T_s = 30°C, then

$$\beta = 0.003354 \ 1/K$$

$$\upsilon = 15.5 \times 10^{-6} \ m^2/s$$

$$g = 9.8 \ m/s^2$$

so that

$$Gr_f = (0.001368 \times 10^{12})x^3$$

For air, Pr = 0.7, k = 26 X 10^{-3} W/m°C, so

$$\bar{Nu}_f = \frac{hx}{k} = 0.15(0.00096 \times 10^{12})^{1/3}x$$

and

$$h = 3.9 \quad W/m^2{}^\circ C$$

If the surface temperature is varied from 30 to 40°C, then

$$Gr_f = (0.002736 \times 10^{12})x^3$$

$$\bar{Nu}_f = \frac{hx}{k} = 0.15(0.00192 \times 10^{12})^{1/3}x$$

and

$$h = 4.8 \quad W/m^2C$$

Therefore, even though the surface temperature variation is as great as 10°C, the h value only deviates from 3.9 to 4.8, which has insignificant effects on the overall heat transfer from the hot water flowing in the embedded tube to the heating space, since the dominant thermal resistance is from panel medium and is about two orders of magnitudes higher than this h value.

APPENDIX E : ILLUSTRATIONS OF NEW METHOD FOR PANEL DESIGN

Illustration 1

A radiant panel built in the master bedroom of the ERH consists of a plaster ceiling of thickness 2.54 cm (1 in.) and embedded copper tubes of 0.95 cm (3/8 in.) O.D. The tubes are spaced 15.24 cm (6 in.) apart. The plaster ceiling has a thermal conductivity of 0.48 W/m°C (0.278 Btu/hr·ft·F) and a gray body surface emissivity of 0.91. The heat transfer coefficient for the room air is estimated at 4.5 $W/m^2°C$ (0.8 $Btu/hr·ft^2F$) (see Appendix C). For a typical field experiment, the panel and room enclosure reached steady state when the room air temperature (measured at 1.5 m from the floor) reached 26°C (78.8F). The measured water inlet (to the panel) temperature is 52°C (125.6F), and the outlet (out of the panel) temperature is 47°C (116.6F). The volume flow rate is 3.4 l/min (0.9 gpm). The coils embedded in the ceiling panel were traced by an infrared camera and the total stretched length of tubing was observed to be about 85.3 m (280 ft).

The following analyses were performed using the above data:

a. The heat output from the whole panel was predicted using the new method;

b. the measured heat losses through the coils were compared with Part a;

c. the heat output was determined using the ASHRAE method and then compared with the measured heat losses through the coils.

Part a.

For an average water temperature between the inlet and outlet of T = 49.5°C (121.1F), L, M, and Hi are

$$L = 15, \quad M = 1.667$$

$$Bi = 0.009, \quad Pi = 0.036, \quad Ti = 0.928$$

and $Hi = 0.2068$

From Eq. (6.47),

$$Qi \cong 0.934$$

The mass flow rate is

$$\dot{m} = \rho\dot{Q} = 0.056 \text{ kg/s}$$

From Eq. (7.6), the outlet temperature can be determined as

$$T_2 = 47.8°C \text{ (118F)}$$

and the heat transfer from the ceiling is predicted at

$$Q = 0.989 \text{ kW (3375 Btu/hr)}$$

The above calculation is based on the assumption that the panel material is homogeneous and isotropic. In reality, the existence of the metal lath layer underneath the tubes considerably improves the heat transfer rate. Accounting for this factor in the analytical model is very difficult. However, this metal lath effect can be approximated by taking an equivalent thermal conductivity of the panel medium consisting of both plaster and metal lath. This equivalent k value is estimated to be k = 0.57 W/m°C (0.33 Btu/hr·ft·F),. Thus the recalculated values of the nondimensional parameters are

$$Bi = 0.076, \quad Pi = 0.029, \quad Ti = 0.928$$

and $Hi = 0.179$

Therefore, from Eq. (6.47),

$$Qi = 0.98$$

The predicted heat output from the whole panel is now

$$Q = 1.12 \text{ kW } (3820 \text{ Btu/hr})$$

Part b.

The measured heat losses from the coils in the panel is

$$Q_m = c\dot{m}(T_1-T_2) = 1.17 \text{ kW } (3996 \text{ Btu/hr})$$

Comparing with the theoretical prediction, the difference is about 15% for the case without taking into account the metal lath effects, and only 5% for the case in which the metal lath effects are accounted for in a lumped and approximate form.

It should be noted that the measured heat output from the coils embedded in the ceiling panel includes the heat losses through the top and perimeter as the insulation is not perfect, while the theoretical prediction is based on the assumption that the insulation is perfect.

Part c.

According to the ASHRAE Handbook (1987), the ceiling panel considered here has an equivalent thermal resistance to downward heat flow (Table 4 in Chapter 7 in the Handbook, assuming perfect insulation on top)

$$R = 0.079 \text{ m}\cdot^2\text{°C/W } (0.45 \text{ ft}^2\cdot\text{F}\cdot\text{hr/Btu})$$

Checking Fig.7 in Chapter 7, for T = 49.8°C (121.6F) and T_∞ = 26°C (78.8F)

$$q_d = 102.5 \text{ W/m}^2 \text{ } (32.5 \text{ Btu/hr}\cdot\text{ft}^2)$$

Since the panel covers approximately 13 m^2 (140 ft^2) of the ceiling, the total heat transfer is

$$Q = q_d A = 1.33 \text{ kW } (4550 \text{ Btu/hr})$$

The difference between this method and the measured value is 14% with the ASHRAE method overestimating the heat output. The difference between ASHRAE method and Part a is 20 to 30%.

Illustration 2

A floor panel consists of concrete with a thickness of 5.1 cm (2 in.) covering the embedded tube of 1.27 cm (0.5 in.) O.D. The tubes are spaced 22.9 cm (9 in.) apart. The concrete has a thermal conductivity of 1.73 W/m°C (1 Btu/hr·ft·F) and surface emissivity of 0.91. The room conditions are h = 6.8 W/m^2°C (0.8 Btu/hr·ft^2F) (due to buoyancy, h is higher than that for the ceiling panel case), and T_∞ = 22°C (72F). The permissible inlet water temperature is T_1 = 54.4°C (130F) and mass flow rate $\dot{Q}$ = 3 l/min (0.8 gpm). The minimum heating load to be met is Q = 1.47 kW (5000 Btu/hr).

The procedure for sizing the floor panel in order to meet the above conditions is described below.

First, determine L = 17, M = 4.

To meet the heating load, the outlet temperature should be

$$T_2 = T_1 - (Q/c\dot{m}) = 47.2°C \text{ (117F)}.$$

So the average ceiling temperature should be

$$T_a = (T_1 + T_2)/2 = 50.8°C \text{ (123.5F)}.$$

Now determine

$Bi = 0.05, \qquad Pi = 0.0125, \qquad Ti = 0.912,$

so $Hi = 0.09$

From Eq. (6.47),

$Qi = 0.761$

From Eq. (7.6) (Rearrangement of this equation is needed),

$S = 40$ m (131.7 ft)

The covered area is approximately

$A = S \cdot 1 = 9.2\ m^2$ or $98.8\ ft^2 \cong 100\ ft^2$

BIBLIOGRAPHY

ADINA "ADINAT user's manual". Automatic Dynamic Incremental Nonlinear Analysis Engineering Inc., Watertown, MA, 1981.

Alexander, J. C. "Calculations of direct energy losses from ceiling mounted radiant heating panels to penetrated areas". Energy Engineering: Journal of Association of Energy Engineers, 78 (1981) 35-48.

Anderson, D. A.; Tannehill, J. C.; and Pletcher, R. H. Computational fluid mechanics and heat transfer, McGraw-Hill, New York, 1984.

Arpaci, V. S. Conduction Heat Transfer, Addison-Wesley, Menlo Park, CA, 1966.

ASHRAE. ASHRAE Handbook-1987 Systems and Application, American Society of Heating, Refrigerating, and Air-Conditioning Engineers, Inc., Atlanta, 1987.

ASHRAE. "Thermal environmental conditions for human occupancy". ASHRAE Standard 55-81, American Society of Heating, Refrigerating, and Air-Conditioning Engineers, Inc., Atlanta, 1981.

Bailey, H. R. "An experimental comparison of energy requirements for space heating with radiant and convective systems". ASHRAE Transactions, 86, Part 1 (1980), 73-81.

Berglund, L.; Rascati, R.; and Markel M. L. "Radiant heating and control for comfort during transient conditions". ASHRAE Transactions, 88, Part 2 (1982), 765-775.

Bryan, W. L. "Comparative energy requirements of radiant space heating". ASHRAE Transactions, 87, Part 1 (1981), 106-115.

Buckley, N. A.; and Seel, T. "Gas-fired low-intensity radiant heating provides a cost-effective. efficient space condition alternative". ASHRAE Transactions, 92, Part 1B (1986), 616-627.

Chapman, A. J. Heat transfer, Macmillan, New York, 1984.

Cinquemani, V.; Owenby, J. R.; and Baldwin, R. C. "Input data for solar systems". Report prepared for U.S. Department of Energy, The National Oceanic & Atmospheric Administration, Washington, D.C., 1978.

Duffie, J. D.; and Beckman, W. A. Solar engineering of thermal processes, John Wiley & Sons, New York, 1980.

Diamant, R. M. E. Energy conservation equipment, Nichols, New York, 1984.

Durland, A. C. "A study of panel heating for a residence". M.S. Thesis. Department of Mechanical Engineering, Iowa State College, Ames, 1942.

Fanger, P. O.; Banhidi, L.; Olesen, B. W.; and Langkilde, G. "Comfort limits for heated ceilings". ASHRAE Transactions, 86, Part 2 (1980), 141-156.

Gastinel, N. Linear numerical analysis, Academic Press, New York, 1970.

Hedgepeth, L. M.; and Sepsy, C. F. "A thermal dynamic simulation of a radiant panel heating system". ASHRAE Transactions, 78, Part 2 (1972), 50-60.

Hogan, R. E. "Heat transfer analysis of radiant heat panels — hot water pipes in concrete slab floor". M.S. Thesis. Louisiana Tech. University, 1979.

Holman, J. P. Heat transfer, McGraw-Hill, New York, 1981.

Howell, R. H. "A study to determine methods for designing radiant heating and cooling systems". Progress Report to ASHRAE TC 6.5 on ASHRAE 394-RP, June 10, 1986.

Jennings, B. H. The thermal environment — conditioning and control, Harper & Row, New York, 1978.

Jones, C. D.; Crall, G. C.; and Jones, J. W. "Simulation and verification of a hydronic sub-system with radiant panels". ASHRAE Transactions, 81, Part 1 (1975), 457-462.

LeBrun, J. J. "Thermal comfort and energy consumption in winter conditions — continuation of the experimental study". ASHRAE Transactions, 84, Part 1 (1978), 150-175.

Lennox. Lennox engineering handbook, accessories Feb. 1979

Lipson, C.; and Sheth, N. J. Statistical design and analysis of engineering experiments, McGraw Hill, New York, 1973.

Liptak, B. G. "Reducing the operation costs of buildings by the use of computers". ASHRAE Transactions, 83, Part 1 (1977), 343-360.

McNall, P. E. "A manufacturer's view of radiant heater control". ASHRAE Transactions, 81, Part 1 (1975), 398-410.

McQuiston, F. C.; and Parker, J. D. Heating, ventilating and air conditioning, John Wiley & Sons, New York, 1982.

Patankar, S. V. Numerical heat transfer and fluid flow, McGraw-Hill, New York, 1980.

Schutrum, L. F.; Parmelee, G. V.; and Humphreys, C. M. "Heat exchanges in a ceiling panel heated room". ASHVE Transactions, 59 (1953), 495.

Thomas, L. H. "Elliptic problems in linear difference equations over a network". Watson Science Computational Laboratory Report, Columbia University, New York, 1949.